Advances in control and estimation of complex systems: living behavior and multistability

Nelson de Figueireido Barroso

University of Lille
Doctoral School: ED Doctorale SPI 072
Research Institution: Inria Lille - Nord Europe

Nelson de Figueiredo Barroso

Advances in control and estimation of complex systems: living behavior and multistability

Lille, France
2020

Nelson de Figueiredo Barroso

Advances in control and estimation of complex systems: living behavior and multistability

Thesis defended on 18^{th} December, 2020 in order to obtain the title of Doctor of Philosophy from University of Lille. Academic field: Automatic Control, Computer Engineering, Signal and Image Processing.

Advisor: Denis Efimov
Co-advisor: Rosane Ushirobira

Université de Lille

Lille, France
2020

Nelson de Figueiredo Barroso
Master in Electrical Engineering – CEFET-MG, Brazil

Advances in control and estimation of complex systems: living behavior and multistability

Thesis defended on 18^{th} December, 2020 in order to obtain the title of Doctor of Philosophy from University of Lille. Academic field: Automatic Control, Computer Engineering, Signal and Image Processing.

Committee menbers:

Advisor: Denis Efimov, Inria Researcher, Inria
Co-advisor: Rosane Ushirobira, Inria Researcher, Inria

Reviwer: David Angeli, Reader, Imperial College London
Reviwer: Antoine Chaillet, Professor, CentraleSupélec

Examiner and Commitee President: Pierre-Alexandre Bliman, Inria Researcher, Inria
Examiner: Jean-Luc Gouzé, Inria Researcher, Inria

Invited: Jean-Charles Massabuau, CNRS, Université de Bordeaux

Lille, France
2020

Nelson de Figueiredo Barroso
Master en génie électrique – CEFET-MG, Brésil

Progrès dans le contrôle et l'estimation de systèmes complexes: comportement vivant et multistabilité

Thèse soutenue le 18 décembre 2020 afin d'obtenir le titre de Docteur en Philosophie de l'Université de Lille. Domaine académique: Contrôle Automatique, Génie Informatique, Traitement du Signal et de l'Image.

Composition du jury:

Directeur: Denis Efimov, Inria Researcher, Inria
Co-directeur: Rosane Ushirobira, Inria Researcher, Inria

Rapporteur: David Angeli, Reader, Imperial College London
Rapporteur: Antoine Chaillet, Professor, CentraleSupélec

Examinateur et président du jury: Pierre-Alexandre Bliman, Inria Researcher, Inria
Examinateur: Jean-Luc Gouzé, Inria Researcher, Inria

Invité: Jean-Charles Massabuau, CNRS, Université de Bordeaux

Lille, France
2020

To my family for being my safe haven.

THANKS

This Ph.D. thesis was supported by Inria and the "Conseil Régional de la Région Hauts-de-France" and conducted at Inria-Lille, whithin the Valse research team.

I extend my sincere thanks to my advisors, Dr. Denis Efimov and Dr. Rosane Ushirobira, for all opportunities, challenges and incentives, and for their invaluable dedication, guidance, support, availability, advice and patience. I learned a lot from you and I will be forever grateful.

I also thank Dr. Jean-Charles Massabuau for his contributions to this work and guidance from the point of view of biology. I extend this thanks to Dr. Mohamedou Sow for his contributions and help with data and to all, without exception, the members of the WaQMoS project. Likewise, I would like to thank Dr. Alexander L. Fradkov for his contribution to one of the works in this thesis related to multistability.

I would like to thank the external members of my defense committee: Dr. David Angeli, Dr. Antoine Chaillet, Dr. Pierre-Alexandre Bliman, and Dr. Jean-Luc Gouzé. Thank you very much for accepting to review my thesis manuscript and for the valuable comments and corrections.

Finally, I would like to thank the professors from the University of Lille, in particular Dr. Lotfi Belkoura and Dr. Chystophe Fiter, whom I had the opportunity to work with, all the members of the Valse team and other people who have been part of my trajectory during these last three years. To Dr. Jean-Pierre Richard and Dr. Andrey Poliakov and in particular to friends Francisco (Paco), Haik, Tonametl (Tona), Youness, Yue, Tatiana, Siyuan, Alex, Quentin, Artem, Anatolli, and Wenjie.

"When I got here the path was already paved.
I just added another small block paving."

Nelson F. B.

ABSTRACT

This Ph.D. thesis takes part in an interdisciplinary collaborative project (ANR WaQ-MoS) joining marine biology, electronics, and applied mathematics. This project's primary goal is to develop an intelligent autonomous biosensor based on the measurement and interpretation of bivalve mollusks' behavioral responses from environmental stimulus. The principal application is remote coastal water quality surveillance and ecosystem change monitoring in sensitive areas due to pollutions or climate change consequences. The biosensor utilizes a high-frequency non-invasive valvometry technology combined with a data acquisition system. In its turn, the data acquisition block includes a complex, intelligent tool, which aims to convert the behavioral responses of bivalve mollusks into a set of useful information for indirect ecological monitoring. The possibility of such a conversion comes from the fact that these animals are quite sensitive to their environmental changes. Moreover, characteristics of their reactions can be captured from the opening/closing movements of its valves, measured by the sensor. However, understanding, isolating, and connecting the information contained in the distance signals to the environmental or climate entrances form a significant challenge to the biosensor's realization.

Following this problematic, motivated by the climate change subject, in the first part of this thesis, we aim to provide a set of time-scaled populational behavioral variables obtained from the distance signal measured along several years of data acquisition in the Arctic region. These aggregated biologically meaningful variables can be related to bioclimatic ones, such as time-scaled air and water surface temperature or their maximum and minimum variations. For this objective, a sequence of data processing tools was proposed, including an intelligent adaptive filter, based on advanced velocity estimation and the dynamic regressor extension and mixing method (DREM) with fixed-(finite-)time estimation approaches. The obtained behavioral variables, especially the speed-related ones, show promise as potential tools to measure the bivalves' level of stress, which can be converted into a welfare and adaptation measurement for these animals regarding environmental temperature variation.

A complementary route in this thesis is related to the study of the robust stability of multistable systems. The multistability phenomenon arises when it is necessary to globally analyze a system's behavior, taking into account all possible final states and motions. Such a phenomenon is present in many areas, including biological, ecosystems, and climate dynamics: several ecosystems have been shown to possess two or more alternative equilibria. The climate theory also presents the multistable character in its models. Perturbations on these systems influence adaptation capacity, resulting in serious consequences such as a decrease of ecosystem stability with loss

of its biodiversity. Therefore, in the second part of this thesis, based on the framework of input-to-state stability (ISS) and integral input-to-state stability (iISS), we aim to provide robustness conditions for stabilization of affine nonlinear systems with multiple invariant sets. In a first approach, we deal with multistable passive systems and obtain iISS/ISS conditions with respect to exogenous disturbances for open-loop and closed-loop cases, where the speed-gradient control is applied. In a second approach, the problem is faced by extending the control Lyapunov functions and universal formula theory within the multistability framework. In this case, a weak iISS condition is also obtained.

Key-words: Mollusks based biosensor, Living behavior estimation, Climate change, Multistability, (integral) Input-to-state stability, Robust stability and stabilization

RÉSUMÉ

Cette thèse de doctorat s'inscrit dans un projet de collaboration interdisciplinaire (ANR WaQMoS) associant la biologie marine, l'électronique et les mathématiques appliquées. L'objectif principal de ce projet est de développer un biocapteur autonome intelligent, basé sur la mesure et l'interprétation des réponses comportementales des mollusques bivalves aux stimuli environnementaux. L'application principale est la surveillance à distance de la qualité des eaux côtières et le suivi des changements des écosystèmes dans les zones sensibles en raison de pollutions ou des conséquences du changement climatique. Le biocapteur utilise une technologie de valvométrie non invasive à haute fréquence combinée à un système d'acquisition de données. Le bloc d'acquisition de données comprend un outil complexe, qui convertit les réponses comportementales des mollusques bivalves en un ensemble d'informations utiles pour la surveillance écologique indirecte, grâce au fait que ces animaux sont très sensibles aux changements de leur environnement. De plus, les caractéristiques de leurs réactions peuvent être captées à partir des mouvements d'ouverture/fermeture de ses valves, mesurés par le capteur. Cependant, la compréhension, l'isolation et la connexion des informations contenues dans les signaux de distance aux entrées environnementales ou climatiques constituent un défi important pour la réalisation du biocapteur.

Suite à cette problématique, dans la première partie de cette thèse, nous visons à fournir un ensemble de variables comportementales à l'échelle du temps obtenues à partir du signal de distance mesuré au long de plusieurs années dans la région arctique. Ces variables agrégées et biologiquement significatives peuvent être liées à des variables bioclimatiques, telles que la température de surface de l'air et de l'eau à l'échelle temporelle, ou leurs variations maximales et minimales. Pour cela, une série d'outils de traitement des données a été proposée, dont un filtre adaptatif intelligent, basé sur l'estimation avancée de la vitesse et la méthode d'extension et de mélange par régression dynamique (DREM) avec des approches d'estimation à temps (fixe) fini. Les variables comportementales obtenues, en particulier celles liées à la vitesse, sont prometteuses en tant qu'outils potentiels pour mesurer le niveau de stress des bivalves, ce qui peut éventuellement être converti en une mesure du bien-être et de l'adaptation de ces animaux à la variation de la température ambiante.

Un autre volet de cette thèse est lié à l'étude de la stabilité robuste des systèmes multistables. Le phénomène de multistabilité survient lorsqu'il est nécessaire d'analyser globalement le comportement d'un système, en prenant en compte tous les états finaux et mouvements possibles. Plusieurs écosystèmes, dans les domaines de la dynamique biologique, les écosystèmes et le climat possèdent deux ou plusieurs

équilibres alternatifs, présentant un caractère multistable dans leurs modèles. Les perturbations de ces systèmes influencent la capacité d'adaptation, ce qui entraîne de graves conséquences telles qu'une diminution de la stabilité de l'écosystème. Dans la deuxième partie de cette thèse, basée sur le cadre de la stabilité d'entrée à l'état (ISS) et de la stabilité intégrale d'entrée à l'état (iISS), nous visons à fournir des conditions de robustesse pour la stabilisation de systèmes affines non linéaires avec des ensembles invariants. Dans une première approche, nous traitons des systèmes passifs multistables et obtenons des conditions iISS/ISS en ce qui concerne les perturbations exogènes pour les cas en boucle ouverte et fermée, où le contrôle du gradient de vitesse est appliqué. Dans une deuxième approche, le problème est abordé en étendant les fonctions de contrôle de Lyapunov et la théorie de la formule universelle dans le cadre de la multistabilité. Dans ce cas, on obtient également une condition iISS faible.

Mots clés: Biocapteur à base de mollusques, Estimation du comportement vivant, Changement climatique, Multistabilité, (intégrale) Stabilité entrée-état, Stabilité et stabilisation robustes

CONTENTS

LIST OF FIGURES

LIST OF TABLES

CHAPTER

ONE

GENERAL INTRODUCTION

1.1 Background and motivation

In this section, we provide a brief background on climate change from the most general aspect of the climate comportment, through the effects on ecological systems, to the specific problems that we deal with in this thesis on detecting climate change using a mollusk-based biosensor and a complementary route related to the study of robust stability of multistable systems. Despite motivating all the work done and presented here, we do not intend to delve into the climate change theory. Our proposal is more practical and related to applied mathematics and data signal processing. That said, we wish you a great reading.

1.1.1 Climate change

These last decades, the topic of climate change has gained significant attention. Extreme weather events such as temperature records, excess or scarce rainfall regimes, droughts and flooding, wildfires, hurricanes are some of the most common and intuitively perceived examples. However, as climate change gains attention, the causes and consequences of the problem are sometimes misunderstood. It happens because climate change, more than a science, is an interconnection involving scientific underpinning, social dynamics, economy, and political implications. Therefore, the multiplicity of simultaneous priorities and interests also generates misinformation. More knowledge about the complexity of social and biophysical systems to avoid gaps in searching for solutions is required [S. L. Burch, 2014].

Climatic changes have always occurred and are part of the history of our planet. Nevertheless, most worries the scientists in the present-days, on a human time-scale, are the abrupt unnatural variability and how fast and how much climate will change. The Earth is getting warmer and the past century of heating (about 0.85^oC) is mostly is due to human activities on atmospheric greenhouse gas emission [Lindsey, 2009, League et al., 2019]. In the current scenario, there exist accurate information about the physical properties of greenhouse gases, how they absorb and re-emit energy, and how long they persist in the atmosphere. Moreover, employing precise conceptual and numerical models, interacting numerous physical, chemical, and biological processes, it has been pointed out that the increase in the greenhouse effect is

the central control factor going in the same direction as the rising global average temperature observation from thousands of measurement data and fingerprints [Pachauri et al., 2014].

Therefore, anthropogenic agents have had a meaningful influence on the balance of our planet. Many studies point out the threat that human actions exert on all ecosystems and how relatively quickly they occur. With this in mind, several direct and indirect forms have been used to measure the variables that describe our climate and generate mathematical and numerical models explaining its behavior and the consequences of the various disturbances suffered by this complex system [Ghil and Lucarini, 2019]. Temperature measurements in the air and aquatic environments and gas concentration measurements in the atmosphere and chemistry are examples of traditional means used to monitor the climate. They have long-term responses and may not produce enough fast and accurate alerts to generate preventive actions. Therefore, more sensitive, autonomous, and low-cost forms of monitoring are desirable. Moreover, we also need better information about what to expect in specific places such as coastlines and agricultural areas. Climate change action plans, proposals, and campaigns depend on it to elaborate and implement better policies to alter emissions pathways and vulnerability. Moreover, climate change science is a powerful opportunity for improving social, economic, and environmental sustainability [S. L. Burch, 2014].

How climate change manifests worldwide is different, with the polar regions being the areas most sensitive to rising temperatures. The Arctic region faces some of the fastest rates of climate change globally, with dramatic transformations taking place in terrestrial, coastal, and offshore environments that have immediate and long-term consequences for socio-ecological systems [Overland et al., 2019, Hanssen-Bauer et al., 2019]. Significant changes in the type, extent, and thickness of the ice cover, melted water input, and mass dynamics, together with the ocean's warming and acidification, have already started to impact the ecosystem process and the flora fauna that inhabits a series of Arctic habitats [Solan et al., 2020]. The pace of change is such that understanding how arctic systems are structured and functioning is insufficient to inform management for mitigation and adaptation efforts across the region. In this sense, foundational concepts and evidence are needed to support sustainable management and policy, preferably focusing on continually acquiring, interpreting, and applying new interdisciplinary knowledge to enhance understanding [Degen et al., 2018, Biresselioglu et al., 2020].

1.1.2 How climate change could be detected?

The complexity of the ecological system in which the bivalves mollusks live is far from the scope of this Ph.D. thesis. Here we are interested in a more basic, practical, and preliminary issue to provide a data processing procedure to support climate change detection in the Arctic zone. However, it would be interesting to provide some insights into these animals' roles in their ecosystem. First of all, we need to understand that bivalves are filter feeders, and its valve movements are linked with respiratory physiology and ethology functions [Pernet et al., 2012]. These functions are interconnected and depend heavily on the environment where these animals live. [Cranford et al., 2011, Dolbeth et al., 2019].

The bivalves are found in the second trophic level of the food chain, primary consumers feeding on algae and phytoplankton. The ocean is where about 50% of the world's primary

productivity occurs. The sea surface temperature varies regionally due to changes in surface air temperature, currents, and upwelling of deeper water. Therefore, the relationship between climatic conditions and the food webs' productivity and structure have been of interest because of the effects of physical conditions on trophic levels productivity, which seem to allow forecasts. The central concept for understanding the effects of ocean temperature on food webs is based on the idea that consumer production is predominantly controlled indirectly by temperature effects on primary production. According to this model, the increase in primary productivity and net autotrophy also increases energy transport throughout the entire food chain [Field et al., 1998, O'Connor et al., 2009, Thomas et al., 2018].

The development of metabolic theory also indicates that respiration-limited metabolism is more sensitive to changing temperature than photosynthesis-limited metabolism and production, suggesting a more robust consumer-driven control with warming [O'Connor et al., 2009]. The metabolic rate, the rate at which organisms use, transform, and expend energy, is associated with the pace of life, and it is a fundamental trait relevant to all organisms. It is related to an organism's capacity for essential maintenance, growth, and reproduction [Bremner et al., 2006]. All of these characteristics interact with fitness. Intuitively, it is expected that there exists an association between this key trait and fitness. Variation in metabolic rate for organismal performance suggests different hypotheses; one of them states compensation, where the organism reallocates energy towards different biological functions [Padfield et al., 2017]. Another hypothesis states that maximal metabolic rates might improve aerobic performance, thermogenesis, and faster energy consumption and mobility. Variation in metabolic effects of temperature across trophic levels suggests that warming may lead to predictable shifts in food web structure and productivity [Pettersen et al., 2016].

Together with associated changes in physical properties, warming has shifted species composition and altered the timing of seasonal spawning and spring bloom events [Neukermans et al., 2018]. These changes' ramifications can be severe for some species and mild for others, causing a mismatch between interacting species. Some of the relationships between prey and predators are falling out of synchronization (a mistiming phenomenon) with important consequences for trophic interactions, altering food-web structures, and ecosystem modifications [Edwards and Richardson, 2004, Durant et al., 2019]. For a biosensor, these interactions seem sufficient to alerts the impacts of climate change on ecological communities.

1.1.3 The ANR WaQMoS project

Monitoring ocean water quality is a major challenge with various social, economic, and ecological implications. Traditional monitoring systems of water quality in the aquatic environments are relatively expensive and based on the intensive exploitation of human resources for sampling collection, chemical analysis, toxicity measurement [Kröger and Law, 2005, Telfer et al., 2009]. A desirable solution is to develop unmanned systems to work at high frequency by remote control, either as sensors or as early warning detectors to trigger a sampling campaign. A particular difficulty of coastal or ocean water monitoring consists of severe environmental conditions, where existing technological instruments may not provide a reliable solution or only be faulting. At the same time, the maintenance cost due to fouling, for example, is usually high,

and the autonomy time is somewhat limited.

This Ph.D. thesis takes part in an ANR (Agence Nationale de la Recherche) project called WaQMoS - coastal waters quality surveillance using bivalve mollusk-based sensors. The WaQMoS is an interdisciplinary collaborative project formed by two research teams that bring together knowledge in marine biology and electronics (EA team - CNRS UMR 5805 EPOC, Arcachon) and applied mathematics (Valse team, Inria, Lille) to develop an intelligent and autonomous biosensor system for long-term ecological monitoring purpose without *in situ* human intervention for at least one full year. In summary, such a biosensor system comprises the bivalve mollusks as the biological part, transducers to measure the relative valve distance (the gap between the two shells), and a data acquisition system to process these distance signals. In its turn, the data acquisition block includes complex intelligent tools, or intelligent subsystems, which aims to convert the behavioral responses into a set of useful information for indirect ecological monitoring. Such a framework received the name MolluSCAN Eye and can be understood as a panoramic view of the WaQMoS project (to learn more about this framework, see https://molluscan-eye.epoc.u-bordeaux.fr/).

As the project's name indicates, the fundamental principle of the MolluSCAN Eye system is the measurement and interpretation of behavioral responses of bivalve mollusks from the environmental stimulus. The stimuli can be captured using valve activities; or valve opening/closing movements [Millman, 1967, Kramer et al., 1989]. To capture these measurements, a high-frequency non-invasive valvometry technology is used to estimate the open state of a mollusk's shell with high precision. The designed method is strongly based on the respiratory physiology and ethology of the bivalves. This system explores the time and characteristics of the bivalves' opening and closing activities as an index of the mollusks' well-being and a possible way to assess their physiological reaction to the environment [Andrade et al., 2016].

For a long time, there is an interest in using the valve movements as a detection method to study both natural environmental changes and the effect of pollutants, *e.g.*, the effects of temperature, light, tidal movements, salinity, food quantity and quality, and a series of toxicants like chemical and organic traces [Bosheim et al., 2008, Dowd and Somero, 2013, Ahmed et al., 2016b]. Therefore, from the applied mathematical point of view, the MolluSCAN Eye is interpreted as a system with multiple inputs and one output from which many estimates can be derived. Of course, such an approach depends on how much observable the system is, and the first step in identify this characteristic is to correlate the different inputs with the output. As the output, in this case, is a distance signal, the velocity can be estimated as a second state, which creates more possibilities [Ahmed et al., 2015]. More than it, it is necessary to put all the involved variables in a suitable form to aggregate biological meaning. For climate change consequences, the temperature is the main input-driver. Therefore, in this Ph.D. thesis, we propose a procedure to obtain suitable output variables to be correlated, for example, with air and seawater temperature.

Furthermore, as a real system, noises can originate from different sources and can also be generated anywhere in the data acquisition system, from the most fundamental level (at the transducers) to the highest level (at the data processing algorithms). Even with hardware preprocessing, it is common to post-process the signal to finally be ready for analysis. An important

and usual step in this direction is the filtering process, used to suppress unwanted components or characteristics of a signal [Lathi, 2009]. This issue is not exclusive to the MolluSCAN Eye system, nowadays, to protect more effectively the marine environment across the world is an absolute priority. In this direction, a new generation of environmental sensors recently appeared in multiple labs, producing huge amounts of data, and also a significant amount of errors needing to be addressed. In conclusion, the measured signals of valves opening/closing seem to be simple but they are riches in pieces of information. The valve activity can, as we saw in subsection 1.1.2, reflect the effect of internal and external forces which are associated with its biological properties [Tran et al., 2016]. However, understanding, isolating, and connect the information contained in the distance signals to such an entrances are one of the biggest challenge to the MolluSCAN Eye biosensor's realization.

1.1.4 Climate and ecological stability

Due to its complex interactions and interconnections, climate and ecological systems, depending on the level of analysis or simplification, naturally, reach a phenomenon called multistability. Multistability means the coexistence of several stable states, or attractors, for a given set of parameters and/or external forcings. The attractors' can be of different nature, ranging from equilibria via a periodic and quasiperiodic motion to chaotic attractors depending on the parameters' specific values or external forcing [Feudel et al., 2018]. In climate science, for example, the coexistence of multiple attractors and critical transitions between them has become a new focus. An interesting discussion about the melting of Arctic ice is given in Eisenman and Wettlaufer [2009], where it was examined physical processes associated with the transition between ice-covered and ice-free Arctic ocean conditions highlighting which of them is more stable. Another famous example is the more general approach considering an Earth system processing the current warm climate and a global snowball state [Lucarini and Bódai, 2017]. Moreover, as we discussed before, ecological systems are characterized by networks of species organized in different trophic levels where the connection between species is determined, for example, by predator-prey interactions and food competition. Such food chains usually possess a complicated structure generating various equilibrium states concerning different species community compositions with different biodiversity levels. A small perturbation on such a system could be sufficient to cause a shift in biodiversity with a long-term recovery [May, 1977, Al-Habahbeh et al., 2020]. These problems also motivate the second subject addressed in this Ph.D. thesis.

1.1.5 Multistability

In numerous scientific disciplines, ranging from mechanics and electronics [Hayachi, 1964, Efimov et al., 2017] to biology [Laurent and Kellershohn, 1999, Pchelkina and Fradkov, 2012] and neurosciences [Pisarchik and Feudel, 2014], the analysis of stability robustness in the context of multistable dynamics has become more and more important. Systems with multiple invariant sets include bistable dynamics (with at least two stable equilibria) [Yakubovich et al., 2004, Chaves et al., 2008], almost globally stable systems (with only one purely attracting invariant set) [Angeli, 2004], and nonlinear systems with a generic structure of invariant sets [Angeli et al.,

2004, Dudkowski et al., 2016, Enciso and Sontag, 2005, Forni and Sepulchre, 2014, Guckenheimer and Holmes, 1983, Rumyantsev and Oziraner, 1987, Stan and Sepulchre, 2007, Vorotnikov, 1998]. Due to the nontrivial relationships between different regions that compose their state space and the complex intertwined boundaries between them, multistable systems are extremely sensitive to initial conditions and perturbations, making their stability analysis and control design extremely challenging. The evaluation of an equilibrium point's stability or a limit cycle can be performed locally (in the first approximation). However, such a local analysis is less pertinent to investigate robustness since a perturbation may push the system to a domain where a linearized model loses its validity. Therefore, a global analysis is required to study robustness. The multistability phenomenon arises naturally since, for complex nonlinear dynamics, the possible final states and motions can be non-unique.

There are many concepts to study multistability (see the papers above), and in this thesis, we will follow the theory initiated in Efimov [2012], where a global asymptotic stability notion has been proposed, as well as the necessary and sufficient Lyapunov characterizations for such multistable systems, considering all compact invariant solutions of the system (including locally stable and unstable ones). In Angeli and Efimov [2015], it has been highlighted that the most natural way of investigating stability properties in this context is to relax the Lyapunov stability requirement by relatively mild additional assumptions on the possibility of decomposition of invariant sets in order to add a restriction on its decomposability and to ask for attractiveness only. This insight has led to a new research line, which starts from the characterizations of input-to-state stability (ISS) for a class of multistable systems in terms of usual Lyapunov dissipation inequalities, generalizing the classical ISS theory [Sontag and Wang, 1995, 1996].

For the analysis of robustness, the ISS framework is one of the most popular. Its development for multistable systems in terms of usual Lyapunov dissipation inequalities has been obtained in Angeli and Efimov [2015]. Next, other useful stability concepts got their extension for this class of systems: the notion of detectability or output-to-state stability (OSS) was generalized in Forni and Angeli [2016a] and the integral input-to-state stability (iISS) [Sontag, 1998, Liberzon et al., 1999, Angeli et al., 2000] was extended in Forni and Angeli [2017]. Specifically, it introduced a notion of iISS as the conjunction of global attractiveness with zero disturbances (0-GATT) and the uniform bounded-energy bounded-state properties (UBEBS) an equivalent characterization again in terms of Lyapunov/LaSalle-like dissipation inequalities. Further research along the lines of multistable systems addressed the analysis and synthesis of specific problems such as conditions of synchronization [Ahmed et al., 2016a], the stability of nonlinear cascades, and feedback interconnections [Forni and Angeli, 2016b] or periodic systems [Efimov et al., 2017].

Once ISS and iISS characterizations in the multistable sense are available, the problem of designing robust stabilizing control laws in this framework naturally arises. In this setting, such a problem consists of finding state feedback control laws that make the closed-loop system ISS or iISS with respect to a family of finite disjoint compact invariant sets in the presence of external disturbances. A popular way of studying the influence of exogenous inputs and the stability of interconnections is based on the concept of passivity. Compared to the ISS theory, the passivity theory was first studied in control almost 30 years earlier by Popov in the 1960's, and it can be formulated using similar tools [Ebenbauer et al., 2009, Willems, 1972]. The

class of passive dynamics is omnipresent in mechanics, electric circuits, and systems biology [Nijmeijer and van der Schaft, 1990, Ortega et al., 1998, Fradkov, 2007]. Unfortunately, the passivity of systems does not imply its robustness against perturbations directly. It is mainly a kind of nonlinear input-output relation. Consequently, the conditions of ISS and iISS of passive systems with respect to a compact and connected invariant set were treated before in the literature: Arcak and Kokotović [2001] and Efimov [2006], Efimov and Fradkov [2008], where the ISS/iISS stabilizability by output feedback for passive and strictly passive systems was considered. In this thesis, in a first development, we aim to extend such a global robustness analysis for passive systems in a context of multiple invariant sets (compact, globally attracting, but maybe disconnected).

In the classical approach, the most generic conditions of stabilizability are formulated within the Control Lyapunov Function (CLF) theory [Artstein, 1983, Sontag, 1989, Lin and Sontag, 1995, Efimov, 2002a,b]. In Artstein [1983] and Sontag [1989], it was shown that the existence of a CLF is necessary and sufficient for the stabilization of an equilibrium point, and that it leads to an explicit formulation for a stabilizing control law. Similar results were proven in Liberzon et al. [2002] for the ISS (iISS) case resulting in an appropriated universal CLF formulation, which is equivalent to the existence of a feedback rendering the closed-loop system with ISS (iISS) properties. Therefore, in a second development, we are interested in the robust stabilization of multistable affine nonlinear systems in the presence of disturbance inputs. This approach is also based on the theory developed in Angeli and Efimov [2015], Forni and Angeli [2017] and it aims to find conditions of a CLF existence in the context of systems with multiple invariant sets (compact and maybe disconnected) and to show how a control formula from Sontag [1989] based on a CLF can be explicitly developed for a robust stabilization in ISS (iISS) multistable sense.

1.2 General problem statement and goals

Following the presented problematics, this thesis considers two complementary issues.

Quantification of living behavior

The possibility of converting the behavioral responses of bivalve mollusks into useful information for indirect ecological monitoring comes from the fact that these animals are quite sensitive to environmental changes. Moreover, characteristics of their reactions can be captured from the opening/closing movements of its valves, measured by the sensor. However, understanding, isolating and connecting the information contained in the distance signals to the environmental or climate inputs form a significant challenge to the biosensor's realization. Following this problematics, motivated by the climate change subject, in the first part of this thesis, we aim to provide a set of time-scaled populational behavioral variables based on the distance signal measured along several years of data acquisition in the Arctic region. These aggregated biologically meaningful variables can be related to bioclimatic ones, such as time-scaled air and water surface temperature, or their maximum and minimum variations in order to help subsidize future developments, alerts, and actions on climate change consequences.

Control of multistability

The multistability phenomenon is present in many areas, including biological, ecosystems, and climate dynamics: several ecosystems have been shown to possess two or more alternative equilibria, and the climate theory also presents the multistable character in its models. Perturbations on these systems influence the adaptation capacity, resulting in serious consequences such as a decrease of ecosystem stability with loss of its biodiversity. Therefore, in the second part of this thesis, based on the framework of ISS and iISS, we aim to provide robustness conditions for stability and stabilization for two different subclasses of input-affine nonlinear systems with multiple invariant sets: multistable passive systems with exogenous disturbances in the input channel and affine multistable systems with an exogenous disturbance input.

1.3 Outline of the thesis

In this Chapter, we introduced the general subject and the context in which this Ph.D. thesis is inserted, followed by the general problem and the objectives for which solutions are sought based on usual data processing tools and advanced control and estimation techniques. The rest of the thesis is organized into two parts: In chapter 2, a development on the detection of climate change using a mollusk-based biosensor will be presented. The chapter describes the studied site and the data acquisition system, followed by the specific problem statement. Next, to obtain a set of time-scale behavioral variables for detecting climate changes, a sequence of data processing procedures will be presented. An important focus in this direction will be given to the development of an intelligent adaptive filter. Chapter 3 will be dedicated to the study of the robust stability of multistable systems. This chapter presents the multistability framework used, followed by two complementary developments in robust stability and stabilization of two subclasses of affine multistable systems. The problem will be addressed by using passive systems and CLF theories for systems with multiple invariant sets. Finally, the general conclusion and perspectives will be presented in Chapter 4.

1.4 List of publications

1.4.1 Peer-reviewed international journals

Published

1. N. F. Barroso, R. Ushirobira, D. Efimov & A. L. Fradkov (2020) “On robustness against disturbances of passive systems with multiple invariant sets,” International Journal of Control, doi: 10.1080/00207179.2020.1750709.

Submitted

1. Nelson F. Barroso, Rosane Ushirobira, Denis Efimov (2020) “Control Lyapunov Function method for robust stabilization of multistable affine nonlinear systems,” Automatica.

1.4.2 Peer-reviewed international conferences

1. N. De Figueiredo Barroso, R. Ushirobira, D. Efimov and A. L. Fradkov, "On robust stability of multistable passive systems," 2019 18th European Control Conference (ECC), Naples, Italy, 2019, pp. 1683-1688, doi: 10.23919/ECC.2019.8796046.

2. N. F. Barroso, R. Ushirobira and D. Efimov, "Universal formula for robust stabilization of affine nonlinear multistable systems," 2019 IEEE 58th Conference on Decision and Control (CDC), Nice, France, 2019, pp. 8024-8029, doi: 10.1109/$textCDC$40024.2019.9029799.

3. Nelson F. Barroso, R. Ushirobira, D. Efimov, Mohamedou Sow, Jean-Charles Massabuau, "Model-based adaptive filtering of harmonic perturbations applied to high-frequency non-invasive valvometry," 2020 21st IFAC World Congress (IFAC-V 2020).

CHAPTER

TWO

CLIMATE CHANGE DETECTION USING A MOLLUSK-BASED BIOSENSOR

2.1 Introduction

This chapter aims to provide a set of time-scaled populational behavioral variables obtained from the distance signal measured along seven years of data acquisition in the Arctic region. The population monthly base variables are the average distance, the percentage of valve opening/closing, the average velocity, and the movement index. These aggregated biologically meaningful variables can be related to bioclimatic ones, such as time-scaled air and water surface temperature or their maximum and minimum variations. For this objective, a sequence of data processing tools is proposed, including an intelligent adaptive filter, based on advanced velocity estimation and the dynamic regressor extension and mixing method (DREM) with fixed/finite-time estimation approaches. The chapter starts describing the site and the data acquisition system (Section 2.2), followed by the main problem description (Section 2.3). The methodology used for data processing is summarized in the diagram shown in Fig.2.1; each step will be described in the same sequence along Sections 2.4 to 2.6. First, we complete and harmonize

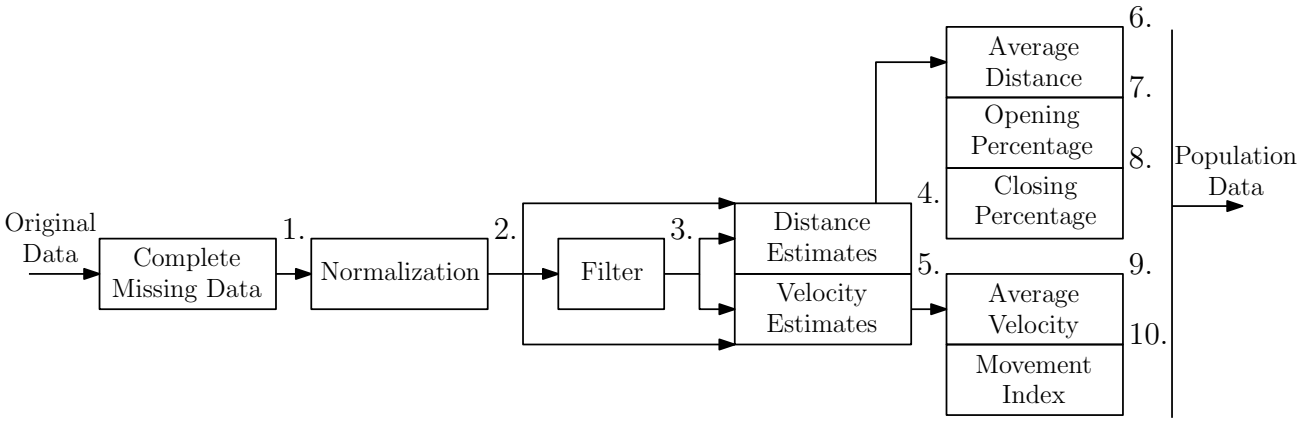

Figure 2.1: Diagram of data processing.

the distance data using a sliding window normalization (steps 1 and 2). Then, motivated by

a practical demand, we propose an intelligent filter to suppress electronic noise and regularize the measured data (step 3). This step is particularly challenging because it deals with a filter problem in which a specific frequency must be suppressed with minor interferences in the rest of the signal spectrum. Therefore, step 3 constitutes one of the most important developments toward our main goal. Next, we estimate the valve opening/closing characteristics and velocity (steps 4 and 5). This estimation is another crucial step since a measure of agitation can give important insights about living beings. Finally, based on the distance and velocity estimates, we obtain the population's behavioral variables (steps 6 to 10). The obtained behavioral variables, especially those related to speed, seem to be promising as potential tools to measure the level of stress of the bivalves, which can be converted into a measure of welfare and adaptation for these animals regarding the environmental temperature variation. Such a result is illustrated in Section 2.7, where the outcomes and discussions are presented. The theoretical tools used in this section will be briefly presented as they are needed to be self-contained.

2.2 The study site and biosensor description

The high-frequency noninvasive (HFNI) valvometer is an essential part of the biosensor monitoring system (MolluSCAN Eye) employed to monitor the valve opening/closing activity of bivalve mollusks [Andrade et al., 2016]. Investigated and implemented at sea since 2006, the HFNI valvometer is a platform for valvometry developed by EA team (Écotoxicologie aquatique) from the University of Bordeaux. Since 2012 such a data acquisition system has been applied to monitor the opening/closing activity of *Chlamys islandica* in Ny-Alesund, Svalbard (Norway, longitude: $11^\circ\ 54'\ 36''$ E, latitude: $78^\circ\ 54'\ 36''$ N).

In a typical field deployment, the system is composed of 16 animals (numbers identify the animals from #1 to #16), each one equipped with two lightweight coils (sensors with approximately $100mg$) fixed on the edge of each valve (Fig.2.2 (a)). One of the coils emits a high-frequency sinusoidal signal, and the second one receives that. The electric field's strength produced between the two coils is proportional to the inverse distance between them, which allows characterizing the relative opening/closing valve activity. The electrodes can estimate the shell's opening status for a mollusk with an accuracy of a few μm. The sensors' lightness allows the online study of bivalve mollusk's natural habitat behavior without significant interference. Usually, the distance measurements are scaled between 0 and 1 for entirely closed and opened, respectively. The measurements are performed every 0.1 seconds successively (with the frequency equal to $\frac{10Hz}{16}$ for each of the sixteen animals). So, the behavior of a particular animal is measured every 1.6 seconds. Every day, 54000 triplets (one animal number, one distance, and one stamped time value) are collected for each animal.

The first level of the data acquisition system is an analog electronic card immersed in the sea close to the animals (Fig.2.2 (b)). This module is protected by a waterproof case and manages the measured signals from the sensors sending them to a second level electronic card held on the sea surface or located on land (Fig.2.2 (c)). This second module, in its turn, is equipped with a GSM/GPRS modem and uses a Linux operating system for driving the first control module immersed in the water, managing the data and meta-data storage, including

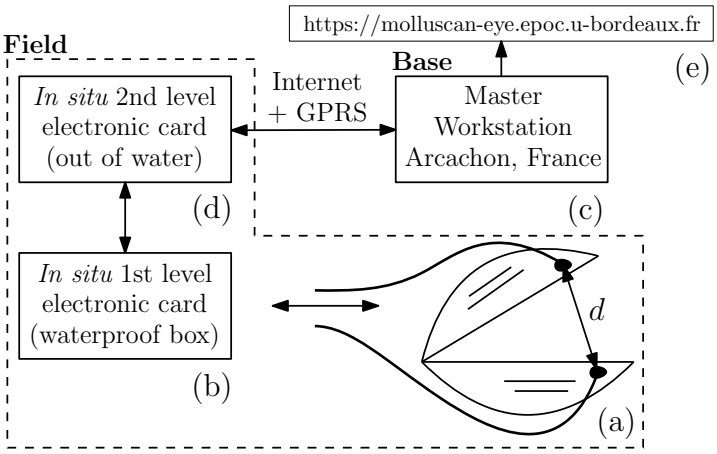

Figure 2.2: Schematic representation of the HFNI valvometer.

timestamp, accessing the internet, and transferring the data to a central workstation server (Master Unit), located in the marine station at Arcachon (France), where the valve-activity data is finally stored in a central database (Fig.2.2 (d)), daily processed, and analyzed. More details about the HFNI valvometer can be found at the "MolluSCAN Eye" website (*https://molluscan-eye.epoc.u-bordeaux.fr*) and in [Andrade et al., 2016].

2.3 Problem statement

The Arctic region was chosen for monitoring because of its sensitivity to climate and environmental variations. However, such an advantage also brings some challenges. For example, due to severe environmental conditions and difficult access to the site and economic issues, the system's autonomy for a long time without human intervention is desirable. In this sense, the first issue for the developments presented in this section concerns constructive aspects to ensure robustness and good quality of measurements, and pre- and post-processing resources need to be employed. In this sense, dealing with problems such as noise, disturbances, and uncertainties is fundamental. A second one is that although all the sensors (electronic part) are built and calibrated under the same conditions, variations may occur over a long period of time. Also, as a biosensor, that is, sensors built from a living being (biological part), each individual has a specific behavior and biological development, so it is necessary to harmonize and regularize the measured signals so that they can be later analyzed under more uniform conditions, *i.e.*, the measurements must be consistent and comparable.

2.4 Missing data and normalization

Since the Arctic has well-defined seasons, it is assumed that the animals' behavior is directly related to each period's characteristics. Thus, it is important to keep the data synchronized with the period in which they were collected. In this way, the first step in data processing was to complete the missing measurements (that happens due to Internet connection losses or failure of electronic cards). With this procedure, it was possible to identify which animals were

missing each year and which days in each month, there was no data acquisition. These results are presented below in Table 2.1 and 2.2, respectively. Such information is important for the last step of data processing, where we are interested in analyzing population behavior. Note that the missing data cannot be completed with approximation due to the gaps' size, causing errors later in interpreting the results.

Table 2.1: Total of animals per year.

Year	Missing Animal	Total of animals
2012	A1	15
2013	A1, A11	14
2014	A1, A6, A11	13
2015	A1, A6, A11	13
2016	A6, A12	14
2017	A1, A2, A6, A12, A16	11
2018	A1, A2, A6, A12, A16	11

Table 2.2: Amount of days with data in each month per year.

Year	Jan.	Feb.	Mar.	Aprl.	May	Jun.	Jul.	Ago.	Sept.	Oct.	Nov.	Dec.
2012	0	0	0	0	12	30	31	30	30	31	30	31
2013	31	28	31	7	0	29	31	31	29	31	30	31
2014	29	28	31	30	31	27	30	31	28	26	17	31
2015	31	26	31	20	0	18	31	7	0	24	30	31
2016	0	0	0	0	31	30	30	31	30	31	28	27
2017	19	28	31	30	31	29	30	30	29	26	29	29
2018	0	28	28	30	30	30	30	31	29	31	0	0

Once the data were completed, the second action was to normalize them using a Min-Max feature scaling. This is important because the animals have small size variations and grow along the years at different rates. To deal with this issue, a moving average normalization is done over a six days window as follows:

$$y_{i,j} = \frac{Y_{i,j} - \min_k(Y_{k,j})}{\max_k(Y_{k,j}) - \min_k(Y_{k,j})} \tag{2.1}$$

where $k = i - N, \cdots, i$. N is the total number of data points in the last 6 days, $Y_{i,j}$ is the original distance, and $y_{i,j}$ is the normalized valve distance for $1 \leq i \leq n$, where n is the amount of data in each year, and $1 \leq j \leq N$, where N is the number of animals in each year. The data is normalized between 0 and 1, where 0 represents the fully closed valve, and 1 represents the fully opened valve. With this procedure, we have reached the first step towards data harmonization. The second step towards this objective, as well as to deal with noise and interferences, is given in the next section.

2.5 Model-based adaptive filter

In this section, we are interested in filtering a harmonic noise in the data of valve opening/closing activity signals of scallops *Chlamys islandica* acquired in 2017 and 2018 by using the HFNI valvometer. A sampling window of such a signal is shown in Fig.2.3(a). It is the normalized distance measured from Animal #4 from 2017. The time axis is in hours base counted from the first day of 2017. The window refers to the data collected from day 314 at $19h33min$ to day 316 at $16h05min$. It was observed that the main behavior of the signal was marked by the presence of almost periodic events (highlighted in the red boxes) occurring with a period of around 4.4 hours. We attribute these events to a malfunction of the equipment since it also appears in measurement channels where the animal is not alive. As we do not know exactly the source of these interferences, we will generally call them electrical noise from here.

The first seven hours of this data window are shown in Fig.2.3(b). It is possible to see how the electrical noise stands out concerning the typical behavior of the valvometry signal. In Fig.2.3(c), an example of these events is shown in a zoomed way. It appears as a periodic oscillation lasting approximately 0.3 hours with a relatively well-defined shape, typical of an electronic noise without biological meaning. Similar samples, with the same characteristics (but with bigger or smallest amplitude), also were detected in the signals measured from other individuals as shown in Fig.2.3(d) to Fig.2.3(f) for Animal 15 from 2017, and 9 and 14 from 2018, respectively.

Our goal is to suppress such a harmonic noise from the measured signal at the server level by applying a post-processing algorithm. Such an algorithm is a model-based adaptive filter that considers the harmonic noise as a fault. First, a simple model is proposed for the system, which is the Fourier series's first term. Next, a dynamic regressor extension and mixing (DREM) method is proposed to allow a decoupled estimation of its parameters. Once the desired regression form of the output model is obtained, a fixed-time estimation approach is used to identify the parameters. By applying these two techniques, a flexible filter structure is obtained to filter the original signal, retaining the major relevant components of interest of the original valve-activity signals.

Notation

- Let $\mathbb{R}_+ = \{x \in \mathbb{R} : x \geq 0\}$ and $\mathbb{N}_+ = \{x \in \mathbb{N} : x > 0\}$. Denote by $|x|$ the absolute value for $x \in \mathbb{R}$ or a vector norm for $x \in \mathbb{R}^n$.

- For a Lebesgue measurable and essentially bounded function $x : \mathbb{R} \to \mathbb{R}^n$ denote $||x||_\infty = \operatorname{ess\,sup}_{t\in\mathbb{R}} |x(t)|$ and define by $\mathcal{L}_\infty(\mathbb{R},\mathbb{R}^n)$ the set of all such functions with finite norms $||\cdot||_\infty$.

- A continuous function $\alpha : \mathbb{R}_+ \to \mathbb{R}_+$ belongs to the class $\mathcal{K}$ if $\alpha(0) = 0$ and the function is strictly increasing; α belongs to the class $\mathcal{K}_\infty$ if it belongs to class $\mathcal{K}$ and $\alpha(s) \to \infty$ as $s \to \infty$. A function $\beta : \mathbb{R}_+ \times \mathbb{R}_+ \to \mathbb{R}_+$ belongs to the class $\mathcal{KL}$ if $\beta(\cdot,t) \in \mathcal{K}$ for each fixed $t \in \mathbb{R}_+$, $\beta(s,\cdot)$ is a decreasing function and $\lim_{t\to\infty} \beta(s,t) = 0$ for each fixed $s \in \mathbb{R}_+$.

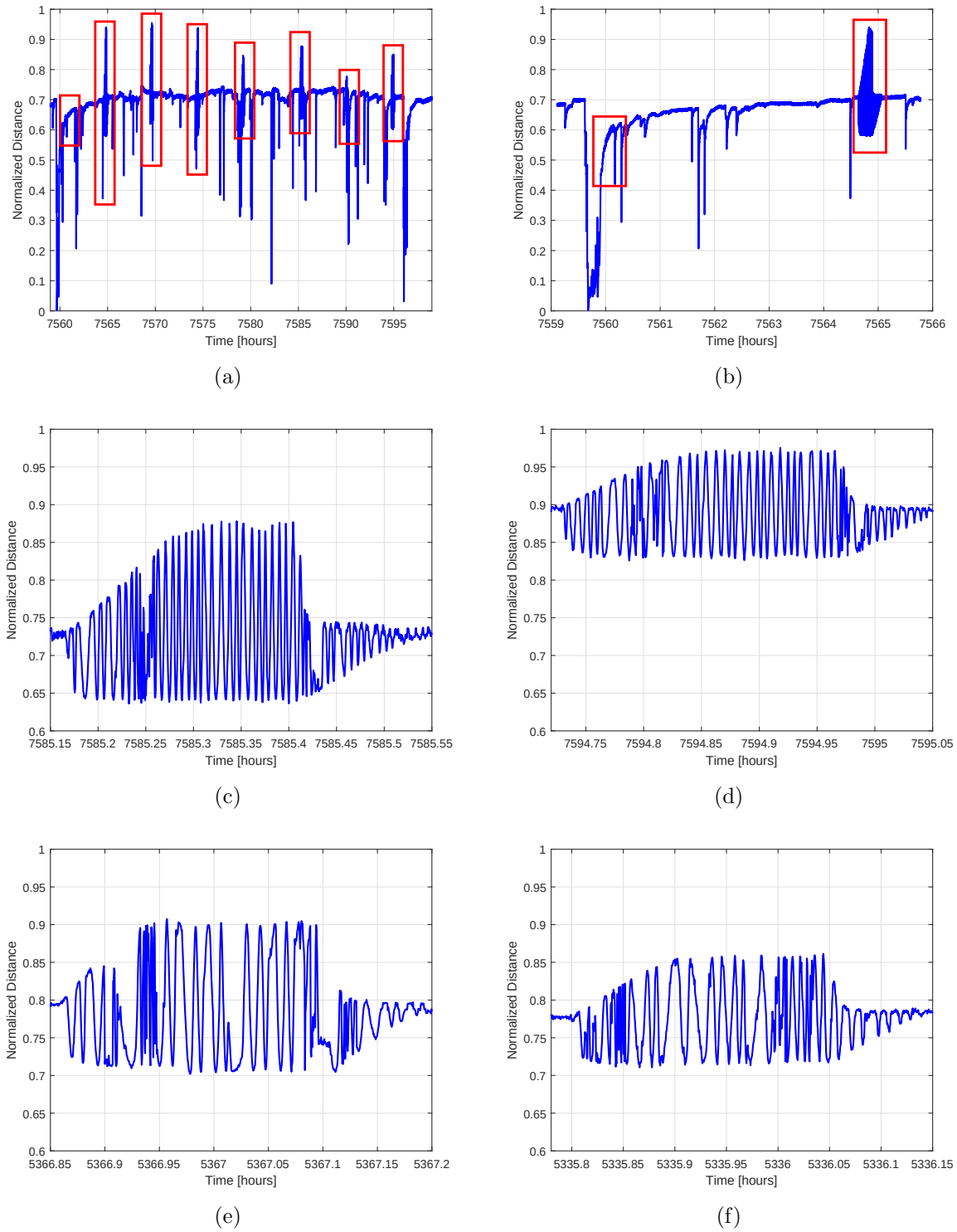

Figure 2.3: (a) A sampling window of the distance signal measured from animal #4 from 2017 (b) First seven hours of the sampling window of the signal in (a) (c) Electronic noise shape in the distance signal measured from animal #4 in 2017 (d) Electronic noise shape in the distance signal measured from animal #15 in 2017 (e) from animal #9 in 2018 (f) from animal #14 in 2018.

It belongs to the class $\mathcal{GKL}$ if $\beta(s,0) \in \mathcal{K}$, $\beta(s,\cdot)$ is a decreasing function and for each $s \in \mathbb{R}_+$, there is $T_f \in \mathbb{R}_+$ such that $\beta(s,t) = 0$ for all $t \geq T_f$.

- Define the Lambert function $\mathbf{W} : \mathbb{R} \to \mathbb{R}$ as the branches of the inverse relation of the function $f(z) = z\mathbf{e}^z$ for $z \in \mathbb{R}$, where $\mathbf{e} = \exp(1)$.
- Denote $\lceil s \rfloor^\nu = |s|^\nu \text{sign}(s)$ for any $s \in \mathbb{R}$ and $\nu \in \mathbb{R}_+$.

2.5.1 Dynamic regressor extension and mixing method

Consider the linear estimation problem:

$$x(t) = \omega^T(t)\theta, \tag{2.2}$$
$$y(t) = x(t) + w(t),\ t \in \mathbb{R}, \tag{2.3}$$

where $x(t) \in \mathbb{R}$ is the model output, $\theta \in \mathbb{R}^n$ is the vector of unknown constant parameters that must be estimated, $\omega : \mathbb{R} \to \mathbb{R}^n$ is the regressor function (usually assumed to be bounded and known), $y : \mathbb{R}_+ \to \mathbb{R}$ is the signal available for measurements (in particular the normalized distance signal), and $w : \mathbb{R} \to \mathbb{R}$ is the measurement noise.

Assumption 2.1. *[Wang et al., 2019] Assume $\omega \in \mathcal{L}_\infty(\mathbb{R},\mathbb{R}^n)$ and $w \in \mathcal{L}_\infty(\mathbb{R},\mathbb{R})$.*

The dynamic regressor extension and mixing (DREM) procedure [Aranovskiy et al., 2017] transforms (2.3) into n new one-dimensional regression models allowing the decoupled estimation of the parameters θ_i with $i = 1,\ldots,n$. For that, $n-1$ linear operators $H_j : \mathcal{L}_\infty(\mathbb{R},\mathbb{R}) \to \mathcal{L}_\infty(\mathbb{R},\mathbb{R})$ for $j = 1,\ldots,n-1$ are introduced, for example, stable linear time-invariant operators selected to filter the noise w or also delay operators. The application of different linear transformations generates various versions of the original signal $y \in \mathcal{L}_\infty(\mathbb{R},\mathbb{R})$. By means of the superposition principle we obtain:

$$\tilde{y}_j(t) = H_j(y(t)) = \tilde{\omega}_j^T\theta + \tilde{w}_j(t),\ j = 1,\ldots,n-1,\ t \in \mathbb{R}_+$$

where $\tilde{y}_j : \mathbb{R} \to \mathbb{R}$ is the j^{th} linear operator output, $\tilde{\omega}_j : \mathbb{R} \to \mathbb{R}^n$ is the j^{th} filtered regression function, and $\tilde{w}_i : \mathbb{R} \to \mathbb{R}$ is the j^{th} noise signal composed by the transformation of w by H_j and other exponentially converging components due to the initial conditions. Hence, a new vector of variables

$$\tilde{Y}(t) = [y(t)\ \tilde{y}_1(t)\ \ldots\ \tilde{y}_{n-1}(t)] \in \mathbb{R}^n,$$
$$\tilde{W}(t) = [w(t)\ \tilde{w}_1(t)\ \ldots\ \tilde{w}_{n-1}(t)] \in \mathbb{R}^n,$$

and a time-varying matrix

$$M(t) = [\omega(t)\ \tilde{\omega}_1(t) \ldots \tilde{\omega}_{n-1}]^T \in \mathbb{R}^{n\times n},$$

are constructed to obtain the extended regressor system

$$\tilde{Y}(t) = M(t)\theta + \tilde{W}(t),\ t \in \mathbb{R}. \tag{2.4}$$

It is known that for any matrix $M(t) \in \mathbb{R}^{n\times n}$, the following equality holds

$$\text{adj}(M(t))M(t) = \det(M(t))I_n,$$

where I_n denotes the identity matrix and adj is the adjoint matrix. By multiplying both sides of (2.4) by adj$(M(t))$ and defining $Y(t) = \text{adj}(M(t))\tilde{Y}(t)$, $W(t) = \text{adj}(M(t))\tilde{W}(t)$, and $\phi(t) = \det(M(t))$, we finally obtain n scalar regressor models of the form

$$Y_i(t) = \phi(t)\theta_i + W_i(t),\ i = 1,\ldots,n. \tag{2.5}$$

By construction, $Y \in \mathcal{L}_\infty(\mathbb{R},\mathbb{R}^n)$, $W \in \mathcal{L}_\infty(\mathbb{R},\mathbb{R}^n)$ and $\phi \in \mathcal{L}_\infty(\mathbb{R},\mathbb{R})$. For the decoupled system (2.5), different estimation algorithms can be applied.

2.5.2 Fixed/Finite-time stability notions

Consider a time-dependent differential equation

$$\dot{x}(t) = f(t,x(t),d(t)),\ \ t \geq t_0,\ \ t_0 \in \mathbb{R}_+ \tag{2.6}$$

where $x(t) \in \mathbb{R}^n$ is the state vector, $d(t) \in \mathbb{R}^m$ is the vector of external inputs, $d \in \mathcal{L}_\infty(\mathbb{R},\mathbb{R}^m)$, $f : \mathbb{R}^{n+m+1} \to \mathbb{R}^n$ is a continuous function with respect to x and d, piecewise continuous with respect to t, and $f(t,0,0) = 0$ for all $t \in \mathbb{R}_+$. Denote by $x(t,t_0,x_0,d)$ a solution of this system, where $x(t_0) = x_0 \in \mathbb{R}^n$ is the initial condition at the initial time $t_0 \in \mathbb{R}_+$. Assume that $x(t,t_0,x_0,d)$ is defined and unique in forward time at least on some finite interval $[t_0,t_0 + T)$, where $T > 0$ may be dependent on x_0, d, and $t_0 \in T^0 = [\underline{T}^0, \bar{T}^0]$, where $\underline{T}^0 > 0$, $\bar{T}^0 = 2\underline{T}^0$.

Definition 2.1. *[Wang et al., 2019] The system (2.6) is said to be*

(a) short-finite-time ISS *with respect to* $(\Omega, \bar{T}^0, T_f, D)$ *if there exist* $\beta \in \mathcal{GKL}$ *and* $\gamma \in \mathcal{K}$ *such that for all* $x_0 \in \Omega \subset \mathbb{R}^n$*, all* $d \in \mathcal{L}_\infty(\mathbb{R},\mathbb{R}^m)$ *with* $||d||_\infty < D$ *and* $t_0 \in T^0$*:*

$$|x(t,t_0,x_0,d)| \leq \beta(|x_0|,t - t_0) + \gamma(||d||_\infty),$$

for all $t \in [t_0,t_0 + T_f]$*, and* $\beta(|x_0|,T_f) = 0$*.*

(b) globally short-finite-time ISS *for* $\bar{T}^0 > 0$ *if there exist* $\beta \in \mathcal{GKL}$ *and* $\gamma \in \mathcal{K}$ *such that for any bounded set* $\Omega \subset \mathbb{R}^n$ *containing the origin there is* $T_f > 0$ *such that for all* $x_0 \in \Omega$ *all* $d \in \mathcal{L}_\infty(\mathbb{R},\mathbb{R}^m)$ *and* $t_0 \in T^0$*:*

$$|x(t,t_0,x_0,d)| \leq \beta(|x_0|,t - t_0) + \gamma(||d||_\infty),$$

for all $t \in [t_0,t_0 + T_f]$*, and* $\beta(|x_0|,T_f) = 0$ *(the system is short-finite-time ISS with respect to* $(\Omega, T^0, T_f, +\infty)$*).*

(c) short-fixed-time ISS *for* $\bar{T}^0 > 0$ *and* $T_f > 0$*, if there exist* $\beta \in \mathcal{GKL}$ *and* $\gamma \in \mathcal{K}$ *such that for all* $x_0 \in \mathbb{R}^n$*, for all* $d \in \mathcal{L}_\infty(\mathbb{R},\mathbb{R}^m)$ *and* $t_0 \in T^0$*:*

$$|x(t,t_0,x_0,d)| \leq \beta(|x_0|,t - t_0) + \gamma(||d||_\infty),$$

for all $t \in [t_0,t_0 + T_f]$*, and* $\beta(|x_0|,T_f) = 0$*.*

For $d \equiv 0$*, the short-finite(fixed)-time stability notions are obtained. Moreover, if (2.6) is short-fixed-time stable, then it is also globally short-fixed-time stable.*

2.5.3 Fixed/Finite-time parameter estimation

We recover the linear regression model (2.2), (2.3) under Assumption 2.1, and assume that the DREM method has been applied to reduce the initial vector estimation problem to n one-dimensional regressor models. Since the problem is decoupled on n independent ones, to simplify the notation, we will omit the index i by assuming $n = 1$:

$$Y(t) = \phi(t)\theta + W(t), \tag{2.7}$$

where $\theta \in \mathbb{R}$, $Y \in \mathcal{L}_\infty(\mathbb{R},\mathbb{R})$, and $W \in \mathcal{L}_\infty(\mathbb{R},\mathbb{R})$. Two adaptive estimation algorithms generating an estimate $\hat{\theta}(t) \in \mathbb{R}^n$ of the unknown parameters $\theta \in \mathbb{R}^n$ have been proposed in [Ríos et al., 2017, 2018] and [Wang et al., 2019]. Such algorithms, according with the following propositions, provide the short-fixed-time stability of the estimation error $e(t) = \theta - \hat{\theta}(t)$ dynamics given some $\bar{T}^0$ and T_f when $||W||_\infty = 0$, and short-fixed-time ISS property when $||W||_\infty \neq 0$.

Algorithm 1 **[Ríos et al., 2017, 2018]:**

$$\dot{\hat{\theta}}(t) = \phi(t)\left\{\gamma_1 \left\lceil Y(t) - \phi(t)\hat{\theta}(t)\right\rfloor^{1-\alpha} + \gamma_2 \left\lceil Y(t) - \phi(t)\hat{\theta}(t)\right\rfloor^{1+\alpha}\right\}, \tag{2.8}$$

for $\gamma_1 > 0$, $\gamma_2 > 0$, and $\alpha \in [0,1)$, with $\hat{\theta}(t_0) \in \mathbb{R}$.

Proposition 2.1. *[Ríos et al., 2017, 2018] Let Assumption 2.1 be satisfied, and for a given $\bar{T}^0 > 0$, and $T_f > 0$,*

$$\int_t^{t+\ell} \min\left\{|\phi(s)|^{2-\alpha},|\phi(s)|^{2+\alpha}\right\} ds \geq \upsilon > 0 \tag{2.9}$$

for all $t \in [\underline{T}^0,\bar{T}^0 + T_f]$ and some $\ell \in \left(0,\frac{T_f}{2}\right)$. Take

$$\min\{\gamma_1,\gamma_2\} > \frac{2^{2+\frac{\alpha}{2}}}{\alpha\upsilon\left(\frac{T_f}{2\ell} - 1\right)}.$$

Then the estimation error $e(t) = \theta - \hat{\theta}(t)$ dynamics of (2.8):

$$\dot{e}(t) = -\phi(t)\{\gamma_1\lceil\phi(t)e(t) + W(t)\rfloor^{1-\alpha} + \gamma_2\lceil\phi(t)e(t) + W(t)\rfloor^{1+\alpha}\},$$

is short-fixed-time ISS *for $\bar{T}^0$ and T_f.*

Algorithm 2 **[Wang et al., 2019]:**

$$\dot{\hat{\theta}}(t) = \text{sign}(\phi(t))\left\{\gamma_1 \left\lceil Y(t) - \phi(t)\hat{\theta}(t)\right\rfloor^{\alpha(t)} + \gamma_2 \left\lceil Y(t) - \phi(t)\hat{\theta}(t)\right\rfloor^{\zeta+\alpha(t)}\right\}, \tag{2.10}$$

for $\gamma_1 > 0$, $\gamma_2 > 0$, $\zeta > 1$, and $\alpha(t) = \frac{|\phi(t)|}{1+|\phi(t)|}$. In this version, the power α is approaching zero together with the regressor ϕ, the contribution of the regressor in the adaptation rate is proportional to $|\phi(t)|^{\alpha(t)}$, $\forall t \in \mathbb{R}$.

Proposition 2.2. *[Wang et al., 2019] Let Assumption 2.1 be satisfied, $\vartheta \in \mathcal{L}_\infty(\mathbb{R},\mathbb{R}^n)$, where $\vartheta(t) = \frac{W(t)}{\phi(t)}$, and for a given $\bar{T}^0 > 0$, and $T_f > 0$,*

$$\int_t^{t+\ell} |\phi(s)|^\zeta ds \geq \upsilon > 0 \tag{2.11}$$

for all $t \in [\underline{T}^0,\bar{T}^0 + T_f]$ and some $\ell \in (0,T_f)$, and

$$\min\{\gamma_1,\gamma_2\} > \sqrt{2}\frac{1 + \phi_{\max} + \frac{4\ell}{(\zeta-1)\upsilon}}{(T_f - \ell)g(x_{\min})}$$

where $\phi_{\max} = \max_{t\in[\underline{T}^0,\bar{T}^0+T_f]} |\phi(t)|$, $g(x) = x^{\frac{x}{1+x}}$ and $x_{\min} = \mathbf{W}(\mathbf{e^{-1}})$, then the estimation error $e(t) = \theta - \hat{\theta}(t)$ dynamics of (2.10),

$$\dot{e}(t) = -sign(\phi(t))\{\gamma_1\lceil\phi(t)e(t) + W(t)\rfloor^{\alpha(t)} + \gamma_2\lceil\phi(t)e(t) + W(t)\rfloor^{\zeta+\alpha(t)}\},$$

is short-fixed-time ISS *for $\bar{T}^0$ and T_f with the input ϑ.*

Note that the condition (2.11) can be skipped for the algorithm (2.10), then the short-finite-time ISS property can be obtained, *i.e*, the convergence time becomes not uniform in the initial conditions. The performance of Algorithms (2.8) and (2.10) are similar. Preliminary investigations demonstrated that a technical difference between them is that (2.10) has more sensitivity to measurement noise, and conversely, (2.8) has a lower mean error and less error oscillation. Therefore, for the next development, we consider (2.8) only.

The quantity $\vartheta(t)$ is the relation between the measurement noise and the regressor vector (it is a signal-noise relation). The requirement that the signal $W(t)/\phi(t)$ is well-defined assumes that the ratio between the useful signal and the noise lies within reasonable limits. Moreover, note that despite the conclusion of Proposition 2.2 concerning ϑ, the robustness result (short-fixed-times ISS) implicitly concerns W, the measurement noise (see the proof in [Wang et al., 2019]). In particular, for the practical problem faced here it is also reasonable, by visual inspection of the typical distance signal, to assume that the well-defined condition for $W(t)/\phi(t)$ holds.

2.5.4 Filter model structure

In our specific problem, a model for the original signal can be chosen as:

$$y(t) = d(t) + f(t) + w(t), \quad \forall t \in \mathbb{R}, \tag{2.12}$$

where d is the filtered signal, f is the fault signal (the harmonic noise) and w is the measurement noise. Since the fault resembles a sinusoidal signal, we can aproximate it by the function

$$f(t) = a(t)\sin(\omega_0 t + \varphi), \quad \forall t \in \mathbb{R} \tag{2.13}$$

where a is the amplitude, ω_0 is the nominal frequency, and φ is the phase shift. Hence, choosing for brevity $a(t) = a_0 = const$ and $d(t) = d_0 = const$ (for a short time window of estimation) we obtain the nominal model with the following equation:

$$y(t) = d_0 + a_0(t)\sin(\omega_0 t + \varphi) + w(t), \quad \forall t \in \mathbb{R}. \tag{2.14}$$

Such a model is the first term of a Fourier series plus a noise term. Other frequency components could be added to this model. However, increasing the model's structure also means increasing the number of parameters to be estimated. Therefore, it should be assessed whether the new component added significantly influences the filtered signal.

The nominal model (2.14) can be rewritten as follows:

$$y(t) = d_0 + a_0 \cos(\varphi) \sin(\omega_0 t) + a_0 \sin(\varphi) \cos(\omega_0 t) + w(t), \quad \forall t \in \mathbb{R}. \tag{2.15}$$

Hence, by assuming $\theta_1 = a_0 \cos(\varphi)$, $\theta_2 = a_0 \sin(\varphi)$, and $\theta_3 = d_0$, we can rewrite the filter problem as a linear regression problem in (2.3):

$$y(t) = \omega(t)^T \theta + w(t), \ \omega(t) = \begin{bmatrix} \sin(\omega_0 t) \\ \cos(\omega_0 t) \\ 1 \end{bmatrix}. \tag{2.16}$$

In this case, the filtered signal results from the estimates of θ_3, *i*.e., a time-dependent parameter which varies relatively slowly in time. In such a model, the parameters θ_1 and θ_2 are proportional to the oscillation amplitude a_0 and varies much faster. As we can see, we need to estimate $n = 3$ parameters under these constraints on θ, so they have to be retained in the adaptation algorithm. Therefore, we need an estimation approach that allows such a decomposition and control on the velocity of adjustment, and DREM is an example of this kind of method.

In other words, the proposed approach takes place in two separate steps. First, to decompose the nominal model so that its parameters are estimated independently. The second step is to adaptively estimate these parameters during a small fixed window of time. We assume that these parameters are slowly varying at this stage, and in the time window of estimation, they stay constant. That is, they can suddenly change the values when the fault appears, being constant meanwhile.

To estimate the nominal frequency, we calculate the average frequency of electrical noise. To do this, we isolate different samples from the noise data, similar to the sampling window shown in Fig.2.3 (c)-(f), from different animals in 2017 and 2018 and calculate the average of their Fast Fourier Transformation (FFT). Fig.2.4 shows the result of this procedure. Observe that the noise's main frequency component is about $0.0396Hz$ or $0.2491rad/s$, and it is this specific frequency that we want to suppress. The averaged FFT of different samples of data is also indicated in the figure.

To apply the DREM method, we choose $n-1$ linear operators $H_j : \mathcal{L}_\infty(\mathbb{R},\mathbb{R}) \to \mathcal{L}_\infty(\mathbb{R},\mathbb{R})$. The first one is a stable linear time-invariant first order filter with transfer function $G_1(s) = \frac{\lambda}{s+\lambda}$, where $s \in \mathbb{C}$ is a complex variable and $\lambda > 0$ is selected to filter the noise w in (2.16). The second one is a delay operator with transfer function $G_2(s) = e^{-\tau s}$, for $\tau > 0$. The choice of λ and τ will be detailed in the next subsection. Finally, once different versions of y and ω are generated, we are able to rewrite the model (2.16) in the form (2.5):

$$Y_i(t) = \phi(t)\theta_i + W_i, \ i = 1, \ldots, 3. \tag{2.17}$$

and apply the algorithm (2.8) or (2.10) to dissociate the desired filtered signal given by the parameter θ_3. To apply the algorithm (2.8), for example, we have to tune the parameters γ_1, γ_2 and α_1 to estimate θ_1; γ_3, γ_4 and α_2 to estimate θ_2; and γ_5, γ_6, and α_3 to estimate θ_3. For (2.10) there is no α_i, but the parameters ζ_i appear for $i = 1, 2, 3$.

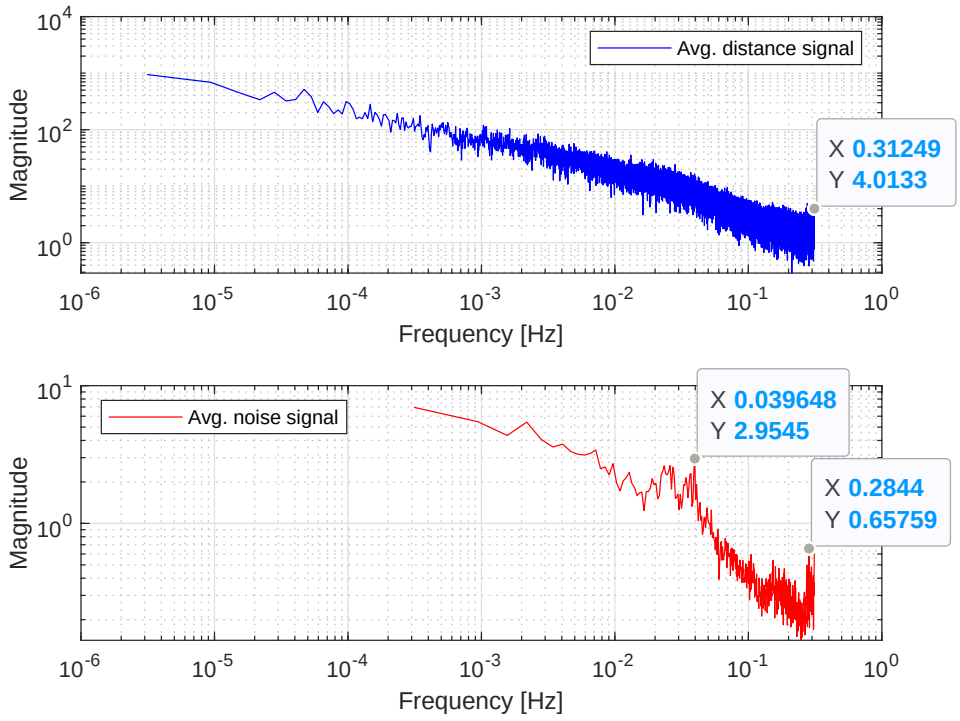

Figure 2.4: The distance signal frequency spectrum (up) and the electronic noise frequency spectrum (down).

2.5.5 Filter parameter tuning

The procedure used to tune the model-based filter parameters is described as follow:

(1) **Choose the cutoff frequency λ of the first-order low-pass filter and the time constant τ of the delay operator:** these parameters must be defined in such a way that the original signal is modified to generate two sufficiently different versions of y and ω such that M in (2.4) is not singular, and ϕ is well-conditioned (condition equivalent to the persistence of excitation). Note that the highest frequency of the distance signal y is approximately $0.31249Hz$, as indicated above in Fig.2.4. However, it is known that the highest frequencies in this signal are due to measurement noise. Therefore, one can choose the frequency of the first-order filter around $0.2844Hz$. In particular, it was chosen $\lambda = 2.9939Hz$, that is, about ten times above the specific frequency we want to suppress. The delay is chosen as a decimation of the sampling time $T_s = 1.6s$, it means that $\tau = T_s\delta$ where $\delta > 1$. In our case, $\delta = 8$ was chosen empirically.

(2) **Using a reference signal without disturbance define the nominal frequency ω_0:** to calculate the parameters θ_i ($i = 1,2,3$) of the decoupled system (2.17), we need to find γ's, α's (ζ's) of the algorithms (2.8) or (2.10). This choice depends on the nominal frequency ω_0, which must be defined for two different cases, *i.e.*, for tuning the algorithms and filtering the electronic noise. For the latter, $\omega_0 = 0.039648Hz$, the cut-off frequency. For the former, as we are interested in obtaining a clean signal ($\hat{y} = \theta_3$), a signal without

electronic noise must be chosen as reference (In particular, we used a signal measured from animal #5 in 2012). This is convenient because, in the first moment, we must prioritize the estimation of θ_3. The nominal frequency ω_0 must be the highest frequency of the reference signal (no filtering is performed at this stage). In particular, we choose $\omega_0 = \lambda = 0.29939Hz$.

(3) **Use an optimization method to calculate the estimator parameters γ's, α's (ζ's):** having defined $\omega_0 = \lambda$, the parameters of the algorithms (2.8) or (2.10) are calculated to minimize the difference between the reference signal y and the estimated signal $\hat{y} = \theta_3$. The minimization method used was a simple interior-point method which minimizes a squared error function $e(t) = (y(t) - \hat{y}(t))^2$, however, to validate the fitting we used the normalized root means square error (NRMSE):

$$\text{NRMSE} = 100 \times \left(1 - \frac{\sqrt{\sum_{k=1}^{n}(y(k) - \hat{y}(k))^2}}{\sqrt{\sum_{k=1}^{n}(y(k) - \bar{y}(k))^2}}\right)$$

where $\bar{y}$ is the average calculated in the window of data, which $\bar{y}$ is taken as a reference to compare the fittings, n is the window size, and k is the available sample. The closer is NRMSE to 100%, the better the estimation fits the measured data.

(4) **Set the nominal frequency ω_0 as the frequency of the electronic noise we want to suppress.**

The results of the four above steps are indicated in Fig.2.5. Fig.2.5(a) and 2.5(b) demonstrate, respectively, the signal used for tuning (in blue) and the estimated signal (in red), and the frequency spectrum for these two signal (the window refers to the data collected of animal #5 from the day 185 at $4h48min$ to $10h05min$ in 2012). The NRMSE index, in this case, is about 94.18%, which means that the estimated signal (estimated by the algorithm (2.8)) is quite close to the original one. To validate this result, a distance signal (with noise) referring to animal #4 collected in 2017 was used. The result of applying the algorithm (2.8) is shown in Fig.2.5(c) and 2.5(d) (the window refers to the data collected from the day 315 at $16h48min$ to $21h00min$). In this case, the NRMSE index is about 92.75%, meaning that the algorithm maintains its quality for a signal different from that used in the tuning process.

Finally, Fig.2.5(e) and 2.5(f) show the model-based filter response, *i.e.*, when $\omega_0 = 0.039648$, the main frequency component of the electrical noise. Note that, in this case, the specific frequency, as well as the high-frequency components correspondent to the measured noise is suppressed while the low-frequency components and the "medium-frequency" components remain. Also, note that on this "medium-frequency" band occurs a small amplitude attenuation, however, the frequency characteristics are kept. Another interesting point is that an attenuation occurs around $0.1189Hz$ which seems to be a harmonic of the removed main frequency by a factor of 3. The parameters obtained for the gains and exponents of the algorithm (2.8) are: $\gamma_1 = 687.7118$, $\gamma_2 = 687.7118$, $\alpha_1 = 0.4949$ estimating θ_1; $\gamma_3 = 687.7118$, $\gamma_4 = 687.7118$, $\alpha_2 = 0.4949$ estimating θ_2, and $\gamma_5 = 1799.9907$, $\gamma_6 = 1799.9907$, $\alpha_3 = 0.0572$ estimating θ_3. The same procedure can be done for the algorithm (2.10).

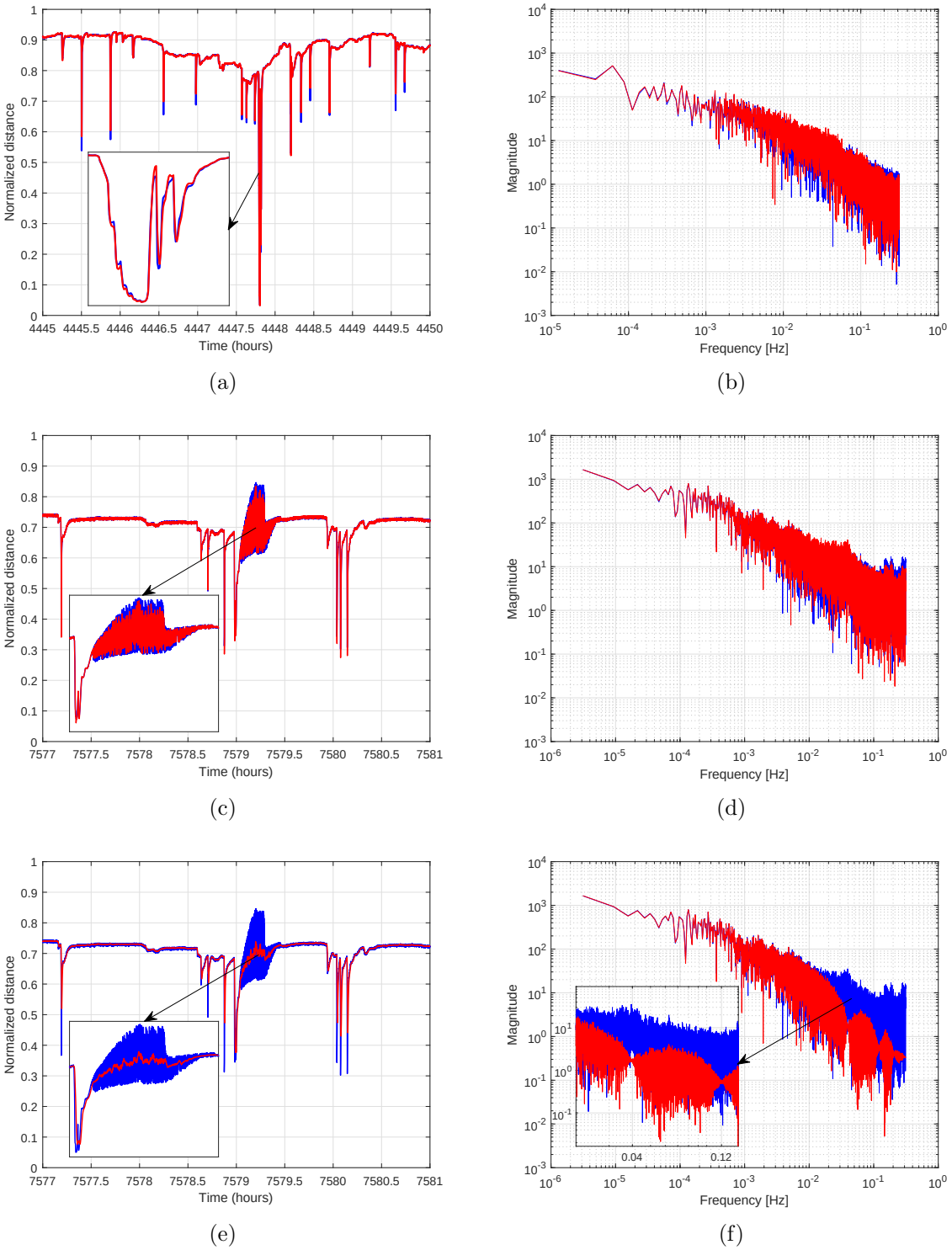

Figure 2.5: (a) Reference signal (in blue) and its estimate by algorithm (2.8) (in red) (b) Frequency spectrum of the signals in (a) (c) Validation signal (in blue) and its estimate by algorithm (2.8) (in red) (d) Frequency spectrum of the signals in (c) (e) Validation signal (in blue) and its filtered vertion by the model-based adaptive filter (in red) (f) Frequency spectrum of the signals in (e).

2.5.6 Filter performance comparison

Analyzing the frequency spectrum of the fault signal, it has been found that its main components are in the range of $0.02Hz$ to $0.04Hz$ as shown in Fig.2.4. Basically, it is the effect of this band that we are interested in suppressing. In this sense, a natural first approach would be to apply a passive bandstop filter or even a lowpass filter. However, as shown below, using conventional solutions, important components of the original signal can also be suppressed, or high-frequency components can be maintained. Such an effect is not desirable, which justifies using the proposed adaptive filter as detailed in the above subsection. Therefore, to illustrate the model-based adaptive filter performance, we compare it with two traditional passive filter solutions, a $6th$ order Butterworth bandstop filter to suppress the frequencies between $0.02Hz$ and $0.04Hz$ and a $6th$ order Butterworth lowpass filter to suppress the frequencies above $0.02Hz$. The Butterworth approach was chosen because it is the most popular in signal processing practice for its simplicity and effectiveness.

Fig.2.6(a) shows the time domain response of the applied bandstop filter to the distance signal from the animal #4 in a sampling window containing the measured signals from the day 316 at $5h36min$ to $6h36min$. This data window was chosen since it contains three main regions typically found in the measured distance signals of the scallops that include the region affected by the electronic noise (I), a low frequency but wide amplitude region (II), and a high-frequency but low amplitude region (III). Note that by using the bandstop filter, there is an attenuation in the amplitude of the signal in the region I, and the filtered signal follows well the behavior in the region II. However, in the region III, by the figure detail, it is possible to see that some high-frequency behavior (measurement noise) is kept. Such a characteristic can also be observed from Fig.2.6(b).

Assuming that the effect in the region III is due to measurement noise, a smoother response would be desirable, so an appropriate solution would be to filter the frequencies above $0.02Hz$. In this case, a Butterworth lowpass filter was designed. The temporal response of this filter is shown in Fig.2.6(c). In this case, the signal was more attenuated in the region III. Besides, the amplitude of the signal was maintained in the region II. It is observed through Fig.2.6(d) that important frequency components may have been lost; the frequency spectrum looks poor. With these two approaches, we illustrate the problem that arises when unwanted frequency components are in the same frequency range as the important frequencies of the original signal (see Fig.2.4).

Finally, the results obtained using the algorithm (2.8) is shown in Fig.2.6(e). By proposing a model for the original signal, including a faulty component model, and identifying its parameters, it was possible to remove from the original signal the electrical noise. Moreover, due to the greater freedom in parameter set-up and the DREM method construction properties, it was also possible to reduce the measurement noise effect. Note that the filtered signal keeps the same characteristics, in terms of frequency, on the three highlighted regions; this is especially observed by comparing regions I and III. The frequency spectrum for the model-based adaptive filtering approach is shown in Fig.2.6(f).

It is important to note that the behavior of the bivalves is under study and it is not clear how much information could be neglected from the original signal. In this case, the less the original

signal was changed the better it would be from the point of view of biology, that is, the more information would be kept. It is possible to verify through the frequency spectra that the three regions of interest for a typical valvometry signal were maintained with the application of the adaptive filter, while in the two other (traditional) approaches, much was lost. This is evident when looking at the frequency spectrum of the low-pass filter, in which the reconstruction of the original signal is very poor.

2.6 Distance and velocity estimates

As mentioned earlier, valve distance activity signals can be rich in relevant biological information and to extract that information from them is a big challenge. The valve velocity seems to provide a more direct and intuitive behavioral interpretation. Since velocity is the time derivative of the valve distance activity, we need to differentiate the distance signals to obtain the velocity. In this section, we use a homogeneous finite-time differentiator for this task. This method is presented in [Perruquetti et al., 2008]. It was also used in [Ahmed et al., 2016c] for automatic spawning detection in oysters. Such a method was chosen because of its simplicity, effectiveness, and noise compensation. Below, we briefly present the homogeneous finite-time differentiator idea and the results we obtained from it.

Homogeneous finite-time differentiator

Consider a nonlinear dynamical system of the form

$$\dot{x}(t) = g(x(t),u(t)), \tag{2.18}$$
$$y(t) = h(x(t)), \tag{2.19}$$

where $x(t) \in \mathbb{R}^d$ is the state vector, $u \in \mathbb{R}^m$ is a known and sufficiently smooth control input, $y(t) \in \mathbb{R}$ is the corresponding output, and $g : \mathbb{R}^d \times \mathbb{R}^m \to \mathbb{R}^d$ is a known continuous vector field. Assume that this system is locally observable and that there exist a local state and output coordinate transformations such that (2.18), (2.19) are transformed into the canonical observable form:

$$\begin{bmatrix} \dot{z}_1 \\ \vdots \\ \dot{z}_n \end{bmatrix} = \underbrace{\begin{bmatrix} a_1 & 1 & 0 & 0 & 0 \\ a_2 & 0 & 1 & 0 & 0 \\ \vdots & \vdots & \vdots & \ddots & \vdots \\ a_{n-1} & 0 & 0 & 0 & 1 \\ a_n & 0 & 0 & 0 & 0 \end{bmatrix}}_{A} z + f(y,u,\dot{u},\cdots,u^r) \tag{2.20}$$

where $z \in \mathbb{R}^n$ is the state, $r \in \mathbb{N}_+$, and $a = [a_1,\ldots,a_n]^T$. Note that, since all nonlinearities are functions of the output and known inputs, the observer design for the system is quite simple

and has the form:

$$\begin{bmatrix} \dot{\hat{z}}_1 \\ \vdots \\ \dot{\hat{z}}_n \end{bmatrix} = \begin{bmatrix} 0 & 1 & 0 & 0 & 0 \\ 0 & 0 & 1 & 0 & 0 \\ \vdots & \vdots & \vdots & \ddots & \vdots \\ 0 & 0 & 0 & 0 & 1 \\ 0 & 0 & 0 & 0 & 0 \end{bmatrix} \hat{z} + ay + f(y,u,\dot{u},\cdots,u^r) - \begin{bmatrix} \chi_1(z_1 - \hat{z}_1) \\ \chi_2(z_1 - \hat{z}_1) \\ \vdots \\ \chi_n(z_1 - \hat{z}_1) \end{bmatrix} \tag{2.21}$$

where $e = z - \hat{z}$ is the error whose the observation dynamics is given by:

$$\begin{cases} \dot{e}_1 = e_2 + \chi_1(e_1) \\ \dot{e}_2 = e_3 + \chi_4(e_1) \\ \vdots \\ \dot{e}_{n-1} = e_n + \chi_{n-1}(e_1) \\ \dot{e}_n = \chi_n(e_1) \end{cases} \tag{2.22}$$

In [Perruquetti et al., 2008], it was prooved that if functions χ_i's are defined as

$$\chi_i(e_1) = -k_i \lceil e_1 \rfloor^{i\alpha-(i-1)}, \;\; 1 \leq i \leq n,$$

the system (2.22) is homogeneous of degree $\alpha - 1$ with respect to the weights $\{(i-1)\alpha - (i-2)\}_{1\leq i\leq n}$ provided that $\alpha > 1 - \frac{1}{n-1}$. Moreover, if the gains $(k_1, \cdots, k_n)$ are chosen such that $A_0 = A - k[1\ 0 \ldots 0]$ is Hurwitz, then, there exists $\varepsilon \in \left[1 - \frac{1}{n-1}, 1\right]$ such that for all $\alpha \in (1-\varepsilon, 1)$, the system (2.22) with χ_i's as defined in (2.22) is globally finite-time stable. To learn more about homogeneous systems, see [Polyakov, 2020].

Finally, considering a chain of integrators, a particular case of (2.20):

$$\dot{z}_i = z_{i+1}, \;\; \text{for} \;\; i = 1, \cdots, n-1,$$

$$\dot{z}_n = u \tag{2.23}$$

$$y = z_1, \tag{2.24}$$

where $z \in \mathbb{R}^n$ is the state vector, $u \in \mathbb{R}$ is the input, and $y \in \mathbb{R}$ is the corresponding output, the following homogeneous finite-time differentiator is obtained:

$$\begin{aligned} \dot{\hat{z}}_1 &= z_2 - k_1 \lceil y - \hat{z}_1 \rfloor^{\alpha}, \\ \dot{\hat{z}}_i &= z_{i+1} - k_i \lceil y - \hat{z}_1 \rfloor^{i\alpha-(i-1)}, \;\; \text{for} \;\; i = 2, \cdots, n-1, \\ \dot{z}_n &= -k_n \lceil y - \hat{z}_1 \rfloor^{n\alpha-(n-1)} + u \end{aligned} \tag{2.25}$$

from which, by applying the Euler discretization, one obtains for the first two states:

$$\begin{aligned} z_1(t_k) &= z_1(t_{k-1}) + T_s(z_2(t_{k-1}) - k_1 \lceil y(t_{k-1} - z_1(t_{k-1})) \rfloor^{\alpha}) \\ z_2(t_k) &= z_2(t_{k-1}) + T_s(-k_2 \lceil y(t_{k-1}) - z_1(t_{k-1}) \rfloor^{2\alpha-1}). \end{aligned} \tag{2.26}$$

where T_s is the sampling period, $t_k = kT_s$ ($k \in \mathbb{N}_+$), $z_1(t_k)$ can be interpreted as a distance estimate and $z_2(t_k)$ is the corresponding velocity [Ahmed et al., 2016c].

To illustrate the obtained results, Fig.2.7 shows an aleatory data window of the filtered and estimated distance and velocity signals measured from Animal #3 in 2014 from the day 289 at $20h30min$ to $21h00min$. It was used an estimator with 4 states, which give us more precision. However, we were interested only in the first two states (position and velocity). The estimator parameters used were $k_1 = 5 \times 10^{-1}$, $k_2 = 5 \times 10^{-2}$, $k_3 = 10^{-6}$, $k_4 = 10^{-9}$, and $\alpha = 0.9975$. As the distance signal was estimated from the filtered distance signal, the estimator parameters were chosen to fit the filtered data sufficiently; thus, we avoid a second filter effect by the differentiator. Fig.2.8 shows the filtered and estimated distance and velocity signals for the same data window showed in Fig.2.6 where the electrical noise was present in the data. In the following developments, instead of velocity, the absolute value of the velocity will be used. This results in a speed measurement that allows us to measure the level of agitation of the valves.

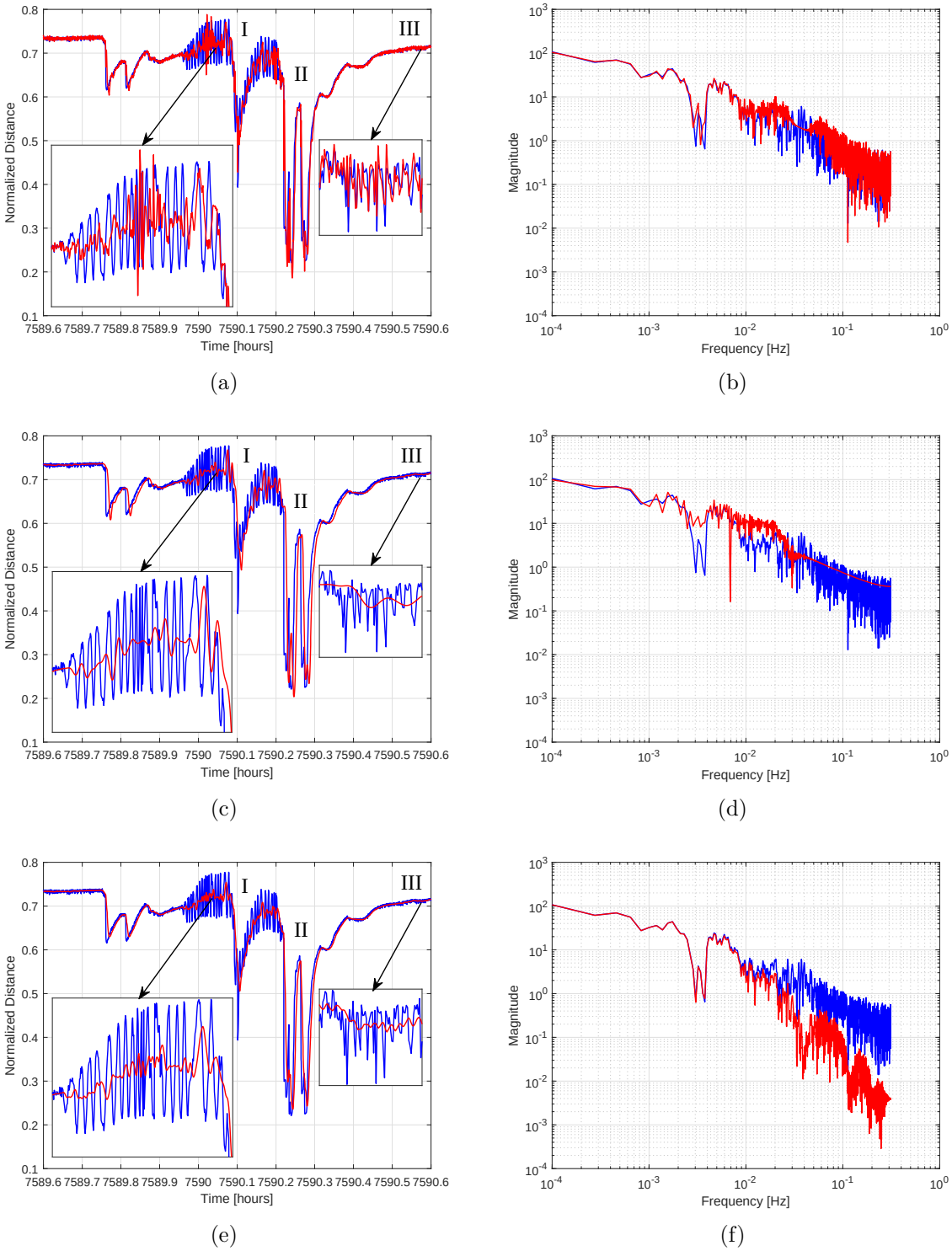

Figure 2.6: (a) Distance signal with electrical noise measured from animal #4 in 2017 (in blue) and its filtered vertion by a $6th$ order stopband filter (in red) (b) Frequency spectrum of the signals in (a) (c) Distance signal with electrical noise measured from animal #4 in 2017 (in blue) and its filtered vertion by a $6th$ order lowpass filter (in red) (d) Frequency spectrum of the signals in (c) (e) Distance signal with electrical noise measured from animal #4 in 2017 (in blue) and its filtered vertion by model-based adaptive filter (in red) (f) Frequency spectrum of the signals in (e).

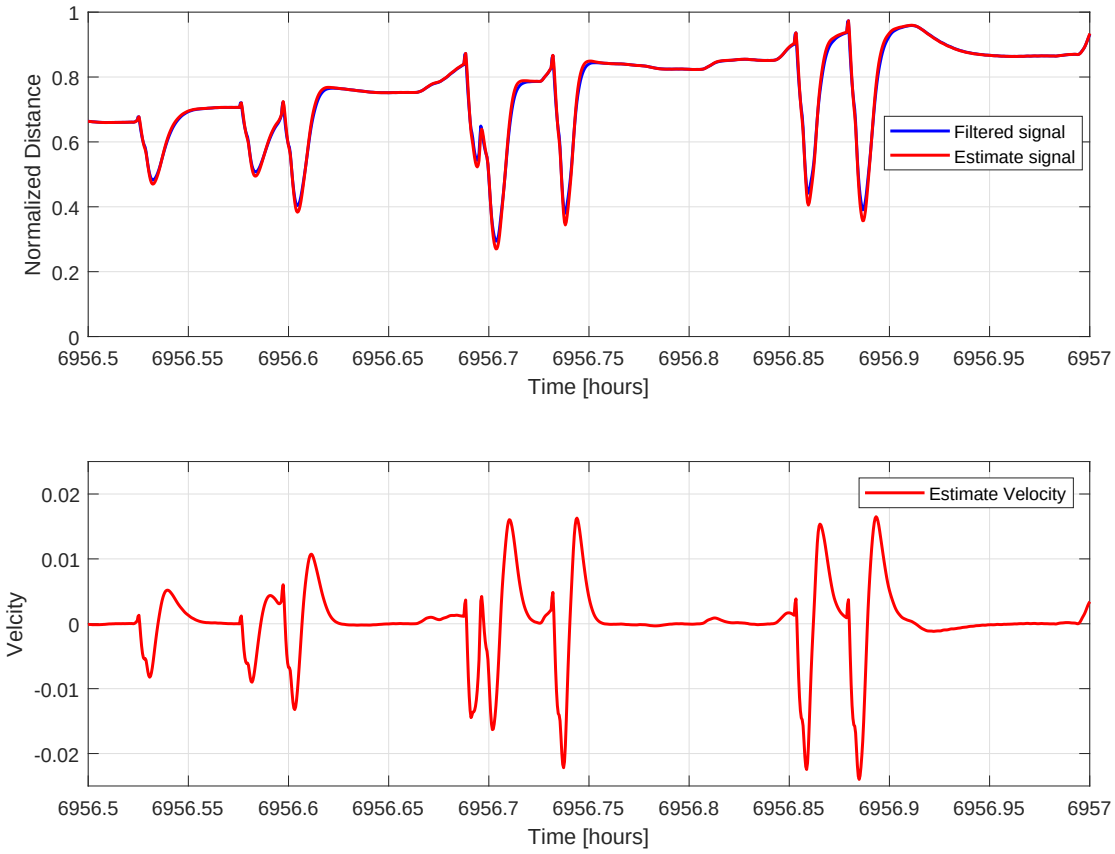

Figure 2.7: Data window of the filtered (blue) and estimated (red) distance signals measured from animal #3 in 2014 from the day 289 at $20h30min$ to $21h00min$ (up) and the estimated velocity (down).

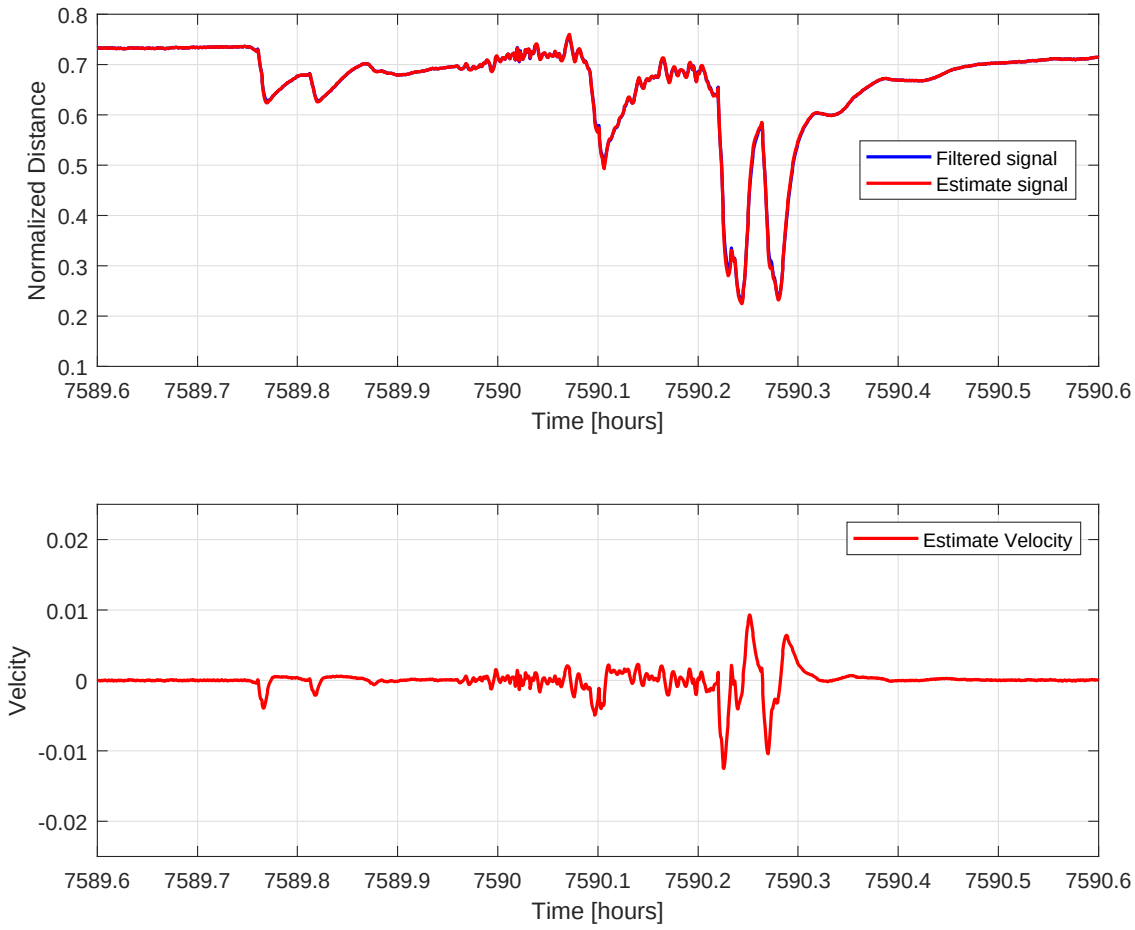

Figure 2.8: Data window of the filtered (blue) and estimated (red) distance signals measured from animal #4 in 2017 from the day 316 at $05h36min$ to $06h36min$ (up) and the estimated velocity (down).

2.7 Results and discussion

Once the distance signals were processed and we estimated the speed, the next step was to calculate the five behavior variables, i.e., the average distance, the percentage of valve opening/closing, the average speed, and the movement index. These signals are direct variations of the only output signal that can be measured from the bivalves. Although there are no conclusive studies on the conditions under which the valves operate, they open and close due to factors related to feeding, breathing, thermal regulation, or defense against threats and predators. Therefore, exploring the time and amplitude of the gaps and the movements' speed and intensity generate the first insights. For these reasons we selected these five behavior variables.

Since the bivalves are living organisms, these animals' reactions to certain stimuli can be relatively different. However, as a community, their expressions should be more homogeneous, so we decided to analyze the population's behavioral variables and not each individual. Also, we realized that analyzing the signals on a short time basis would be less intuitive. We were interested in detecting changes in behavior due to climatic factors. In this case, even though the bivalves can react quickly to changes in temperature, significant abrupt variations in the environment would be unlikely mainly because they are in an aquatic environment. In this case, through preliminary tests using a smaller time basis, we chose to calculate the variables monthly.

The calculation performed to obtain the population monthly average behavior variables was done in the following order. First, we calculate the monthly average behavior variables for each individual. Then, we calculate the average according to the number of individuals in the population each year (16 animals maximum), obtaining the population monthly average behavior variables. Note that the same criteria can be used to obtain them on any time basis, for example, the population weekly or hourly average behavior variables. The resampling of these signals depends heavily on the application. However, the average behavior is almost always more accurate to understand living beings. Bellow, we discuss the results obtained.

First, it is shown in Figs. 2.9 and 2.10, respectively, the monthly air and water temperatures in Ny-Alesund from 2012 to 2018. These temperatures are courtesy of the "Tu.Tiempo.net" (see https://en.tutiempo.net/climate/ws- 10070.html) and "SEA TEMPERATURE.INFO" (see https://seatemperature.info/january/ny-alesund-water-temperature.html) websites. The graphs are presented here for illustrative purposes. Both series have the same temperature profile, with the warmest period occurring between June and September. A more accurate analysis of the temperature in the studied region can be found in Cisek et al. [2017].

Fig.2.11 shows the result obtained for the population monthly average distances during the seven years of data acquisition. To illustrate the filter effect, we also plot the result obtained without filtering. Note that the filter does not affect this variable, and the result is the same using the filtered or the non filtered distance signals. We also plot a trend-line that visually indicates a decreasing tendency. We stress that analyzing these data and correlating them with temperature is not in the scope of this work, and the significance of this trend must be investigated.

Fig.2.12 is a variant of the first and shows the population percentage monthly average opening/closing variables. The objective of these variables concerning temperature is, for example,

to indicate whether there exists a temperature event where the bivalves react closing/opening the valves for more time. The same observation is done concerning trends. They must be investigated.

Fig.2.14 shows the population monthly average velocity variable (actually the valve speed) estimated from the filtered and non filtered distance signals. In this case, we can make some qualitative observations. The first one is that the trend-line of the signal estimated from the non filtered distance signals increases. This fact could be associated with the presence of harmonic noises in 2017 and 2018, which indicates the importance of filtering since these noises can distort the conclusions. For example, one could state that the increasing trend in the speed signal is associated with the temperature data trend, which is not possible to assume directly. On the other hand, we observe that the population monthly average velocity data calculated from the filtered distance signals does not present these trends. In any case, to affirm something, it would be necessary first to investigate whether the trends are significant for both cases and then to examine how the two data sets correlate with temperature. Despite this, it is possible to observe that the temperature and velocity data profile seem to have some connection. For instance, the periods of high-speed coincide (visually) with periods of high-temperatures. Therefore, the velocity data has the potential as a measure of the agitation of bivalves.

The last behavioral variable, the population monthly average movement index shown in Fig. 2.14, derives from velocity signals. To calculate this variable first, we defined a speed threshold in the speed signals. Then, we calculate how many times in one month the velocity cross this threshold. In other words, such a threshold could be interpreted as a stress level for the bivalves. The same qualitative correlation with temperature is observed. Therefore, for example, we could say that in periods of high-temperature, the valves move with more intensity, implying a good stress indicator.

In conclusion, we can only affirm that the obtained behavioral variables, especially the speed-related ones, show promise as potential tools, for instance, to measure the bivalves' agitation and level of stress, which can be converted into a welfare and adaptation measurement for these animals, regarding environmental temperature variation. To illustrate this potential, we show in Fig.2.15 and 2.16 the relationship between water temperature and the speed-related behavioral variables, the monthly velocity, and the monthly movement index, respectively. It is possible to note, for both cases, an accentuated slope in the trendlines increasing in the same direction of temperature. Such a tendency must be better investigated in the light of biology and complementary bioclimatic inputs in future works.

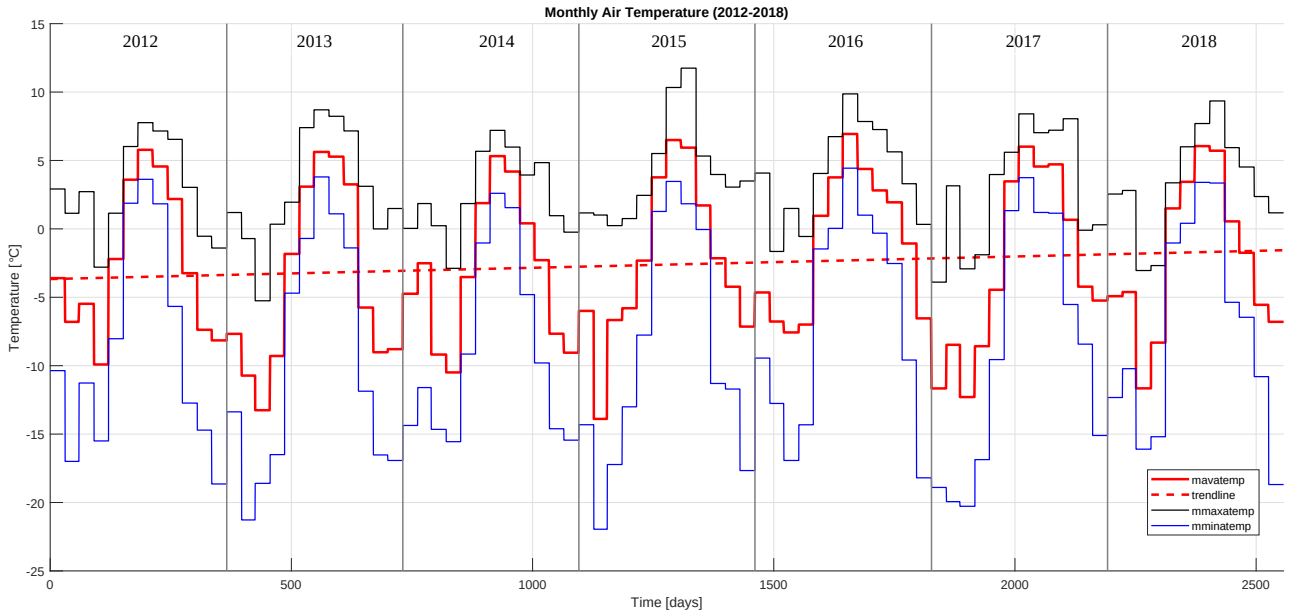

Figure 2.9: Air temperature measured in Ny-Alesund from 2012 to 2018 (mavatemp: monthly average air temperature; mmaxtemp: monthly maximum air temperature; mmintemp: monthly minimum air temperature).

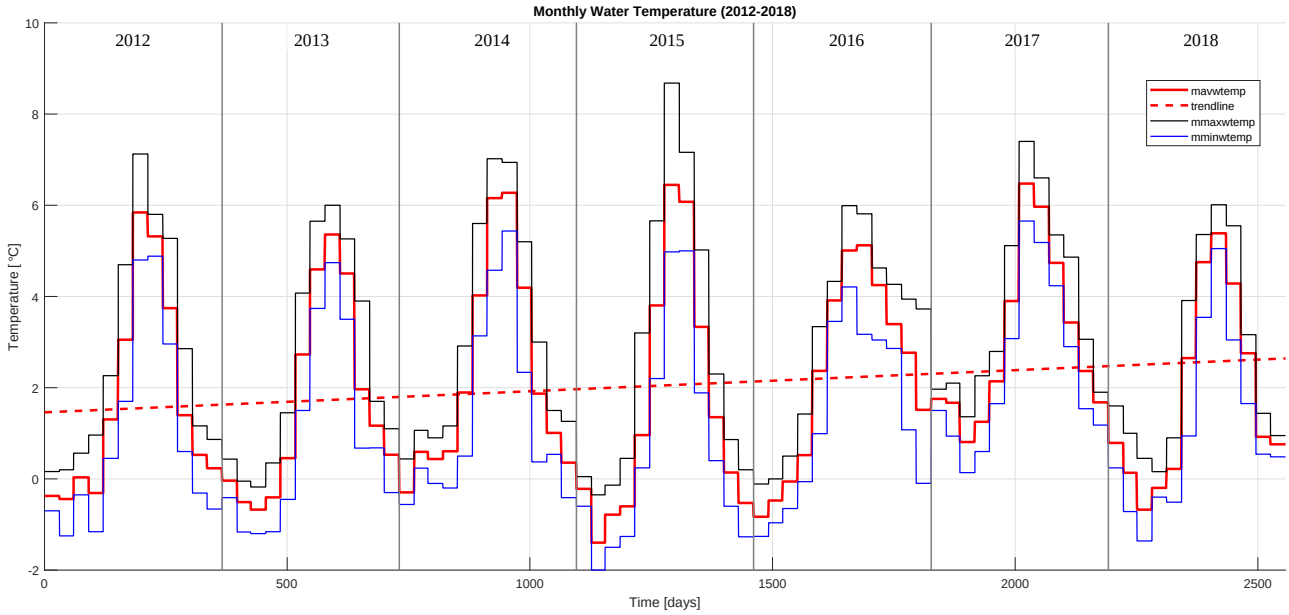

Figure 2.10: Water temperature measured in Ny-Alesund from 2012 to 2018 (mavwtemp: monthly average water temperature; mmaxtemp: monthly maximum water temperature; mmintemp: monthly minimum water temperature).

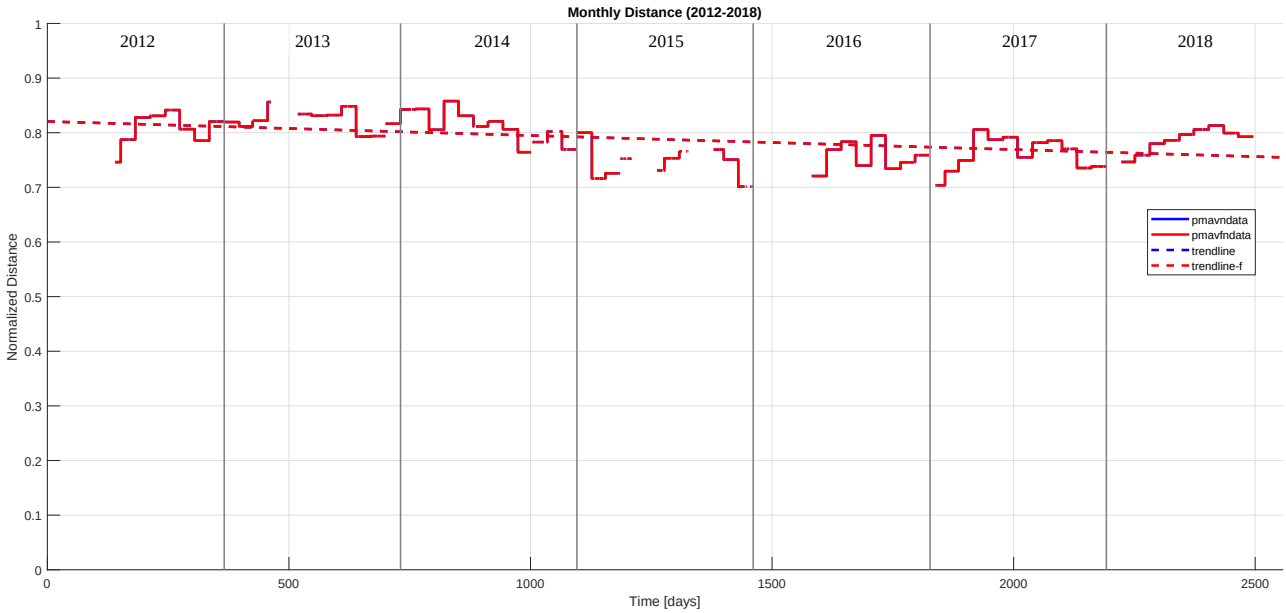

Figure 2.11: Population monthly average distance obtained from the original and filtered distance signals (pmavndata: population monthly average from normalized data; pmavfndata: population monthly average from filtered normalized data).

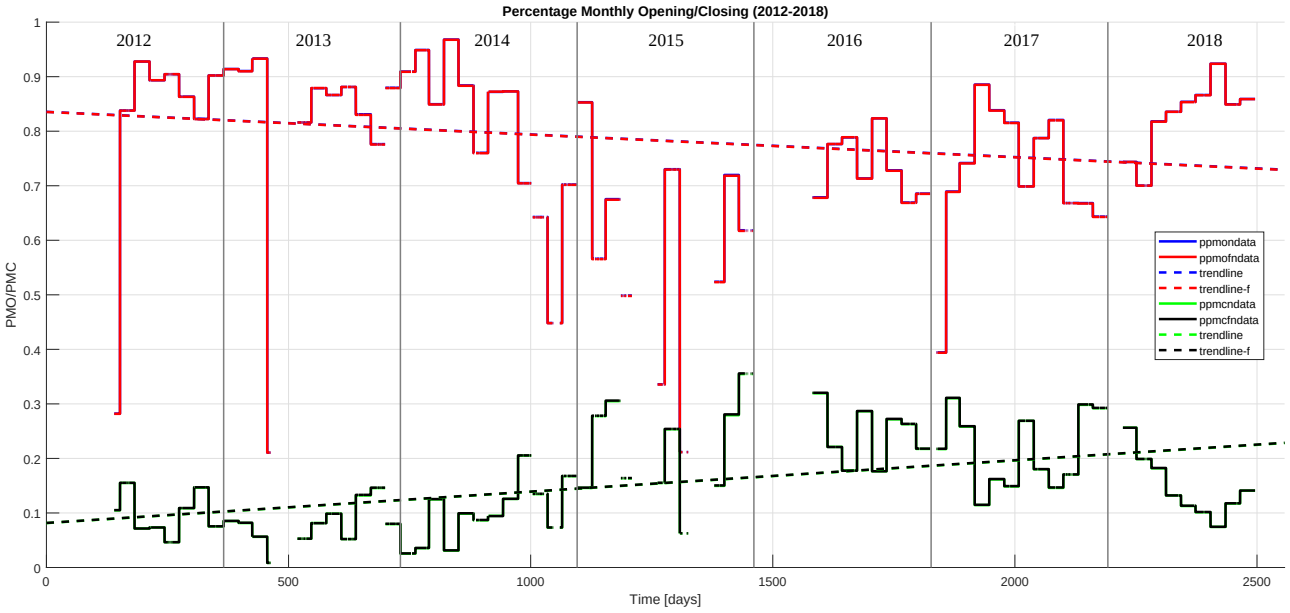

Figure 2.12: Population percentage monthly onpening/closing obtained from the original and filtered distance signals (ppmondata: population percentage monthly opening normalized data; ppmondata: population percentage monthly closing normalized data; ppmofndata: population percentage monthly opening filtered from normalized data; ppmondata: population percentage monthly closing from filtered normalized data).

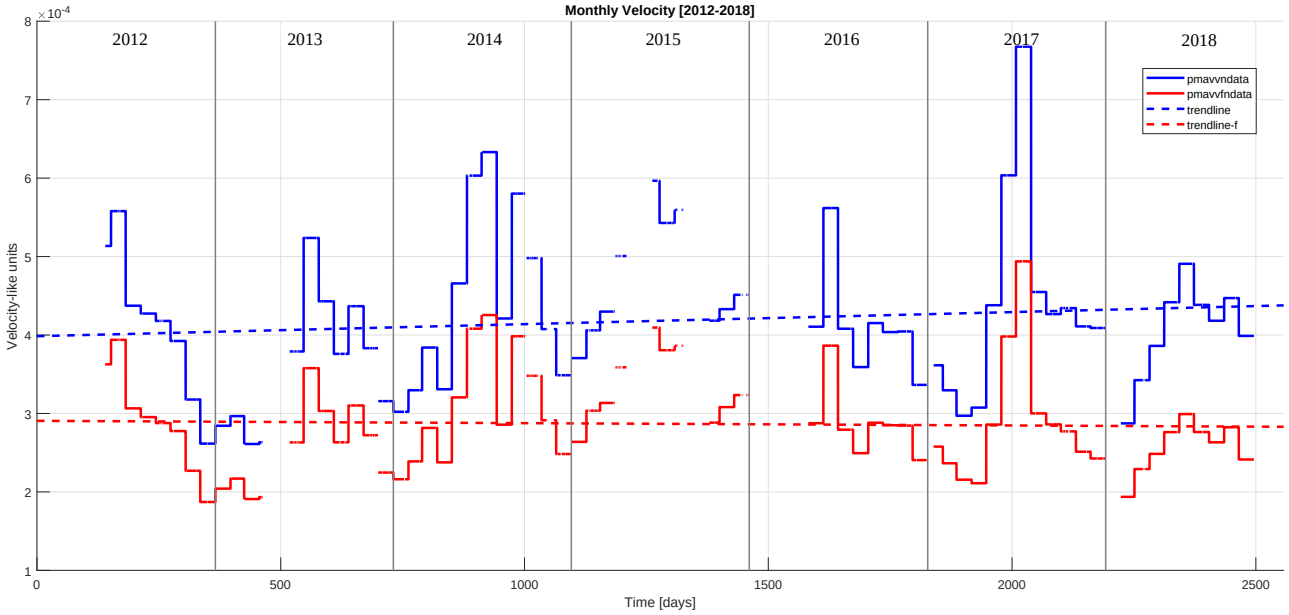

Figure 2.13: Population monthly average velocity obtained from the original and filtered distance signals (pmavvndata: population monthly average velocite from normalized data; pmavvfndata: population monthly average velocite from filtered normalized data).

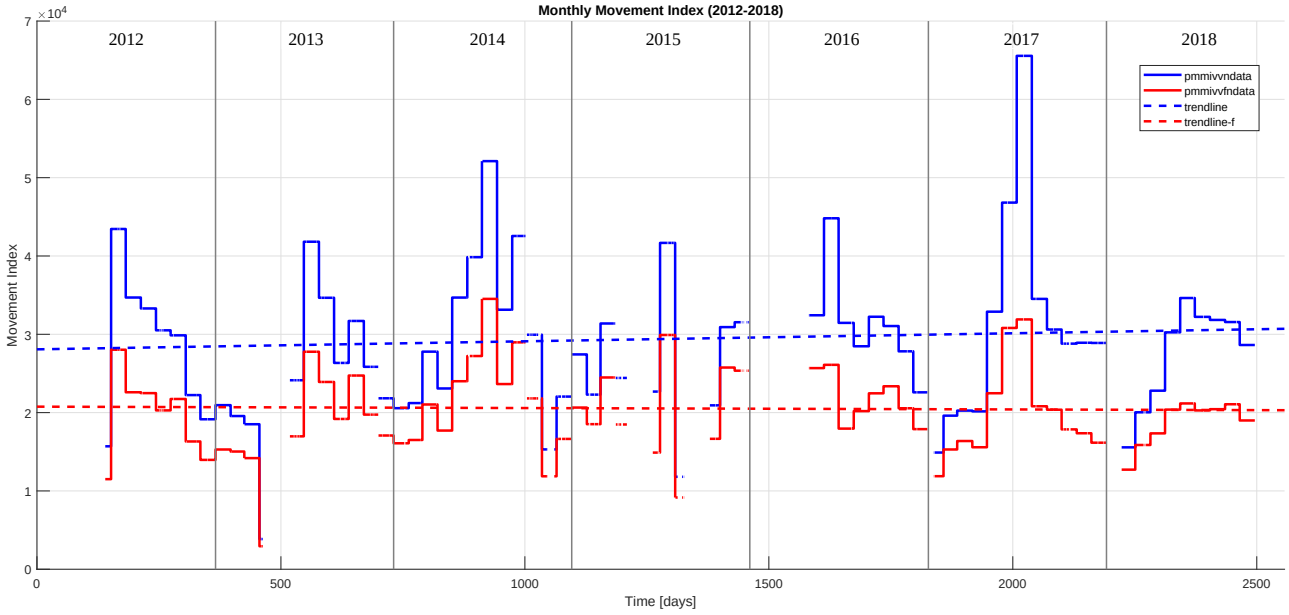

Figure 2.14: Population monthly movement index obtained from the original and filtered distance signals (pmmivndata: population monthly movement index of velocity from normalized data; pmmivfndata: population monthly movement index of velocity from filtered normalized data).

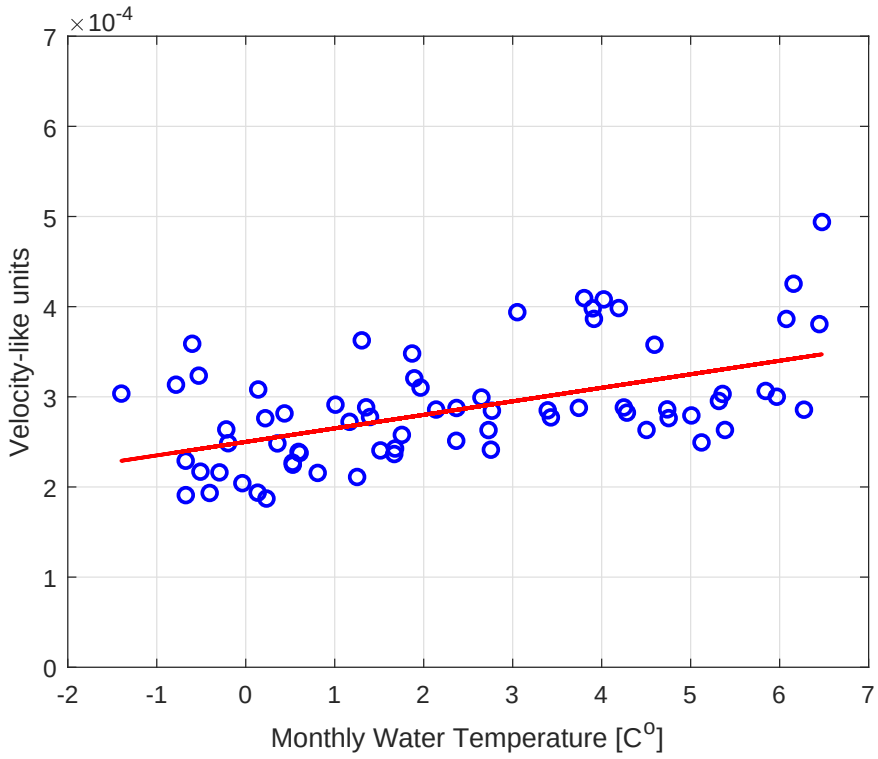

Figure 2.15: Relation between water temperature and monthly velocity.

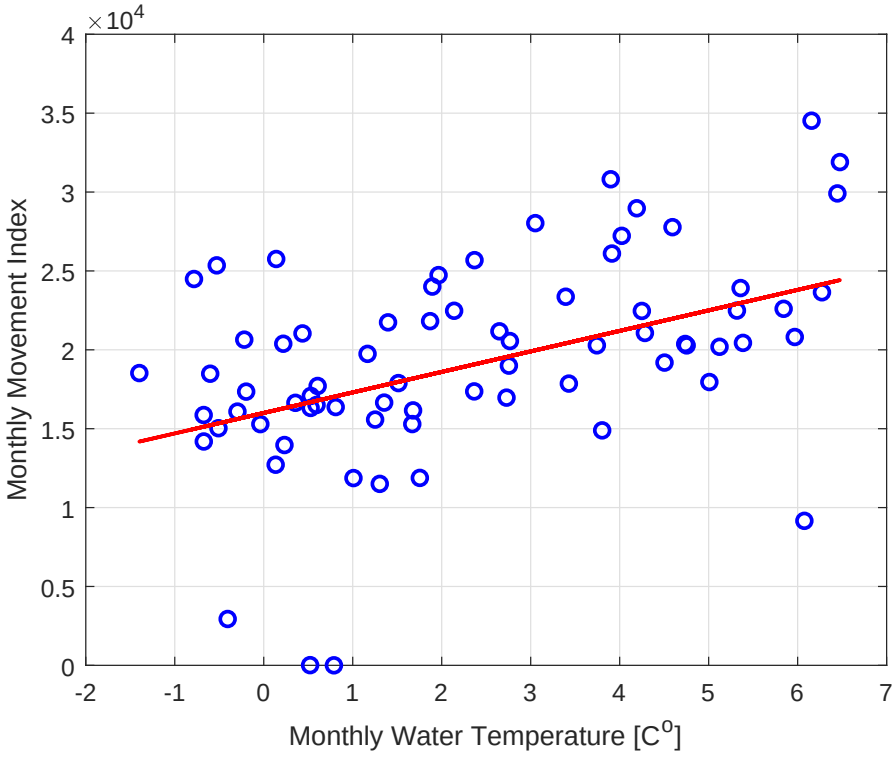

Figure 2.16: Relation between water temperature and monthly movement index.

CHAPTER

THREE

ROBUST STABILIZATION OF AFFINE MULTISTABLE SYSTEMS

3.1 Introduction

In this chapter, based on the framework of input-to-state stability (ISS) and integral input-to-state stability (iISS), we aim to provide robustness conditions for stability and stabilization of two different subclasses of input-affine nonlinear systems with multiple invariant sets. In Section 3.2, the multistability framework is presented. We introduce its main constructive properties and assumption and several robust stability notions with respect to a compact invariant set $\mathcal{W}$; the main object of analysis and the starting point for the theoretical development. In the first approach (Section 3.3) we deal with multistable passive systems with exogenous disturbances in the input channel. The problem is stated under the argumentation that passive and strict-passive systems can be driven into instability over small input perturbations despite its stable nature. Then we provide iISS/ISS conditions for the open-loop and closed-loop cases, where additional output feedback is required to ensure robustness. In the second approach (Section 3.4) we deal with a subclass of affine multistable systems with an exogenous disturbance input. The problem is faced by extending the control Lyapunov functions and universal formula theory within the multistability framework. In each section, we provide suitable examples to illustrate both approaches. A general conclusion for the chapter is given in Section 3.5. To clarify the multistable scenario adopted, we will start this chapter with a simple example.

A simple multistable system

Let us consider the following nonlinear dynamical system (a Duffing system). We wish to make a qualitative analysis of the evolution of its states:

$$\begin{aligned} \dot{x}_1(t) &= x_2(t), \\ \dot{x}_2(t) &= -x_2(t) - x_1(t)(x_1^2(t) - 1), \quad x \in \mathbb{R}^2_+. \end{aligned} \tag{3.1}$$

The phase portrait of this system is shown in Fig.3.1. It has three equilibria, the first equilibrium, at the origin, is a saddle point (with one positive and one negative real eigenvalue), and the

last two are stable sinks (with complex conjugate eigenvalues with negative real parts). We can group all of these points in a compact set $\mathcal{W}$, the set of all *invariant solutions* of (3.1). It means that for an initial condition $x_0 \in \mathcal{W}$, the solution $x(t)$ of (3.1) remains in $\mathcal{W}$ for all $t \in \mathbb{R}$.

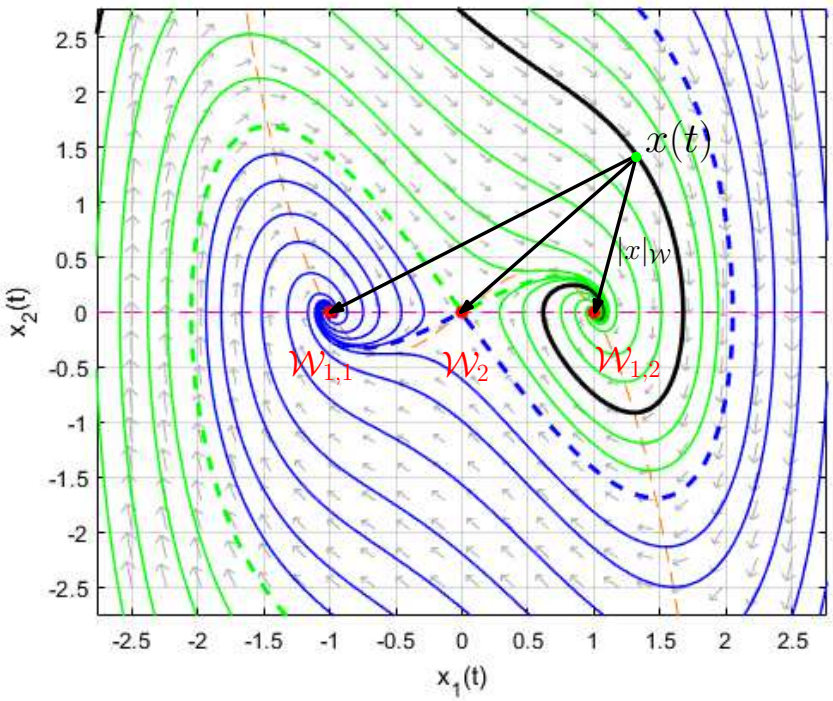

Figure 3.1: Phase portrait of a Duffing system.

For $x_0 \notin \mathcal{W}$, all trajectories converge to one of the stable equilibria. To characterize this motion, we can decompose $\mathcal{W}$ into two subsets: $\mathcal{W} = \{\mathcal{W}_1 = ((-1,0),(1,0)), \mathcal{W}_2 = (0,0)\}$, the set of attracting and repulsing solutions respectively and define a metric $|x|_{\mathcal{W}}$ which denotes the smallest distance between $x(t)$ traveling on $\mathbb{R}^2$ and $\mathcal{W}$. There is also a solution that connects $\mathcal{W}_1$ to $\mathcal{W}_2$; but no path connects any component of $\mathcal{W}$ and returns to itself.

A Lyapunov function for (3.1) is given by:

$$V(x) = \frac{1}{4}(x_1^2 - 1)^2 + \frac{1}{2}x_2^2.$$

Such a function is equal to zero at $\mathcal{W}_1 = \{(-1,0),(1,0)\}$ and it is positive otherwise as shown in Fig.3.2 (the level curves of V). The gradient of V with respect to the trajectories of (3.1) is given by:

$$\dot{V}(x) = -y^2, \quad y = x_2.$$

As $\dot{V}$ depends only on x_2, we must apply the Krasovskii-LaSalle invariance principle to analyze the system behavior, which indicates that all trajectories are bounded and converges to the set $\mathcal{W}$. The stable subset $\mathcal{W}_2$ attracts trajectories for almost all initial conditions, except the equilibrium at the origin and the stable separatrices of this equilibrium. Such behavior is characterized by the Lyapunov function V, equal to zero on the attracting limit set and positive otherwise, where their time derivative is negative semidefinite.

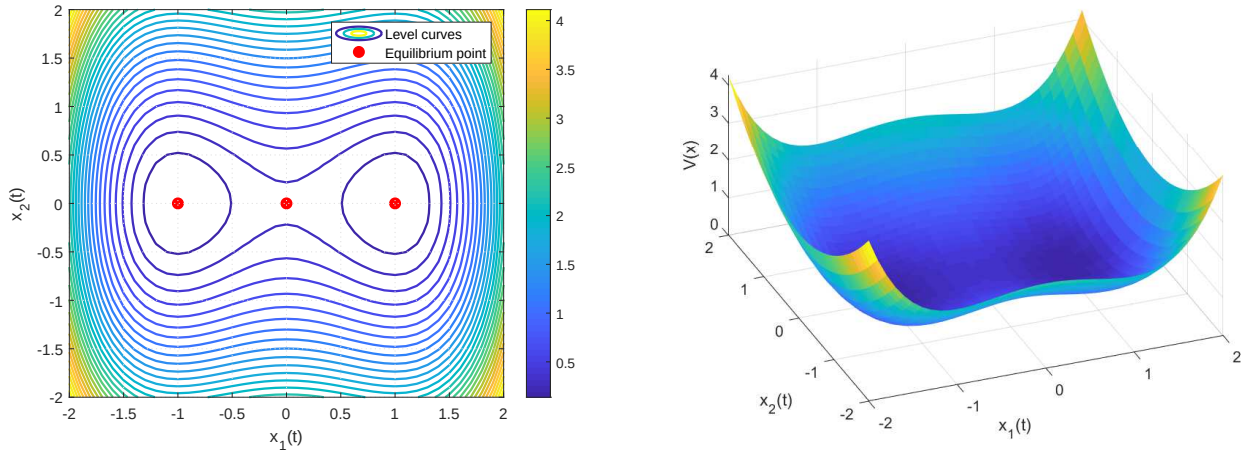

(a) (b)

Figure 3.2: Lyapunov function shape: (a) Level curves of $V(x)$ (b) Surface of $V(x)$

The system (3.1) is a simple example in $\mathbb{R}^2$ of a multistable system, precisely a bistable one. With the above scenario, we can summarize, for our further analysis, the main properties of the multistability framework introduced by [Efimov, 2012], as well as the corresponding robust stability notions for systems with multiple invariant sets, as introduced by [Angeli and Efimov, 2015, Forni and Angeli, 2017]. To do so, we need to assume that the system is evolving on a Riemannian manifold $\mathcal{M}$ ($\mathcal{M} = \mathbb{R}^2$ for the previous example).

3.2 The multistability framework

Consider a nonlinear dynamical system of the following form:

$$\dot{x}(t) = f(x(t),u(t)), \quad \forall t \in \mathbb{R}_+, \tag{3.2}$$

$$y(t) = h(x(t)), \tag{3.3}$$

evolving on a n-dimensional connected and orientable Riemmanian manifold $\mathcal{M}$ without boundary, with $u \in \mathcal{U} = \mathcal{L}_\infty(\mathbb{R}_+,\mathbf{U})$, where $\mathbf{U}$ defines the set of admissible values for the control; and let $f : \mathcal{M} \times \mathbf{U} \to T_x\mathcal{M}$ be a locally Lipschitz continuous function on $\mathcal{M}$ mapping the state vector $x(t) \in \mathcal{M}$ and the input vector $u(t) \in \mathbf{U} \subseteq \mathbb{R}^m$ to the tangent space $T_x\mathcal{M} \subseteq \mathbb{R}^n$; $y(t) \in \mathcal{Y} \subseteq \mathbb{R}^p$ is the corresponding output vector, $h : \mathcal{M} \to \mathcal{Y}$ is a continuous function. We also assume that $f(0,0) = h(0) = 0$ (without losing generality let $0 \in \mathcal{M}$).

For any $x_0 \in \mathcal{M}$ and $u \in \mathcal{U}$, we denote by $x(t,x_o,u)$ the uniquely defined solution of (3.2) at time $t \in \mathbb{R}_+$ such that $x(0,x_0,u) = x_0$ (the short notation $x(t)$ is used when the initial conditions x_0 and the input u are apparent). However, to characterize the evolution of $x(t)$ on $\mathcal{M}$ in the multistability framework, let us first consider the unperturbed version of (3.2):

$$\dot{x}(t) = f(x(t),0), \quad t \in \mathbb{R}_+, \tag{3.4}$$

and a set $\mathcal{W}$ as a reference for the evolution of $x(t,x_0,0)$, where the distance from a point $p \in \mathcal{M}$

to the set $\mathcal{W}$ is given by:

$$|p|_{\mathcal{W}} = \inf_{a\in\mathcal{W}} \delta(p,a),$$

and $\delta(x_1,x_2)$ denotes the Riemannian distance between x_1 and x_2 in $\mathcal{M}$, with the convention that for a point x_{or}, selected as the origin on $\mathcal{M}$, $|p| = |x|_{x_{or}}$ can be considered as a norm of $p \in \mathcal{M}$ (with a small ambiguity, we use the same symbol for the Euclidean norm).

Definition 3.1. *A set $\mathcal{W} \subset \mathcal{M}$ is called (forward)* invariant*, if for all initial conditions $x_0 \in \mathcal{W}$ the solutions of (3.4) do not leave this set,* i.e.*, if $x_0 \in \mathcal{W}$, then $x(t,x_0,0) \in \mathcal{W}$ for all $t \in \mathbb{R}_+$.*

Definition 3.2. *A point $\underline{x}$ is called an* α-limit point *of (3.4) if there exists a sequence of time instants $t_0, \cdots, t_\ell, \cdots$, such that $t_k \to -\infty$ as $k \to +\infty$, for which the following holds:*

$$x(t_k,x_0,0) \to \underline{x}, \quad k \to +\infty. \tag{3.5}$$

The set of all such points is called α-limit of $x(t,x_0,0)$ and it is denoted by $\alpha(x_0)$.

Definition 3.3. *A point $\bar{x}$ is called an* ω-limit point *of (3.4) if there exists a sequence of time instants $t_0, \cdots, t_\ell, \cdots$, such that $t_k \to +\infty$ as $k \to +\infty$, for which the following holds:*

$$x(t_k,x_0,0) \to \bar{x}, \quad k \to +\infty. \tag{3.6}$$

The set of all such points is called ω-limit of $x(t,x_0,0)$ and it is denoted by $\omega(x_0)$.

In the sequel we will assume that $\mathcal{W}$ is a compact invariant set of (3.4), which contains all α- and ω-limit sets for (3.4).

3.2.1 Decomposition of a compact invariant set $\mathcal{W}$

To characterize the evolution of $x(t,x_0;0)$ along $\mathcal{M}$, it is useful to decompose $\mathcal{W}$ and explicitly determine the existence of solutions traveling between its components.

Definition 3.4. *[Nitecki and Shub, 1975] A* decomposition *of a compact invariant set $\mathcal{W} \subset \mathcal{M}$ is a finite and disjoint family of compact invariant sets $\mathcal{W}_1, \cdots, \mathcal{W}_z$ such that:*

$$\mathcal{W} = \bigcup_{i=1}^{z} \mathcal{W}_i. \tag{3.7}$$

The attracting and repulsing subsets of an invariant set $\mathcal{W} \subset \mathcal{M}$ can be defined, respectively, as follows:

$$\mathfrak{A}(\mathcal{W}) = \{x_0 \in \mathcal{M} : |x(t,x_0;0)|_{\mathcal{W}} \to 0 \text{ as } t \to +\infty\},$$
$$\mathfrak{R}(\mathcal{W}) = \{x_0 \in \mathcal{M} : |x(t,x_0;0)|_{\mathcal{W}} \to 0 \text{ as } t \to -\infty\}.$$

Based on it, we can define a relation between two invariant sets $\mathcal{W}_1 \subset \mathcal{M}$ and $\mathcal{W}_2 \subset \mathcal{M}$ by $\mathcal{W}_1 \prec \mathcal{W}_2$ if $\mathfrak{A}(\mathcal{W}_1) \cap \mathfrak{R}(\mathcal{W}_2) \neq \emptyset$. This relation implies that there is a solution connecting the set $\mathcal{W}_1$ with the set $\mathcal{W}_2$ as follows:

Definition 3.5. *[Nitecki and Shub, 1975] Let $\mathcal{W}_1, \cdots, \mathcal{W}_z$ be a decomposition of a compact invariant set $\mathcal{W}$. Then,*

(1) An r-cycle *($r \geq 2$) is an ordered r-tuple of distinct indices $i_1, \cdots, i_r$ such that $\mathcal{W}_{i_1} \prec \cdots \prec \mathcal{W}_{i_r} \prec \mathcal{W}_{i_1}$.*

(2) A 1-cycle *is an index i such that $[\mathfrak{R}(\mathcal{W}_i) \cap \mathfrak{A}(\mathcal{W}_i)] \setminus \mathcal{W}_i \neq \emptyset$.*

(3) A filtration ordering *is a numbering of the $\mathcal{W}_i$ so that $\mathcal{W}_i \prec \mathcal{W}_j \Rightarrow i \leq j$.*

Note that the existence of an r-cycle with $r \geq 2$ results in a *heteroclinic cycle* for (3.4). Also, the existence of a 1-cycle results in a *homoclinic cycle*. It was recognized in [Angeli and Efimov, 2015] that if one wishes to have a strict Lyapunov function (with a proper negative definite derivative) in the multistable scenario, the presence of cycles has to be ruled out, and we need a strict Lyapunov function for robust stability analysis. Therefore, for the development of the next two sections, we will assume the following restriction on $\mathcal{W}$.

Assumption 3.1. *[Angeli and Efimov, 2015] The compact invariant set $\mathcal{W}$, containing all α- and ω-limit sets of the unperturbed system (3.4), admits a finite decomposition without cycles: $\mathcal{W} = \bigcup_{i=1}^{z} \mathcal{W}_i$ for some non-empty disjoint compact sets $\mathcal{W}_i$ and a finite $z > 0$, which form a filtration ordering of $\mathcal{W}$.*

3.2.2 Robust stability notions with respect to a compact invariant set $\mathcal{W}$

Below we list several stability properties for (3.2), (3.3) of a compact invariant set $\mathcal{W}$. Most of these properties are direct extensions of the classical ISS and iISS notions introduced in [Sontag and Wang, 1995, 1996, Liberzon et al., 1999, Angeli et al., 2000].

Definition 3.6. *[Angeli and Efimov, 2015, Forni and Angeli, 2017] The system (3.2) has the* practical asymptotic gain (pAG) *property if there exist $\eta \in \mathcal{K}_\infty$ and $q \geq 0$ such that for all $x_0 \in \mathcal{M}$ and $u \in \mathcal{U}$, the solutions are defined for all $t \geq 0$ and the following holds:*

$$\limsup_{t \to +\infty} |x(t,x_0,u)|_{\mathcal{W}} \leq \eta(||u||_\infty) + q. \tag{3.8}$$

If $q = 0$, then we say that the asymptotic gain (AG) *property holds. Moreover, if (3.8) is satisfied for $q = 0$ for the system (3.4) only, then we say that (3.2) has the* zero-global attraction (0-GATT) *property with respect to $\mathcal{W}$.*

Definition 3.7. *[Angeli and Efimov, 2015] The system (3.2) has the* limit property (LIM) *with respect to $\mathcal{W}$ if there exists $\mu \in \mathcal{K}_\infty$ such that for all $x_0 \in \mathcal{M}$ and all $u \in \mathcal{U}$ the solutions are defined for all $t \geq 0$ and the following holds:*

$$\inf_{t \geq 0} |x(t,x_0,u)|_{\mathcal{W}} \leq \mu(||u||_\infty).$$

Definition 3.8. *[Angeli and Efimov, 2015] The system (3.2) has the* practical global stability (pGS) *property with respect to $\mathcal{W}$ if there exists $\beta \in \mathcal{K}_\infty$ and $c \geq 0$ such that for all $x_0 \in \mathcal{M}$ and all $u \in \mathcal{U}$, the solutions are defined for all $t \geq 0$ and the following holds:*

$$|x(t,x_0,u)|_{\mathcal{W}} \leq \beta\left(\max\{|x_0|_{\mathcal{W}} + c, ||u||_\infty\}\right).$$

Definition 3.9. *[Angeli and Efimov, 2015, Forni and Angeli, 2017] A continuously differentiable function $V : \mathcal{M} \to \mathbb{R}_+$ is a* practical ISS-Lyapunov function *for (3.2) if there exist $\mathcal{K}_\infty$ functions α_1, α_2, α_3 and γ, and $q \geq 0$, $c \geq 0$ such that*

$$\alpha_1(|x|_{\mathcal{W}}) \leq V(x) \leq \alpha_2(|x|_{\mathcal{W}}) + c, \tag{3.9}$$

and the following dissipation inequality holds:

$$DV(x)f(x,u) \leq -\alpha_3(|x|_{\mathcal{W}}) + \gamma(|u|) + q. \tag{3.10}$$

If (3.10) holds for $q = 0$, then V is an ISS-Lyapunov function*. If (3.9) is satisfied and (3.10) holds for $q = 0$ and $\alpha_3 : \mathbb{R}_+ \to \mathbb{R}_+$ a positive definite function, then V is an* iISS-Lyapunov function*.*

The existence of α_2 and c follows, without any additional hypothesis, by standard continuity arguments.

Definition 3.10. *[Forni and Angeli, 2017] The system (3.2) has the* uniform bounded-energy bounded-state (UBEBS) *property if there exist $\alpha,\gamma,\sigma \in \mathcal{K}_\infty$ and $c \geq 0$ such that the following estimate holds for all $t \geq 0$, all $x_0 \in \mathcal{M}$ and all $u \in \mathcal{U}$:*

$$\alpha(|x(t,x_0,u)|_{\mathcal{W}}) \leq \gamma(|x_0|_{\mathcal{W}}) + \int_0^t \sigma(|u(\tau)|)d\tau + c.$$

Definition 3.11. *[Forni and Angeli, 2017] The system (3.2), (3.3) has the* smooth dissipativity *property if there exist a $\mathcal{C}^1$ function $V : \mathcal{M} \to \mathbb{R}_+$, α_1, α_2, $\sigma \in \mathcal{K}_\infty$, a continuous positive definite function α_4, and a continuous output map $h : \mathcal{M} \to \mathcal{Y} \subseteq \mathbb{R}^p$ with*

$$|x|_{\mathcal{W}} = 0 \;\Rightarrow\; h(x) = 0, \quad \forall x \in \mathcal{M}$$

such that (3.9) is satisfied for all $x \in \mathcal{M}$ and the following dissipation inequality holds:

$$DV(x)f(x,u) \leq -\alpha_4(|h(x)|) + \sigma(|u|). \tag{3.11}$$

Definition 3.12. *[Forni and Angeli, 2017] The system (3.2), (3.3) has the* weak zero-detectability *property if:*

$$h(x(t,x_0,0)) = 0, \, \forall t \geq 0$$

implies $|x(t,x_0,0)|_{\mathcal{W}} \to 0$ as $t \to +\infty$.

The principal results connecting these properties are given by:

Theorem 3.1. *[Angeli and Efimov, 2015] Consider a nonlinear system (3.2) and let Assumption 3.1 hold. Then the following are equivalent:*

(1) The system enjoys the pAG or AG property.

(2) The system admits an ISS Lyapunov function.

(3) The system admits an ISS Lyapunov function constant on $\mathcal{W}$.

(4) The system admits a practical ISS Lyapunov function.

(5) The system enjoys the LIM property and the pGS.

A system (3.2) satisfying these properties is called ISS in the multistable sense *from the input u with respect to the set $\mathcal{W}$.*

Theorem 3.2. *[Forni and Angeli, 2017] Consider a nonlinear system (3.2) and let Assumption3.1 hold. Then the following are equivalent:*

(1) 0-GATT and UBEBS properties.

(2) Existence of an iISS Lyapunov function constant on $\mathcal{W}$.

(3) Existence of an iISS Lyapunov function.

(4) Existence of an output function that makes the system smoothly dissipative and weakly zero-detectable.

A system (3.2) satisfying these properties is called iISS in the multistable sense *from the input u with respect to the set $\mathcal{W}$.*

Lemma 3.1. *[Forni and Angeli, 2017] Let system (3.14) be 0-GATT. Then, there exist a smooth function $U : \mathcal{M} \to \mathbb{R}$, ν_1, ν_2, $\delta \in \mathcal{K}$, a continuous positive definite function $\varpi : \mathbb{R}_+ \to \mathbb{R}_+$ and a positive constant c such that:*

$$\nu_1(|x|_{\mathcal{W}}) \leq U(x) \leq \nu_2(|x|_{\mathcal{W}} + c),$$
$$DU(x)f(x,u) \leq -\varpi(|x|_{\mathcal{W}}) + \delta(|u|),$$

for all $x \in \mathcal{M}$ and $u \in \mathbf{U}$. Moreover, $DU(x) = 0$ for all $x \in \mathcal{W}$.

Note that if the function U in Lemma 3.1 were proper, *i.e.*, $\nu_1 \in \mathcal{K}_\infty$, then it would qualify U as an iISS-Lyapunov function. Unfortunately, this is not necessarily the case; therefore, U needs to be used in addition to a proper function V to obtain a new iISS-Lyapunov function such that the iISS property holds:

Corollary 3.1. *Consider a nonlinear system (3.14) in the conditions of Theorem 3.2. Then the following properties are equivalent:*

(1) iISS with respect to the set $\mathcal{W}$ and input u.

(2) 0-GATT and existence of an output function making the system smoothly dissipative.

Proof. The iISS property comes from the fact that the sum $V + U$ is an iISS-Lyapunov function, with V and U given in Definition 3.11 and Lemma 3.1, respectively. The converse is a consequence of Theorem 3.2. □

3.3 Robustness upon disturbances of affine passive multistable systems

Robustness of stability upon external perturbations is an important property characterizing the dynamics' ability to counteract the influence of uncertainties. In the present section, such property is investigated for passive and strictly passive systems, which have several invariant compact and globally attracting subsets in the unforced scenario. It is assumed that the storage and supply rate functions are sign-definite on these sets. The results are obtained within the framework of input-to-state stability and integral input-to-state stability for multistable systems. The robustness conditions are obtained for open-loop and closed-loop cases, *i.e.*, when output feedback is required to guarantee robustness. Two applications (related to the model of multispecies populations) of the proposed theory illustrate its efficiency.

3.3.1 Multistable passive systems

For further analysis, assuming that the dimensions of the input and the output spaces are the same and $m = p$, we introduce, in the multistability context, the formal definition of passive and strict passive systems [Hill and Moylan, 1980].

Definition 3.13. *The system (3.2), (3.3) is* passive *with a continuous function $V : \mathcal{M} \to \mathbb{R}_+$ if for all $x_0 \in \mathcal{M}$, $u \in \mathcal{U}$, and $t \geq 0$, the following inequality is satisfied:*

$$V(x(t,x_0,u)) \leq V(x_0) + \int_0^t \varpi(x(\tau,x_0;u),u(\tau),y(\tau,x_0;u))d\tau, \tag{3.12}$$

$$\varpi(x,u,y) = y^T u - \beta(|x|_{\mathcal{W}}), \tag{3.13}$$

where $\beta : \mathcal{M} \to \mathbb{R}_+$ is a continuous function. Then ϖ and V are called, respectively, supply rate *and* storage functions. *It is called* passive with a certain rate of dissipation β *if the equality sign holds in (3.12). It is called* passive without losses *if it is possible to use the equality sign and $\beta \equiv 0$ in (3.12). Finally, if in (3.13) β is a positive definite function, the system is called* strictly passive.

The Kalman-Yakubovich-Popov Lemma claims that for the system (3.2), (3.3), the output function for passive and strict passive systems with a differentiable storage function can be defined in the following way:

$$h(x) = (DV(x)G(x))^T = \left(\frac{\partial V}{\partial x}G(x)\right)^T.$$

If the storage function V is continuously differentiable, then the inequality on the trajectories (3.12) gives a simpler form:

$$DV(x)f(x,u) \leq \varpi(x,u,h(x))$$

that has to be verified for all $x \in \mathcal{M}$, and $u \in \mathbf{U}$. Moreover, the solution of a system that admits the passive property with a proper storage function V is Lyapunov stable for $u(t) \equiv 0$, $t \geq 0$. The solution of a strictly passive system in such a case is asymptotically stable with a Lyapunov function V (these facts can be proven using LaSalle arguments since positive definiteness of the storage function V has not been claimed).

3.3.2 Problem statement

Passivity and strict passivity mean that the system solution is respectively Lyapunov stable and asymptotically stable for zero inputs. However, in the general case, these properties are not robust with respect to input perturbations, and an arbitrary small input signal may initiate unstable processes in the system [Efimov, 2006, Efimov and Fradkov, 2008]. Therefore, the task of iISS (ISS) stabilization of such a kind of system is of great interest. In this section, we deal with a class of nonlinear (strict)passive dynamical systems affine in the input of the following form:

$$\dot{x}(t) = f(x(t)) + G(x(t))u(t), \quad t \in \mathbb{R}_+, \tag{3.14}$$

$$y(t) = h(x(t)), \tag{3.15}$$

where $x(t) \in \mathcal{M}$ is the state vector; $u(t) \in \mathbf{U} \subseteq \mathbb{R}^m$ is the input vector and $u \in \mathcal{U} = \mathcal{L}_\infty(\mathbb{R}_+,\mathbf{U})$, where $\mathbf{U}$ defines the set of admissible values for the control; $y(t) \in \mathcal{Y} \subseteq \mathbb{R}^p$ is the corresponding output vector. For this system, $f : \mathcal{M} \to \mathbb{R}^n$ and the columns of the matrix $G : \mathcal{M} \to \mathbb{R}^{n\times m}$ are assumed to be locally Lipschitz continuous on $\mathcal{M}$. We also assume that $f(0) = h(0) = 0$ (without loosing generality let $x_{or} = 0 \in \mathcal{M}$).

The output stabilizability notion is extended from Sontag [1990] to the multistability case as follows:

Definition 3.14. *The system* (3.14), (3.15) *is* iISS (ISS) output stabilizable *if there exists for it a control law*

$$u(t) = \varphi(y(t)) + v(t),$$

where $\varphi : \mathcal{Y} \to \mathbf{U}$ is a Lipschitz continuous function and $v(t) \in \mathbb{R}^k$, $v \in \mathcal{L}_\infty(\mathbb{R}_+,\mathbb{R}^k)$ is a new input vector that makes the closed-loop system iISS (ISS) with respect to v.

Therefore, the problem studied in this section can be formally written by introducing the following hypothesis:

Assumption 3.2. *A passive or strict passive system described by the affine nonlinear model (3.14), (3.15) has a decomposable compact invariant set $\mathcal{W}$ as in Assumption 3.1, and its storage function $V : \mathcal{M} \to \mathbb{R}_+$ is continuously differentiable and satisfies* (3.9) *and* (3.12) *for all $x \in \mathcal{M}$, while the supply function has the form:*

$$\varpi(x,u,y) = y^T u - \beta(|x|_{\mathcal{W}}), \tag{3.16}$$

where $\beta : \mathbb{R}_+ \to \mathbb{R}_+$ is a continuous function.

Problem 3.1. *Under Assumption 3.2, find the conditions for iISS (ISS) output stabilisability for (3.14), (3.15) (according to Definition 3.14).*

To choose a control law that provides the iISS (ISS) property for a strict passive system (3.14), (3.15) in the setting of multiple invariant sets, we need to introduce some specifications on the storage function and the supply rate (these additional requirements do not contradict the

definition of passive systems Definition 3.13). Hence the evolution of the state $x(t) \in \mathcal{M}$ must be evaluated with respect to the invariant set $\mathcal{W} \subset \mathcal{M}$ (the functions V and β are defined for $|x|_{\mathcal{W}}$), and we have to assume that this set is globally attractive for $u \equiv 0$. Another interesting point consists in distinguishing the situations where an additional feedback $\varphi(y)$ is required or where we can select $\varphi(y) = 0$.

3.3.3 Conditions on robust stability and stabilizability

This subsection presents several results about different conditions on the robust stability and stabilizability of passive systems.

Theorem 3.3. *Assume that a strict passive system (3.14), (3.15) satisfies Assumption 3.2. If one of the following conditions holds:*

$$\lim_{|x|_{\mathcal{W}} \to +\infty} \frac{|h(x)|}{V(x)} < +\infty, \tag{3.17}$$

$$y^T \varphi(y) \geq \varepsilon |y|^2, \quad \forall y \in \mathcal{Y}, \varepsilon > 0, \tag{3.18}$$

then the control law

$$u = -\varphi(y) + v \tag{3.19}$$

with $\varphi : \mathcal{Y} \to \mathbf{U}$ a Lipschitz continuous function satisfying $y^T \varphi(y) > 0$ for all $y \neq 0$ and $v \in \mathcal{L}_\infty(\mathbb{R}_+, \mathbb{R}^k)$, ensures the iISS property for the system with respect to $\mathcal{W}$ and the disturbance input v, where β is a positive definite function. If the condition (3.18) is satisfied and β is an element of $\mathcal{K}_\infty$ or $|h(x)| \geq \varrho(|x|_{\mathcal{W}})$ for all $x \in \mathcal{M}$ and some $\varrho \in \mathcal{K}_\infty$, then the control (3.19) guarantees the ISS property with respect to $\mathcal{W}$ and the disturbance input v, and V is an ISS-Lyapunov function.

Proof. The derivative of the storage function V under the introduced restrictions for the strict passive system (3.14), (3.15) can be upper estimated with respect to $\mathcal{W}$ as follows:

$$\dot{V} \leq y^T u - \beta(|x|_{\mathcal{W}}),$$

where β is a positive definite function. Substituting the control law we obtain:

$$\dot{V} \leq y^T(-\varphi(y) + v) - \beta(|x|_{\mathcal{W}}).$$

Let us consider a new storage function for the system which inherits all properties of the function V:

$$U(x) = \ln(1 + V(x)).$$

Consequently, U is a positive definite, continuously differentiable and proper function with respect to the set $\mathcal{W}$. The derivative of U is given by (taking into account the equality $y = (DV(x)\ G(x))^T$):

$$\dot{U} = \frac{DV(x)[f(x) - G(x)\varphi(y)] + DV(x)G(x)v}{1 + V(x)} \leq \frac{-\beta(|x|_{\mathcal{W}})}{1 + V(x)} + \frac{|h(x)||v|}{1 + V(x)}.$$

Under condition (3.17) there exists a constant $\lambda > 0$ such that

$$\frac{|h(x)|}{1+V(x)} \leq \lambda, \quad \forall x \in \mathcal{M},$$

and the time derivative of U for the system can be rewritten as follows:

$$\dot{U} \leq \frac{-\beta(|x|_{\mathcal{W}})}{1+V(x)} + \lambda|v|.$$

Thus, according to Definition 3.12, the function U is an iISS-Lyapunov function for the system, which is equivalent to the iISS property. Now, if (3.18) is satisfied, then:

$$\dot{V} \leq -\varepsilon|y|^2 + |y||v| - \beta(|x|_{\mathcal{W}}).$$

Hence, using the inequality $2|y||v| \leq \varepsilon|y|^2 + \varepsilon^{-1}|v|^2$ that is valid for any $\varepsilon > 0$, this last estimate can be transformed to the following one:

$$\dot{V} \leq -\beta(|x|_{\mathcal{W}}) - 0.5\varepsilon|y|^2 + 0.5\varepsilon^{-1}|v|^2.$$

Therefore, from the definitions of iISS- and ISS-Lyapunov functions, the desired conclusions can be obtained, and V is an iISS- or ISS-Lyapunov function. □

Theorem 3.3 establishes the connection between the form of the function β and the robustness property of the system with respect to inputs bounded in $\mathcal{L}_\infty$ or $\mathcal{L}_2$ sense. An important consequence of this theorem consists in the ability of a strict passive system to become robust with respect to an additive perturbation in the input channel under any output feedback with an arbitrary small gain ε [Efimov, 2006, Efimov and Fradkov, 2008, Pchelkina and Fradkov, 2012].

The following proposition is a particular case of the Theorem 3.3 when output feedback is not needed to guarantee the iISS property for the system. In this case, the 0-GATT property is enough because there is no disturbance in the input channel. This is a technical detail that illustrates the range of the iISS property for strict passive systems.

Proposition 3.1. *Assume that a strict passive system (3.14), (3.15) satisfies Assumption 3.2 and the following inequality holds:*

$$|h(x)| \leq b(V(x)), \ \forall x \in \mathcal{M}$$

where $b : \mathbb{R}_+ \to \mathbb{R}_+$ is a function satisfying the integral constraint:

$$\int_0^{+\infty} \frac{dr}{1+b(r)} = +\infty.$$

Then the system is iISS with respect to $\mathcal{W}$ and the input u.

Proof. The derivative of the storage function V under introduced restrictions for the strict passive system (3.14), (3.15) can be upper estimated with respect to $\mathcal{W}$ as follows:

$$\dot{V} \leq y^T u - \beta(|x|_{\mathcal{W}}),$$

where β is a positive definite function. Note that a strict passive system satisfies the 0-GATT property since for $u \equiv 0$ we have

$$\dot{V} \leq -\beta(|x|_{\mathcal{W}}).$$

In other words, V is a Lyapunov function for the system $\dot{x} = f(x)$. Now, let us consider a new storage function for the system (3.14), (3.15):

$$U(x) = \int_0^{V(x)} \frac{dr}{1 + b(r)}$$

which is clearly proper and positive definite by the introduced hypotheses (note that by the chain rule $U(x) = 0$ for all $x \in \mathcal{W}$ such that $V(x) = 0$). Then, the derivative of U along the trajectories of (3.14), (3.15) is given by:

$$\dot{U} = \frac{DV(x)(f(x) + G(x)u)}{1 + b(V(x))} = \frac{DV(x)f(x)}{1 + b(V(x))} + \frac{|DV(x)G(x)|}{1 + b(V(x))}|u|.$$

Finally, using $|DV(x)G(x)| \leq b(V(x))$ we achieve:

$$\dot{U} \leq \frac{-\beta(|x|_{\mathcal{W}})}{1 + b(V(x))} + \frac{b(V(x))}{1 + b(V(x))}|u| \leq \frac{-\beta(|x|_{\mathcal{W}})}{1 + b(V(x))} + |u|.$$

Therefore, from the iISS-Lyapunov function definition, the desired result is obtained, and U is an iISS-Lyapunov function. □

Now let us consider the same issues for passive systems only.

Theorem 3.4. *Assume that a passive system (3.14), (3.15) satisfies Assumption 3.2. If the system satisfies the weak zero-detectability property, the condition (3.17) and the inequality*

$$\frac{h^T(x)}{1 + V(x)}\varphi(h(x)) \geq \kappa(|h(x)|), \quad \forall x \in \mathcal{M}, \tag{3.20}$$

with a positive definite continuous function $\kappa : \mathbb{R}_+ \to \mathbb{R}_+$ holds, then the control law (3.19) provides the iISS property for this system with respect to $\mathcal{W}$ and the input v.

Proof. The passivity property implies that for some $\mathcal{C}^1$ storage function $V : \mathcal{M} \to \mathbb{R}_+$, which satisfies the relations (3.9) for all $x \in \mathcal{M}$, the following inequality holds:

$$\dot{V} \leq y^T u.$$

Substituting in this inequality the control law (3.19), from the Theorem 3.3 we obtain

$$\dot{V} \leq -y^T\varphi(y) + y^T v.$$

Introducing again the new storage function $U(x) = \ln(1 + V(x))$ we achieve

$$\dot{U} \leq -\frac{y^T\varphi(y)}{1 + V(x)} + \frac{|y||v|}{1 + V(x)},$$

which according to the condition (3.17) and (3.20) can be rewritten as:

$$\dot{U} \leq -\kappa(|y|) + \lambda|v|,$$

where $\lambda > 0$. It follows that the system has the smooth dissipativity property and it is weakly zero-detectable. Therefore, the system zero solution is iISS by means of the property 4 from Theorem 3.2. □

Note that Assumption 3.2 implies 0-GATT property (it refers to Assumption 3.1, where it is stated that $\mathcal{W}$ contains all α- and ω-limit sets of the unperturbed system $\dot{x} = f(x,0)$, thus it is the global attractor in the system for $u = 0$).

Theorem 3.5. *Assume that a passive system (3.14), (3.15) satisfies Assumption 3.2. If the control (3.19) is applied under (3.18) and an additional restriction:*

$$\delta(2|\varphi(y)|) \leq \epsilon|y|^2, \quad \forall y \in \mathcal{Y}, \epsilon > 0,$$

where $\delta \in \mathcal{K}$ is given in Lemma 3.1, then the control law (3.19) provides the iISS property for this system with respect to $\mathcal{W}$ and the input v.

Proof. In the light of the condition (3.18), substituting the control (3.19) in the upper estimate for the derivative of the storage function leads to

$$\dot{V} \leq -\varphi(y)^T y + y^T v \leq -0.5\varepsilon|y|^2 + 0.5\varepsilon^{-1}|v|^2.$$

where the inequality $2a^T b \leq \varepsilon|a|^2 + \varepsilon^{-1}|b|^2$ is used during the last step (which is satisfied for any $a,b \in \mathbb{R}^p$, $\varepsilon > 0$). From this inequality, it is easy to see that the smooth dissipativity property holds. Assuming that the 0-GATT property also holds, there exists a semi-proper function $U : \mathcal{M} \to \mathbb{R}_+$ as shown in Lemma 3.1. Let us consider a candidate iISS-Lyapunov function $W = U + V$, then

$$\alpha_1(|x|_{\mathcal{W}}) \leq W(x) \leq \alpha_2(|x|_{\mathcal{W}} + c_1) + \nu_2(|x|_W c + c_2),$$

and the derivative of W along the trajectories of the system (substituting $u = -\varphi(y) + v$) can be written as

$$\dot{W} \leq -\varpi(|x|_{\mathcal{W}}) - 0.5\varepsilon|y|^2 + 0.5\varepsilon^{-1}|v|^2 + \delta(|v - \varphi(y)|),$$

which by means of the inequality $\delta(a + b) \leq \delta(2a) + \delta(2b)$ satisfied for any function from class $\mathcal{K}$, it can be rewritten as

$$\dot{W} \leq -\varpi(|x|_{\mathcal{W}}) - 0.5\varepsilon|y|^2 + \delta(2|\varphi(y)|) + 0.5\varepsilon^{-1}|v|^2 + \delta(2|v|).$$

The last inequality, under an additional restriction: $-0.5\varepsilon|y|^2 + \delta(2|\varphi(y)|) \leq 0$, which can be ensured by taking $\varepsilon = 2\epsilon$, is an iISS-Lyapunov function. □

3.3.4 N-species Lotka-Volterra system.

To exemplify an iISS (ISS) theory application, we will consider a controlled version of the N-species Lotka-Volterra (*predator-pray*) model [Rouche et al., 1977, Pchelkina and Fradkov, 2012]. In this model, we assume that for the population of $N > 1$ species, the birth rate of the species $x_\ell \in \mathbb{R}_+$, $\ell = M+1,\ldots,N$ can be controlled with the index $0 \leq M \leq N$. Then the interaction between the species is described by the following system of differential equations:

$$\begin{aligned}
\dot{x}_i(t) &= x_i(t)\left(k_i + \beta_i^{-1}\sum_{j=1}^{N} a_{ij}x_j(t)\right), \quad i = 1,2,\ldots,M,\\
\dot{x}_\ell(t) &= x_\ell(t)\left(k_\ell + \beta_\ell^{-1}\sum_{j=1}^{N} a_{\ell j}x_j(t) + u_\ell(t)\right), \quad \ell = M+1,\ldots,N,
\end{aligned} \tag{3.21}$$

where $u = [u_{M+1},\ldots,u_N]^T \in \mathbb{R}^{N-M}$ is the control, k_i (k_ℓ) is the speed of the natural increase or death rate of the i-th (ℓ-th) species in the absence of all others with the following convention: $k_i < 0$ ($k_\ell < 0$), if the i-th (ℓ-th) species lives at the expense of others and $k_i > 0$ ($k_\ell > 0$) otherwise. The parameter $\beta_i > 0$ ($\beta_\ell > 0$) reflects the fact that the appearance of a predator is usually connected with the vanishing of one or more preys. The quantities a_{ij}, $i \neq j$ ($a_{\ell j}$, $\ell \neq j$) evaluate the type and the intensity of the interaction between i-th (ℓ-th) and j-th species and form an asymmetric matrix.

Assume that there exists at least one positive equilibrium of (3.21) with $u = 0$ for some values of the system parameters:

$$n = (n_1, n_2, \cdots, n_N), \qquad n_i > 0 \quad i = 1,\ldots,N, \tag{3.22}$$

and consider an auxiliary function W:

$$W(x) = \sum_{i=1}^{N} \beta_i n_i \left(\frac{x_i}{n_i} - \ln\left(\frac{x_i}{n_i}\right)\right).$$

If the condition (3.22) holds, then W is constant along the trajectories of (3.21), *i.e.*, W is an invariant of (3.21) ($\dot{W} = 0$, see [Pchelkina and Fradkov, 2012]). As the Hessian matrix of W is positive definite, then $W(x) > W(n)$ for any $x \neq n$, and it can be used to indirectly measure the amplitude of oscillations [Pchelkina and Fradkov, 2012]. Hence, by introducing the control goal

$$W(x(t)) \to W^*, \quad t \to +\infty, \tag{3.23}$$

a desired amplitude of oscillations can be achieved by means of a desired level of the quantity W as $t \to +\infty$. Note that If $W^* = W(n) = \min_{x\in\mathcal{M}} W(x)$, the goal (3.23) means the achievement of the equilibrium $x = n$. Therefore, the problem is to find a control function u stabilizing the desired level W^* of the function W and hence providing an oscillatory property to the system with the needed amplitude of oscillations. As it has been shown in [Pchelkina and Fradkov, 2012], this problem can be solved by employing the speed gradient (SG) method [Fradkov, 2007]. To this end, it is necessary to introduce another auxiliary function

$$Q(x) = \frac{1}{2}(W(x) - W^*)^2,$$

that can be considered as a storage function for (3.21), when the goal (3.23) is achieved provided that $Q(x(t)) \to 0$ as $t \to \infty$. According to the SG method to design the control one needs to evaluate, first, the time derivative of Q along the system (3.21), and after the gradient of $\dot{Q}$ with respect to u. The first step yields:

$$\dot{Q}(x,u) = (W(x) - W^*) \sum_{\ell=M+1}^{N} (x_\ell(t) - n_\ell)u_\ell, \tag{3.24}$$

while the second one gives:

$$\frac{\partial \dot{Q}(x,u)}{\partial u_\ell} = (W(x) - W^*)(x_\ell(t) - n_\ell), \quad \ell = M+1, \ldots, N.$$

Note that by means of equation (3.24) the system is passive without losses with respect to the output

$$y = (W(x) - W^*) \sum_{\ell=M+1}^{N} (x_\ell(t) - n_\ell).$$

Following the SG method the control action is chosen as

$$u_\ell(t) = -\gamma_\ell (W(x) - W^*)(x_\ell(t) - n_\ell) + v_\ell, \tag{3.25}$$

for some $\gamma_\ell > 0$ and all $\ell = M+1, \ldots, N$, where $v = [v_{M+1}, \ldots, v_N]^T \in \mathbb{R}^{N-M}$ is a disturbance input (essentially bounded function of time) added to the system in order to investigate the iISS (ISS) stabilizability property and to represent the model uncertainty and environmental influences on the populations.

Substituting (3.25) in (3.24) we achieve:

$$\dot{Q}(x,u) \leq -\gamma |(W(x) - W^*) \sum_{\ell=M+1}^{N} (x_\ell(t) - n_\ell)|^2 + |(W(x) - W^*) \sum_{\ell=M+1}^{N} (x_\ell(t) - n_\ell)||v_\ell|,$$

where $\gamma = \min_{\ell=M+1,\ldots,N} \{\gamma_\ell\}$. Therefore, the set of all invariant solutions of the system for $v = 0$ is given by $\mathcal{W} = \{n\} \cup \Gamma$, where $\Gamma := \{x : W(x) = W^*\}$.

Finally, we have:

$$\dot{Q}(x,u) \leq -\gamma |y|^2 + |y||v| \leq -0.5\varepsilon |y|^2 + 0.5\varepsilon^{-1}|v|^2 \tag{3.26}$$

for some $\varepsilon > 0$. Using the same arguments as in Theorem 3.5, it is easy to see that the smooth dissipativity property holds for this system. Also, one can show that for $M = 0$ (which means that all species' birth rate can be controlled), the equation (3.26) guarantees the convergence of all solutions to the set $\mathcal{W}$. It means that (3.26) can be written, according with the characterization of Definition 3.9, as an ISS-Lyapunov function in the form:

$$\dot{Q}(x,u) \leq -\alpha_3(|x|_{\mathcal{W}}) + 0.5\varepsilon^{-1}|v|^2.$$

where α_3 is a $\mathcal{K}_\infty$ function rendering to the system the ISS property.

For $M > 0$, beyond the dissipativity and 0-GATT properties (already satisfied) according to Theorem 3.5, an additional restriction must be checked to render iISS property for the system. For the present example, this restriction implies the existence of a function $\delta \in \mathcal{K}$ such that $\delta(2|y|) \leq \epsilon|y|^2$ for some $\epsilon > 0$. However, as this function is unknown, the restriction cannot be analytically verified to the example treated in this work.

Now, we will illustrate by means of a simple numerical experiment the convergence of the system trajectories to a set $\mathcal{W}$ with and without perturbations. For that, let us consider a system with one predator and one prey. The manifold $\mathcal{M}$ for this case is $\mathbb{R}^2_+$, and the model for the system can be written as follows:

$$\begin{aligned} \dot{x}_1 &= k_1 x_1 + \beta_1^{-1} a_{12} x_1 x_2, \\ \dot{x}_2 &= k_2 x_2 + \beta_2^{-1} a_{21} x_1 x_2 + x_2 u_2, \end{aligned} \tag{3.27}$$

where $x_1(t) \in \mathbb{R}_+$ and $x_2(t) \in \mathbb{R}_+$ represent, respectively, the predator and the prey populations; $k_1 = -50$, $k_2 = 100$, $\beta_1 = 4$, $\beta_2 = 2$, $a_{12} = 20$, and $a_{21} = -a_{12}$. The equilibrium for the system (3.27) for these parameters is $n_1 = 10$ and $n_2 = 10$. Therefore, the quantity $W(n) = 60$. For simulations, we choose as the initial condition the point $x(0) = [25\ 25]^T$. We will test two scenarios for W^*: $W(n) < W^* < W(x(0))$ and $W^* \leq W(n) < W(x(0))$.

For the case $W(n) < W^* < W(x(0))$ (which means that the amplitude of oscillation of the system trajectory, indirectly measured by W, will decrease from the $W(x(0))$ level to the one corresponding to the set $\Gamma = \{x : W(x) = W^*\}$), we will choose $W^* = 70$, and apply the control law (3.25) without and with the disturbance input v. In particular, the control action (3.25) for our example is given by:

$$u_2(t) = -\gamma_2(W(x) - W^*)(x_2(t) - n_2) + v_2,$$

where it has been selected for simulations $\gamma_2 = 0.1$ and $v_2 = 10\sin(30t)$.

The phase portrait for the controlled system (3.27) is shown in Fig.3.3(a). As we can conclude, for the case without disturbance the trajectories of the closed-loop system converge to the desired limit cycle, indirectly measured by W, *i.e.*, the amplitude of oscillations of the system decreases from the initial level specified by $W(x(0))$ to the one corresponding to the set $\Gamma = \{x : W(x) = W^*\}$. For the case where there exists a disturbance, it is possible to see that the boundedness is kept with some deviations of trajectories around the limit cycle without achieving zero for none of the species. The behavior of W for the controlled system (3.27) without and with disturbance input is shown in Fig.3.3(b). Note that the signal W oscillates around the desired level W^* for the system with disturbance. This oscillation can be conveniently decreased by increasing the gain γ_2.

Fig.3.4 shows the results of simulation for the case $W^* < W(n) < W(x(0))$ where $W^* = 50$ was chosen. It is possible to see that the amplitude of oscillation of the system trajectory for the system (3.27), without disturbance, instead of to go to the desired oscillation level W^*, goes to the equilibrium point, and for the case where the disturbance is present, it oscillates with a small amplitude around the equilibrium point. The behavior of W can be seen in Fig.3.4(c).

Therefore, these results of numerical experiments confirm the theoretical findings of this section. However, let us consider in the next example a more practical and realistic problem in the electronics field.

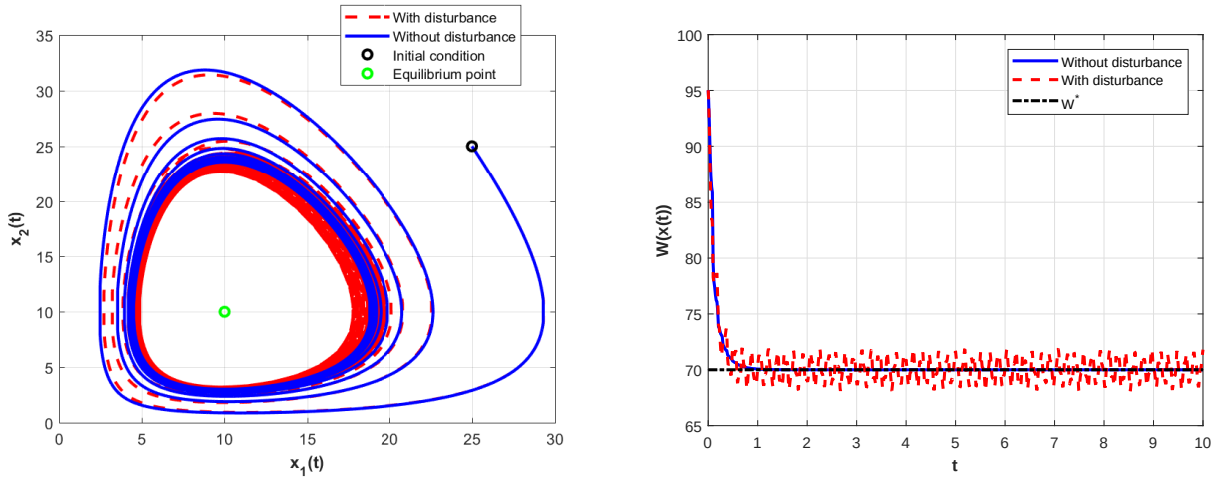

(a) (b)

Figure 3.3: (a) Phase portrait for the controlled system (3.27) without and with disturbance input (b) Behavior of W for the controlled system (3.27) without and with disturbance input. $W^* = 70$.

3.3.5 Noise-induced transition in a semiconductor-gas-discharge gap system

In this example, we consider a nonlinear dynamical model of a semiconductor-gas-discharge gap system. Such a system is presented schematically in Fig.3.5. It consists of two main components: a semiconductor layer (A) and a gas discharge domain (B). The planar structure is fed by a voltage source U_m that is connected to plane electrode (C) and (D), which are in contact with the semiconductor and gas discharge components, respectively [Kim et al., 2001]. The model of the system is supposed to be properly described by the following differential equations [Kim et al., 2001, Astrov et al., 2008]:

$$\begin{aligned} \dot{x}_1 &= -\frac{x_1}{\tau} + \frac{x_1 x_2}{\tau(E_c + v)}, \\ \dot{x}_2 &= -a x_2 - b x_1 x_2 + a E_m. \end{aligned} \tag{3.28}$$

where x_1 is the density of free charge carriers in the gap, and x_2 is the electric field strength in the discharge gap.

The first equation describes the dynamics of free carriers' density in the gap, which is governed by their generation and decay process. It is supposed that their generation's process prevails over their recombination when x_2 is larger than some critical electric field strength E_c.

The second equation describes the charging of capacity of the discharge gap from a source of feeding voltage and its discharging due to free carriers' presence in the gap. The characteristic time of the charging process is $\tau_E = 1/a$, and b is a coefficient. The maximal value of x_2 in the gap provided by a source of constant voltage is $E_m = U_m/d$ where U_m is the voltage of the fielding source d is the length of the gap in the direction of the electric current.

The generation of free carriers in the gas-discharge gap is provided by the avalanche of gas atoms and molecules' ionization. The efficiency of this process is known to fluctuate in time, which serves as a source of intrinsic noise. At a small current density, the device's intrinsic noise

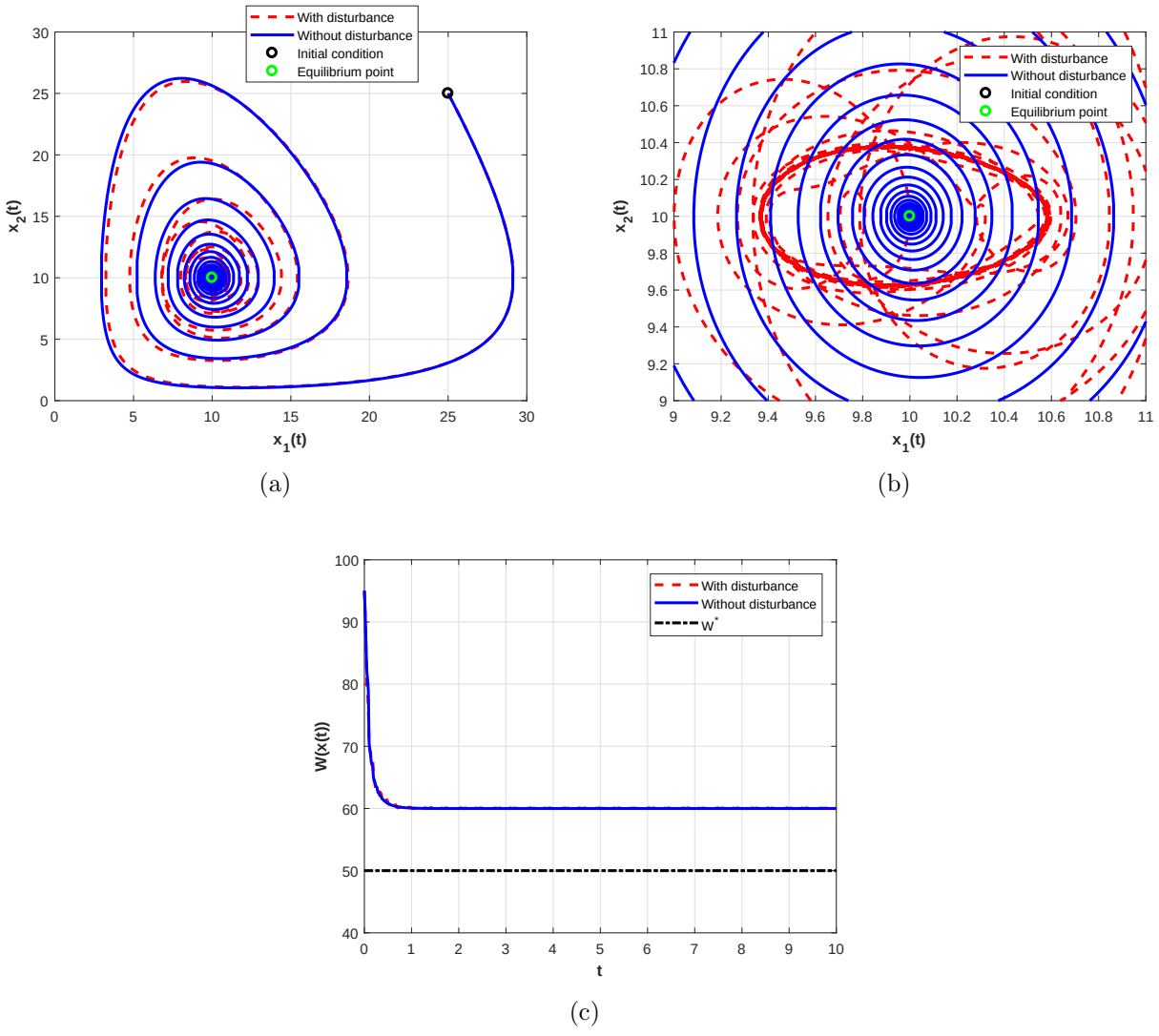

Figure 3.4: (a) Phase portrait for the controlled system (3.27) without (solid) and with (dashed) disturbance input (b) Fig.3.4(a) in zoomed version (c) Behavior of W for the controlled system (3.27) without (solid) and with (dashed) disturbance input. $W^* = 50$.

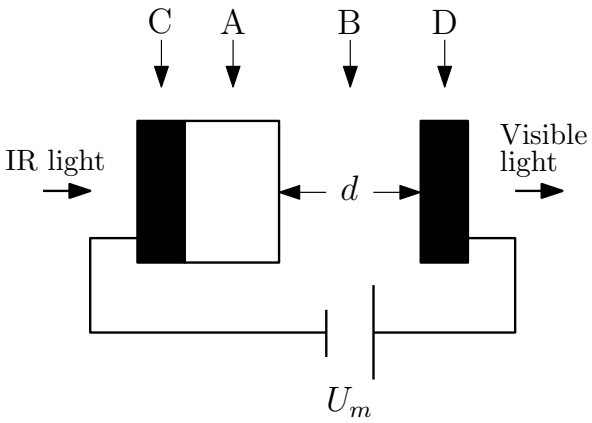

Figure 3.5: Schematic representation of a semiconductor-gas-discharge gap system

can initiate large amplitude oscillations in current, resulting in spontaneous interruption of the discharge process in the gap, *i.e.*, a transition from the conductive to the dielectric state of the system can occur [Astrov et al., 2008].

In a simple approach, the noise's influence on the system's dynamics can be simulated by adding a stochastic noise v to the parameter E_c. On the other hand, by physical principles of the device under consideration, it is suggested that control action can be played by properly varying the electric field strength E_m in time [Astrov et al., 2008]. Therefore, in this example, we are interested in defining the conditions for robust stabilization of the system with respect to the disturbance input $v > -E_c$. In other words, we are interested in knowing under what conditions the system dynamics remain within an appropriate operating region (in the vicinity of a given steady-state mode). For that, we proceed with the following analysis.

First let us analyze the system (3.28) for $E_m = 0$ and $v = 0$, therefore we have

$$\begin{aligned} \dot{x}_1 &= -\frac{x_1}{\tau} + \frac{x_1 x_2}{\tau E_c}, \\ \dot{x}_2 &= -a x_2 - b x_1 x_2, \end{aligned} \tag{3.29}$$

whose the stationary solutions are given by $n = (0,0)$ and $n = (-\frac{a}{b},E_c)$, and the latter equilibrium is unfeasible since the first state component is negative. For this system one could try to use

$$W(x) = \alpha_1 x_1 + \alpha_2 \ln(x_1) + \beta_1 x_1 + \beta_2 \ln(x_2) \tag{3.30}$$

as an invariant function, with posterior stabilization of its level using the SG method, it has been proposed in [Astrov et al., 2008]. If the values of the parameters α_1, α_2, β_1 and β_2 are properly chosen, then the derivative of W in the direction of the system (3.29) can be made equal to zero for $u = 0$. However, as it has been observed in our analysis, the level curves of this function are not closed and drive the system solutions to the origin, then stabilization of a level set of W does not lead to a solution for the proposed problem since almost all trajectories in the closed-loop are converging to the origin.

Another way to deal with this problem is to properly transform the original system (3.28), by means of an intermediate input signal in order to use the same auxiliary function (3.30), but with closed level curves. For instance, let us consider

$$E_m = u_0 x_2 + \delta u, \tag{3.31}$$

thus, the system (3.28) becomes

$$\begin{aligned} \dot{x}_1 &= -\frac{x_1}{\tau} + \frac{x_1 x_2}{\tau(E_c + v)}, \\ \dot{x}_2 &= a(u_0 - 1)x_2 - b x_1 x_2 + a\delta u. \end{aligned} \tag{3.32}$$

In this case, by choosing $u_0 > 1$, the system will have a positive equilibrium point $n = \left(\frac{a(u_0-1)}{b},E_c\right)$ and the auxiliary function (3.30) can be used as a conserved quantity for it with $\delta u = 0$. To illustrate better the problem, we can see by means of Fig.3.6 the behavior of W with respect to the system (3.32) when $\delta u = 0$, for $u_0 = 0$ and $u_0 = 2$, respectively.

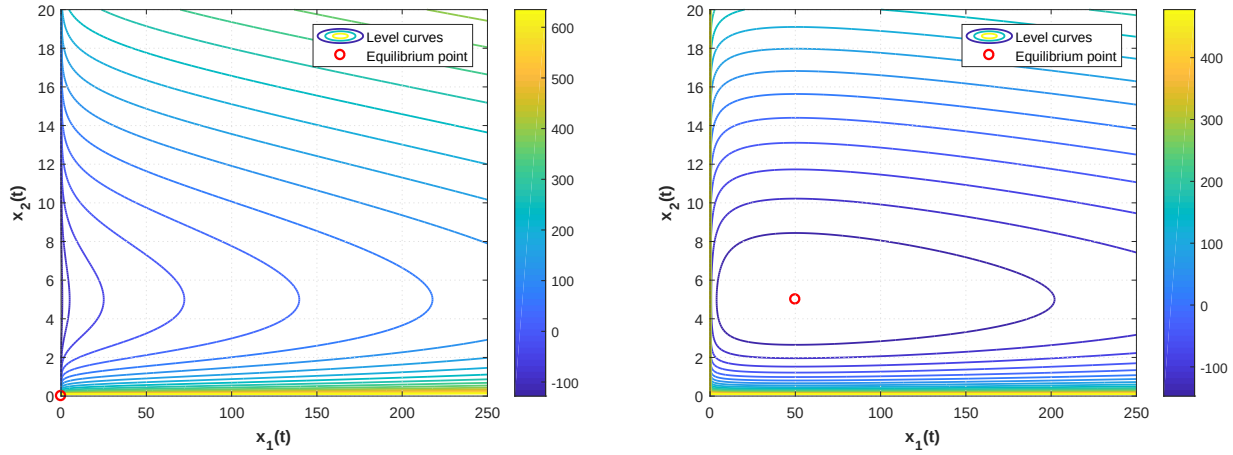

(a) (b)

Figure 3.6: Level curves of the function W for the system (3.32) in the cases (a) $u_0 = 0$, and (b) $u_0 = 2$

In the second case, the set of level curves that compose the phase space is formed by a set of closed orbits around the equilibrium point. Thus, the original problem's solution consists of finding a control law δu such that the regulated system oscillates as close as possible to the equilibrium point even under the influence of disturbances. To do so, let us first find the parameters α_1, α_2, β_1, and β_2 such that W is a constant quantity for the system (3.32) with $\delta u = 0$. For that we proceed with the derivative of W with respect to (3.32) assuming $v = 0$ and $\delta u = 0$. In this way, we achieve

$$\dot{W}(x) = \left(-\frac{\alpha_1}{\tau} - \beta_2 b\right) x_1 + \left(\beta_1 a(u_0 - 1) + \frac{\alpha_2}{\tau E_c}\right) x_2 + \left(\frac{\alpha_1}{\tau E_c} - \beta_1 b\right) x_1 x_2 + \beta_2 a(u_0 - 1) - \frac{\alpha_2}{\tau}, \quad (3.33)$$

that is equal to zero for $\alpha_1 = b$, $\alpha_2 = -a(u_0 - 1)$, $\beta_1 = \frac{1}{\tau E_c}$, and $\beta_2 = -\frac{1}{\tau}$. Therefore, we can rewrite (3.30) as

$$W(x) = bx_1 - a(u_0 - 1)\ln(x_1) + \frac{x_2}{\tau E_c} - \frac{\ln(x_2)}{\tau}. \quad (3.34)$$

Then, proceeding with the derivative of W in the direction of the system (3.32) for $v \neq 0$ and $\delta u \neq 0$ we obtain

$$\dot{W}(x,u) = \frac{a}{\tau}\left(\frac{x_2 - E_c}{E_c x_2}\right)\delta u + (a(u_0 - 1) - bx_1)\frac{x_2}{\tau}\frac{v}{E_c(E_c + v)}. \quad (3.35)$$

Introducing the auxiliary function

$$Q(x) = \frac{1}{2}(W(x) - W^*)^2, \quad (3.36)$$

where W^* is a desired level of W, which is reached provided that $Q(x(t)) \to 0$ as $t \to 0$, and calculating its derivative, we have

$$\dot{Q}(x,u) = (W(x) - W^*)\frac{a}{\tau}\left(\frac{x_2 - E_c}{E_c x_2}\right)\delta u + (W(x) - W^*)(a(u_0 - 1) - bx_1)\frac{x_2}{\tau}\frac{v}{E_c(E_c + v)}, \quad (3.37)$$

and as we can see, the system is passive without losses for $v = 0$ and $y = (W(x) - W^*)\frac{a}{\tau}\left(\frac{x_2 - E_c}{E_c x_2}\right)$.

Following the SG method, by calculating the derivative of Q with respect to δu we have

$$\frac{\partial \dot{Q}(x,u)}{\partial \delta u} = (W(x) - W^*)\frac{a}{\tau}\left(\frac{x_2 - E_c}{E_c x_2}\right), \quad (3.38)$$

therefore, we can choose

$$\delta u = -\gamma(W(x) - W^*)\frac{a}{\tau}\left(\frac{x_2 - E_c}{E_c x_2}\right), \quad (3.39)$$

where $\gamma > 0$ is a tuning gain. Then, by substituting (3.39) in ((3.40) we found

$$\dot{Q}(x,u) = -\gamma\left((W(x) - W^*)\frac{a}{\tau}\left(\frac{x_2 - E_c}{E_c x_2}\right)\right)^2 + (W(x) - W^*)(a(u_0 - 1) - bx_1)\frac{x_2}{\tau}\frac{v}{E_c(E_c + v)}. \quad (3.40)$$

As in the previous example, the set of all invariant solutions of the system for $v = 0$ is given by $\mathcal{W} = \{n\} \cup \Gamma$, where $\Gamma = \{x : W(x) = W^*\}$ and n is the positive equilibrium point.

Finally, to define the robust stability properties for the controlled system, let us introduce a new storage function $U(x) = \ln(1 + Q(x))$ and calculate its derivative. In this way, we obtain

$$\dot{U}(x,u) = \frac{-\gamma|y|^2}{1 + Q(x)} + \frac{r(x)\sigma(v)}{1 + Q(x)}. \quad (3.41)$$

where $r(x) = (W(x) - W^*)(a(u_0 - 1) - bx_1)\frac{x_2}{\tau}$, and $\sigma(v) = \frac{v}{E_c(E_c + v)}$. From (3.40) we can readily conclude that the weak zero-detectability property holds for the controlled system with respect to the input v (Definition 3.12). However, to provide the robust stability it is still necessary to analyze the behavior of the system for $v \neq 0$, *i.e.* verify the behavior of the functions r and σ. Fig.3.7 helps us to understand what is happen when x is evolving in $\mathcal{M} = \mathbb{R}^2_+$.

We can divide the analysis of r into two parts. By taking $n_1 = \frac{a(u_0 - 1)}{b}$ as a reference, one can see that the term $(a(u_0 - 1) - bx_1)x_2$ is positive when $x_1 < n_1$ and negative when $x_1 > n_1$. On the other hand, $(W - W^*)$ is positive outside the closed region bounded by W^* and negative inside this region. Thus, outside of the ball on the left-hand side and inside of the ball, we need to compute an upper bound of $\frac{r(x)}{1+Q(x)}$, and outside of the ball on the right-hand side, this term is already negative. Therefore, the second term's boundedness now depends on the sign of v that already cannot be equal to $-E_c$. Thus, by assuming that

$$v(t) \geq 0 \quad \forall t \geq 0$$

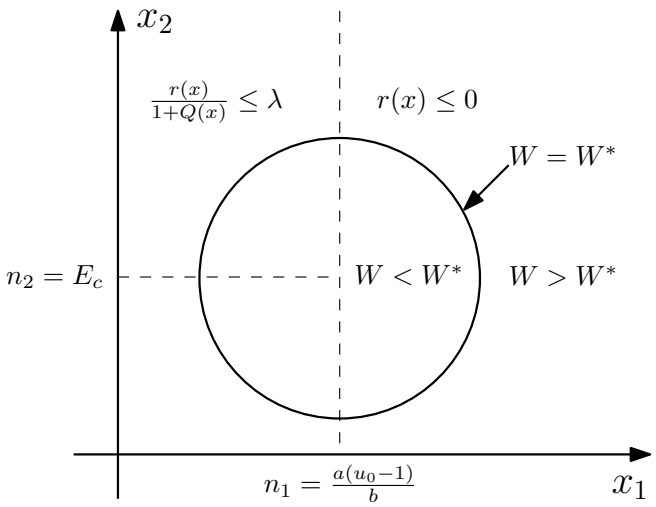

Figure 3.7: Scheme of the behavior of $r(x)$

we can guarantee that $\frac{r(x)}{1+Q(x)}$ is bounded:

$$\frac{r(x)}{1+Q(x)} \leq \begin{cases} 0 & \text{if } x_1 \geq n_1 \wedge W(x) \geq W^* \\ \lambda & \text{if } x_1 < n_1 \vee W(x) < W^*, \end{cases}$$

where $\lambda > 0$ is a constant, and we used boundedness of x_1 and W for its computation. Therefore, under this assumption, we conclude that the smooth dissipativity property holds (Definition 3.11) for the controlled system and the controlled system is iISS by means of the property 4 from Theorem 3.2:

$$\dot{U}(x,u) \leq -\frac{\gamma|y|^2}{1+Q(x)} + \lambda\sigma(v), \tag{3.42}$$

which is in accordance with Theorem 3.4.

To illustrate the convergence of the system trajectories to the set $\mathcal{W}$, specifically for $W = W^*$, a desired oscillation level, we choose for the system (3.32) the parameters $a = 20s^{-1}$, $b = 0.4cm^3/s$, $\tau = 5 \times 10^{-3}s$, and $E_c = 5V/cm$. It is used a uniformly distributed stochastic noise with an amplitude equal to 0.02, representing 0.4% of E_c. These values were re-scaled to facilitate the result's simulation and analysis. Values in correspondence with physical parameters of the real device can be found in [Kim et al., 2001, Astrov et al., 2008]. The control input applied to the system is given by

$$u = -\gamma(W(x) - W^*)\frac{a}{\tau}\left(\frac{x_2 - E_c}{E_c x_2}\right) + u_0 x_2. \tag{3.43}$$

where $u_0 = 2$.

As we can see in Fig.3.8(a) the system states evolve near to the equilibrium point $n = (50{,}5)$ with the desired amplitude, which makes the state x_1 approximately oscillating between 49.5 and 50.5 and x_2 between 4.98 and 5.02, for that, it was chosen $W^* = W(n) + 0.001$, where $W(n)$ is an energy level of the system in the equilibrium point. From Fig.3.8(b) it is possible to observe that $Q(x) \to 0$ as $t \to \infty$ for the system without disturbance. In another way, we can note that the proposed control is working to keep Q tending to zero as the time goes to infinity for the system with disturbances.

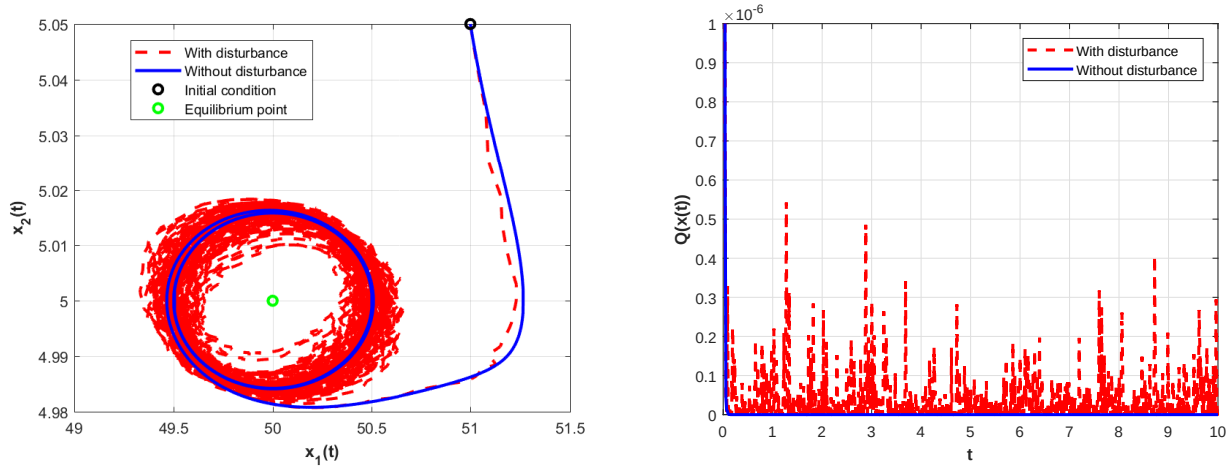

(a) (b)

Figure 3.8: (a) Phase portrait for the controlled system (3.32) without and with disturbance input (b) Behavior of the function Q

3.4 Control Lyapunov Function for robust stabilization of affine multistable systems

In this section, we continue to study the problem of robust stabilization of affine nonlinear multistable systems in the presence of exogenous disturbances. The results are based on the theory of input-to-state stability (ISS) and integral input-to-state stability (iISS) for systems with multiple invariant sets, introduced previously in this chapter. The notions of ISS and iISS control Lyapunov functions (CLFs) and the small control property are extended within the multistability framework. Such properties are also complemented by the concept of a weak iISS CLF and corresponding small control property. It is verified that the universal control formula can be applied to yield the ISS (iISS or weak iISS) property for the closed-loop system. The extended CLF framework's efficiency in the multistable sense is illustrated for two academic examples, a Duffing and Brockett oscillator systems and in application to a noise-induced transition in a semiconductor-gas-discharge gap system.

3.4.1 Problem statement

In this section, we deal with a class of nonlinear dynamical systems that are affine in the input of the following form:

$$\dot{x}(t) = f(x(t),v(t)) + G(x(t))u(t), \quad t \in \mathbb{R}_+, \tag{3.44}$$

$$y(t) = h(x(t)), \tag{3.45}$$

where $x(t) \in \mathcal{M}$ is the state vector; $v(t) \in \mathbb{R}^k$ is a disturbance with $v \in \mathcal{L}_\infty(\mathbb{R}_+,\mathbb{R}^k)$; $u(t) \in \mathbf{U} \subseteq \mathbb{R}^m$ is the input vector and $u \in \mathcal{U} = \mathcal{L}_\infty(\mathbb{R}_+,\mathbf{U})$, where $\mathbf{U}$ defines the set of admissible values for the control; $y(t) \in \mathcal{Y} \subseteq \mathbb{R}^p$ is the corresponding output vector. For this system, $f : \mathcal{M} \times \mathbb{R}^k \to \mathbb{R}^n$ and the columns of the matrix $G : \mathcal{M} \to \mathbb{R}^{n\times m}$ are assumed to be locally

Lipschitz continuous on $\mathcal{M}$. We also assume that $f(0,0) = h(0) = 0$ (without loosing generality let $x_{or} = 0 \in \mathcal{M}$).

Definition 3.15. *Systems in the form (3.44), (3.45) are said to be* iISS (ISS) stabilizable *if there exists a control law $u = K(x)$, where $K : \mathcal{M} \to \mathbf{U}$, rendering the closed-loop system with the iISS (ISS) property from v with respect to a given set $\mathcal{W} \subset \mathcal{M}$.*

Therefore, the problem studied in this section can be formally determined as follows:

Problem 3.2. *For the model (3.44), (3.45) under Assumption 3.1 find the conditions of its ISS(iISS) stabilizability by u from v with respect to $\mathcal{W}$.*

3.4.2 Practical iISS (ISS) CLF and small control property

As in the case of iISS/ISS stabilization with respect to a compact set [Liberzon et al., 1999, Sontag, 1989], we search for existence conditions of stabilizing feedback using the CLF framework. To present our main result, we introduce a suitable notion of iISS (ISS) CLF in a multistability framework.

Definition 3.16. *A* practical ISS CLF *for the system* (3.44), (3.45) *and control $u \in \mathcal{U}$ is a continuously differentiable function $V : \mathcal{M} \to \mathbb{R}_+$ satisfying:*

(1) There exist $\mathcal{K}_\infty$ functions α_1, α_2 and $c \geq 0$ such that

$$\alpha_1(|x|_{\mathcal{W}}) \leq V(x) \leq \alpha_2(|x|_{\mathcal{W}}) + c \tag{3.46}$$

for all $x \in \mathcal{M}$, and $\frac{\partial V(x)}{\partial x} = 0$ for any $x \in \mathcal{W}$.

(2) There exist $\mathcal{K}_\infty$ functions χ, α_3 and $q \geq 0$ such that for all $x \in \mathcal{M}$ and all $v \in \mathbb{R}^k$:

$$\inf_{u \in \mathbf{U}} \{a(x,v) + b(x)u\} \leq -\alpha_3(|x|_{\mathcal{W}}) + \chi(|v|) + q, \tag{3.47}$$

where $a(x,v) = DV(x)f(x,v)$, $b(x) = DV(x)G(x)$.

If (3.47) *holds for $q = 0$, then V is an* ISS CLF. *In addition, V is an* iISS CLF *if both items are satisfied for $q = 0$ and for a continuous positive definite function $\alpha_3 : \mathbb{R}_+ \to \mathbb{R}_+$.*

Observe that the inequality (3.47) can be rewritten as follows:

$$\inf_{u \in \mathbf{U}} \{a(x,v) - \tilde{\chi}(|v|) - q + b(x)u\} \leq -\alpha_3(|x|_{\mathcal{W}}),$$

where $\tilde{\chi} \in \mathcal{K}_\infty$ satisfies $\tilde{\chi}(s) \geq \chi(s)$ for all $s \in \mathbb{R}_+$ and such that there exists a function

$$\psi(x) = \sup_{v \in \mathbb{R}^k} \{a(x,v) - \tilde{\chi}(|v|) - q\}, \, \forall x \in \mathcal{M}$$

(supremum over all disturbances v), *e.g.*, take $\tilde{\chi}(s) = \max\{\chi(s), \sup_{|x|,|v| \leq s} |a(x,v)|\}$ for any $s \in \mathbb{R}_+$ [Liberzon et al., 1999], then with such a choice

$$\psi(x) = \sup_{|v| \leq |x|} \{a(x,v) - \tilde{\chi}(|v|) - q\}.$$

By construction $\psi(x) \leq 0$ for all $x \in \mathcal{W}$. Since a is at least Lipschitz continuous in x, then the function ψ admits the same property. In addition, for all $x \in \mathcal{M}$

$$\inf_{u \in \mathbf{U}} \{\psi(x) + b(x)u\} \leq -\alpha_3(|x|_{\mathcal{W}}).$$

Finally, define $\Psi(x) = \psi(x) + \frac{1}{2}\alpha_3(|x|_{\mathcal{W}})$, then, for all $x \in \mathcal{M}$ and all $v \in \mathbb{R}^k$:

$$\Psi(x) \geq \frac{1}{2}\alpha_3(|x|_{\mathcal{W}}) + a(x,v) - \tilde{\chi}(|v|) - q,$$
$$\inf_{u \in \mathbf{U}} \{\Psi(x) + b(x)u\} \leq -\frac{1}{2}\alpha_3(|x|_{\mathcal{W}}).$$

Conclude that now the condition (3.47) can be replaced with another one:

$$b(x) = 0 \Rightarrow \Psi(x) \leq -\frac{1}{2}\alpha_3(|x|_{\mathcal{W}}) \tag{3.48}$$

for all $x \in \mathcal{M}$, and α_3 is in the class $\mathcal{K}_\infty$ or a positive definite function for the cases of ISS or iISS, respectively. Therefore, the condition (3.48) formulates the main restriction to be checked for an iISS (ISS) CLF in the system (3.44),(3.45).

Definition 3.17. *A continuously differentiable function $V : \mathcal{M} \to \mathbb{R}_+$ possesses* small control property *(SCP) if for each $\varepsilon > 0$ there is a $\delta > 0$ such that whenever $0 < |x|_{\mathcal{W}} < \delta$ there exists some control $u \in \mathbf{U}$ with $|u| < \varepsilon$ such that*

$$\Psi(x) + b(x)u < 0.$$

Let $\mathbf{U} = \mathbb{R}^m$, then following the CLF framework from [Sontag, 1989, Liberzon et al., 2002], we will use the "universal" control formula, which in our case takes the form for all $x \in \mathcal{M}$:

$$u = K(x) = \begin{cases} \kappa(\Psi(x), |b(x)|^2) b(x)^\top & \text{if } x \notin \mathcal{W} \\ 0 & \text{if } x \in \mathcal{W} \end{cases}, \tag{3.49}$$

where $\kappa : \mathbb{R}_+ \times \mathbb{R}_+ \to \mathbb{R}$ is defined by

$$\kappa(s,r) = -\frac{s + \sqrt{s^2 + r^2}}{r}. \tag{3.50}$$

The chosen form of the function κ in (3.50) corresponds to $\mathbf{U} = \mathbb{R}^m$. Then with mild modifications and by applying the formulas given in [Lin and Sontag, 1995], for example, similar results can be obtained for other classes of $\mathbf{U}$ (with bounded controls). According to the above developments, we propose the following theorem:

Theorem 3.6. *Let Assumption 3.1 be satisfied. If the function $V : \mathcal{M} \to \mathbb{R}_+$ is an iISS (ISS) CLF, then the feedback law (3.49) is continuous in $\mathcal{M} \setminus \mathcal{W}$ and it provides for (3.44) the iISS (ISS) property from v with respect to $\mathcal{W}$. If such a CLF satisfies the SCP (given in Definition 3.17), then the control (3.49) is continuous on $\mathcal{M}$.*

Proof. First of all note that the control (3.49) is continuous on $\mathcal{M}\setminus\mathcal{W}$ by the standard argumentation [Sontag, 1989]. Indeed, it was shown in the proof of Theorem 1 of [Sontag, 1989] that the function $\kappa(s,r)$ is continuous for $(s,r) \in S = \{(s,r) \in \mathbb{R}^2 : r > 0 \text{ or } s < 0\}$, and $(\Psi(x),|b(x)|^2) \in S$ due to (3.48) and the definition of the control (3.49). Next, consider (3.44) and assume that V is an ISS CLF. With (3.49) and since $\tilde{\chi}(|v|)+q-\frac{1}{2}\alpha_3(|x|_{\mathcal{W}}) \geq a(x,v)-\Psi(x)$ by construction, computing the derivative of V along the solution of the closed-loop system, $\dot{x} = f(x,v)+G(x)K(x)$, we obtain for all $x \notin \mathcal{W}$ (denote a short hand $\dot{V} = DV(x)[f(x,v) + G(x)K(x)]$):

$$\begin{aligned}
\dot{V} &= a(x,v) + b(x)K(x) \\
&= a(x,v) + \kappa(\Psi(x),|b(x)|^2)|b(x)|^2 \\
&= a(x,v) - \Psi(x) - \sqrt{\Psi^2(x) + |b(x)|^4} \\
&\leq \tilde{\chi}(|v|) + q - \frac{1}{2}\alpha_3(|x|_{\mathcal{W}}) - \sqrt{\Psi^2(x) + |b(x)|^4} \\
&\leq -\frac{1}{2}\alpha_3(|x|_{\mathcal{W}}) + \tilde{\chi}(|v|) + q, \qquad (3.51)
\end{aligned}$$

which shows that V is an ISS Lyapunov function for the closed-loop system. Therefore, according to Theorem 3.1, the closed-loop system is ISS from v with respect to $\mathcal{W}$ as needed. The same analysis can be done by considering V as an iISS CLF for (3.51). In this case, $q = 0$ and α_3 is just a positive definite function, and the closed-loop system is iISS by means of the existence of an iISS Lyapunov function (Theorem 3.2).

Now, we will show that if V satisfies the SCP, then u is also continuous at $\mathcal{W}$. Since $u = 0$ whenever $b(x) = 0$ or $x \in \mathcal{W}$, we can assume that $b(x) \neq 0$ and $x \notin \mathcal{W}$ in what follows. Let us analyze the amplitude of the control law (3.49) rewriting it as

$$|u| = |\kappa(\Psi(x),|b(x)|^2)||b(x)| = \frac{|\Psi(x) + \sqrt{\Psi(x)^2 + b(x)^4}|}{|b(x)|}. \qquad (3.52)$$

The gradient of V is continuous and zero on the set $\mathcal{W}$, then for any $\varepsilon > 0$ there is $\delta > 0$ such that $|b(x)| \leq \varepsilon$ when $|x|_{\mathcal{W}} \leq \delta$. Similarly for $\Psi(x) = \psi(x) + \frac{1}{2}\alpha_3(|x|_{\mathcal{W}})$, where the function ψ is locally Lipschitz continuous, from SCP of V (Definition 3.17) we know that for each $\varepsilon > 0$ there is a $\delta > 0$ such that

$$\Psi(x) < |b(x)|\varepsilon$$

with $|x|_{\mathcal{W}} \leq \delta$, hence, the positive value of Ψ is upper bounded in the vicinity $|x|_{\mathcal{W}} \leq \delta$ by ε^2.

Now let us analyze (3.52) for $\Psi(x) \leq 0$ and any $|x|_{\mathcal{W}} \leq \delta$:

$$|u| \leq \frac{|\Psi(x) + |\Psi(x)| + b(x)^2|}{|b(x)|} = |b(x)| \leq \varepsilon.$$

On the other hand, in the case when $\Psi(x) > 0$, we obtain for $|x|_{\mathcal{W}} \leq \delta$:

$$|u| \leq \frac{|\Psi(x)| + \sqrt{\Psi(x)^2 + b(x)^4}}{|b(x)|} \leq 2\frac{|\Psi(x)|}{|b(x)|} + |b(x)| \leq 3\varepsilon,$$

and since ε is arbitrary, that implies the continuity of the control (3.49) on the set $\mathcal{W}$ also. □

Note that $V(x) = 0$ for $x \in \mathcal{A}$ in some subset $\mathcal{A} \subset \mathcal{W}$ (where V reaches its minimum; and it has other kinds of extremum for the decomposition components in $\mathcal{W} \setminus \mathcal{A}$), then the control (3.49) provides almost global or local attraction of the set $\mathcal{A}$ in the case $v = 0$. A direct consequence of our main result is given as follows:

Lemma 3.2. *Let Assumption 3.1 be satisfied. Then there exists a continuous control $u = K(x)$ that provides for* (3.44) *the iISS (ISS) property from v with respect to $\mathcal{W}$ if and only if the system admits an iISS (ISS) CLF with SCP.*

Proof. The proof that the existence of a CLF with SCP implies the corresponding stability property under a continuous control (3.49) is presented in Theorem 3.6. Conversely, assume that there is a continuous feedback u that renders the closed-loop system iISS (ISS) in v with respect to $\mathcal{W}$, then by Theorem 3.2 or 3.1 there is a corresponding Lyapunov function (constant on $\mathcal{W}$), which can serve as a searched CLF. □

3.4.3 Weak iISS CLF and small control property

The notion of CLF can be extended for the iISS case by means of *relaxed* concepts of the output smooth dissipativity and the weak zero-detectability (definitions 3.11 and 3.12, respectively), whose existence also is equivalent to iISS (Theorem 3.2). In such a case we can introduce a weak iISS CLF as follows:

Definition 3.18. *A* weak iISS CLF *for the system* (3.44), (3.45) *and control $u \in \mathcal{U}$ is a continuously differentiable function $V : \mathcal{M} \to \mathbb{R}_+$ satisfying:*

(1) There exist $\mathcal{K}_\infty$ functions α_1,α_2, and χ, a continuous positive definite function $\alpha_4 : \mathbb{R}_+ \to \mathbb{R}_+$, and a continuous output map $h : \mathcal{M} \to \mathbb{R}^p$ with

$$\mathcal{W} \subseteq \mathcal{Z} = \{x \in \mathcal{M} : h(x) = 0\}$$

such that (3.46) *is satisfied for all $x \in \mathcal{M}$, $b(x) = 0$ for any $x \in \mathcal{Z}$, and the following dissipation inequality holds for all $x \in \mathcal{M}$ and all $v \in \mathbb{R}^k$:*

$$\inf_{u \in \mathbf{U}} \{a(x,v) + b(x)u\} \leq -\alpha_4(|h(x)|) + \chi(|v|). \tag{3.53}$$

(2) The system (3.44), (3.45) *has the weak zero-detectability property for $v \equiv 0$ and $u \equiv 0$.*

Following the same reasoning as above, we can rewrite (3.53) as:

$$\inf_{u \in \mathbf{U}} \{a(x,v) - \tilde{\chi}(|v|) + b(x)u\} \leq -\alpha_4(|h(x)|),$$

where $\tilde{\chi} \in \mathcal{K}_\infty$ is such that $\tilde{\chi}(s) \geq \chi(s)$ for all $s \in \mathbb{R}_+$, then, $\psi_o(x) = \sup_{v \in \mathbb{R}^k}\{a(x,v) - \tilde{\chi}(|v|)\}$ is well defined. The function $\tilde{\chi}$ is selected in a way that $\psi_o(x) \leq 0$ for all $x \in \mathcal{Z}$, and since a is at least Lipschitz continuous in x, then the function ψ_o admits the same property. In addition,

$$\inf_{u \in \mathbf{U}} \{\psi_o(x) + b(x)u\} \leq -\alpha_4(|h(x)|)$$

for all $x \in \mathcal{M}$. Finally, by defining $\Psi_o(x) = \psi_o(x) + \frac{1}{2}\alpha_4(|h(x)|)$ we have:

$$\Psi_o(x) \geq \frac{1}{2}\alpha_4(|h(x)|) + a(x,v) - \tilde{\chi}(|v|),$$

therefore,

$$\inf_{u\in\mathbf{U}}\{\Psi_o(x) + b(x)u\} \leq -\frac{1}{2}\alpha_4(|h(x)|),$$

for all $x \in \mathcal{M}$ and $v \in \mathbb{R}^k$. Observe that for this case the condition (3.53) can be replaced by:

$$b(x) = 0 \Rightarrow \Psi_o(x) \leq -\frac{1}{2}\alpha_4(|h(x)|) \tag{3.54}$$

for all $x \in \mathcal{M}$ and a positive definite function α_4.

Definition 3.19. *A weak iISS CLF $V : \mathcal{M} \to \mathbb{R}_+$ possesses a variant of SCP if for each $\varepsilon > 0$ there is $\delta > 0$ such that there exists some control $u \in \mathbf{U}$ with $|u| < \varepsilon$ providing*

$$\Psi_o(x) + b(x)u < 0 \tag{3.55}$$

whenever $0 < |x|_{\mathcal{Z}} < \delta$.

Hence, taking into account the weakly zero-detectability property, the condition (3.54) formulates the main restriction to be checked for a weak iISS CLF in the system (3.44), (3.45) and we can formulate the following theorem.

Theorem 3.7. *Let Assumption 3.1 be satisfied. If the function $V : \mathcal{M} \to \mathbb{R}_+$ is a weak iISS CLF, then the feedback law*

$$u = K(x) = \begin{cases} \kappa(\Psi_o(x),|b(x)|^2)b(x)^\top & \text{if } x \notin \mathcal{Z} \\ 0 & \text{if } x \in \mathcal{Z} \end{cases}, \tag{3.56}$$

is a continuous function in $\mathcal{M}\setminus\mathcal{Z}$ (with κ as in (3.50)*) providing* (3.44), (3.45) *the iISS property from v with respect to $\mathcal{W}$. If such a CLF satisfies the SCP (given in Definition 3.19), then the control (3.56) is continuous on $\mathcal{M}$.*

Proof. The proof comes from the same ideas applied in the proof of Theorem 3.6. Note, first, that the control (3.56) is continuous on $\mathcal{M}\setminus\mathcal{Z}$ by the usual argumentation [Sontag, 1989]. Next, consider (3.44), (3.45) and assume that V is a weak iISS CLF. By means of control (3.56) and since $\tilde{\chi}(|v|) - \frac{1}{2}\alpha_4(|h(x)|) \geq a(x,v) - \Psi_o(x)$ by construction, the derivative of V along the solution of the closed-loop system, $\dot{x} = f(x,v) + G(x)K(x)$, is given by

$$\begin{aligned}
\dot{V} &= a(x,v) + b(x)K(x) \\
&= a(x,v) + \kappa(\Psi_o(x),|b(x)|^2)|b(x)|^2 \\
&= a(x,v) - \Psi_o(x) - \sqrt{\Psi_o^2(x) + |b(x)|^4} \\
&\leq \tilde{\chi}(|v|) - \frac{1}{2}\alpha_4(|h(x)|) - \sqrt{\Psi_o^2(x) + |b(x)|^4} \\
&\leq -\frac{1}{2}\alpha_4(|h(x)|) + \tilde{\chi}(|v|),
\end{aligned}$$

which shows that and V provides the output dissipation inequality, then under the weak-zero detectability property the closed-loop system is iISS with respect to $\mathcal{W}$ (by Theorem 3.2).

The SCP in this case implies that for any $\varepsilon > 0$ there is $\delta > 0$ such that $|b(x)| \leq \varepsilon$ when $|x|_{\mathcal{Z}} \leq \delta$. Similarly for $\Psi_o(x) = \psi_o(x) + \frac{1}{2}\alpha_4(|h(x)|)$, where the function ψ_o is locally Lipschitz continuous and α_4 is a positive definite function of a continuous function h with $|x|_{\mathcal{W}} = 0$ implying $h(x) = 0$. Then, from the SCP (Definition 3.19) we know that for each $\varepsilon > 0$ there is a $\delta > 0$ such that

$$\Psi_o(x) = \psi_o(x) + \frac{1}{2}\alpha_4(|h(x)|) < |b(x)|\varepsilon.$$

Therefore, the rest of the proof follows the same arguments given in Theorem 3.6 and we can conclude the continuity of the control (3.56) on the set $\mathcal{Z}$. □

Remark 3.1. *A difference between iISS CLF (Definition 3.16) and its weak formulation (Definition 3.18) is that the derivative of the latter, when $u = 0$ in (3.56) and $v = 0$, is not zero (in general case, the trajectory is in $\mathcal{Z}$ and has to converge to $\mathcal{W}$) while the former with the control (3.49) in such a case implies that the trajectory is already at $\mathcal{W}$.*

3.4.4 Duffing system

Consider the following variant of Duffing system (our motivating example in this chapter):

$$\begin{aligned} \dot{x}_1(t) &= x_2(t) + u(t) + v_1(t), \\ \dot{x}_2(t) &= -x_2(t) + x_1(t)(x_1^2(t) - 1) + v_2(t), \end{aligned} \tag{3.57}$$

where $x(t) = (x_1(t)\ x_2(t))^\top \in \mathcal{M} = \mathbb{R}^2$, $u(t) \in \mathbb{R}$ and $v(t) = (v_1(t)\ v_2(t))^\top \in \mathbb{R}^2$ have the same sense as before. It is straightforward to check that for $u = 0$ and $v = 0$ the system has three equilibria, thus, $\mathcal{W} = \{(-1,0),(0,0),(1,0)\}$. Linearization shows that the origin is a locally asymptotically stable steady-state, and the two equilibria, $(-1,0)$ and $(1,0)$ are unstable foci (see Fig.3.9(a)). Select $\mathcal{A} = \{(-1,0),(1,0)\}$ as the subset of $\mathcal{W}$ that will be almost globally attractive in the closed-loop system. To this end, as a CLF candidate, choose

$$V(x) = \frac{1}{4}(x_1^2 - 1)^2 + \frac{1}{2}x_2^2,$$

whose derivative for the oscillator takes the usual form $\dot{V} = a(x,v) + b(x)u$, where $a(x,v) = 2x_1(x_1^2 - 1)x_2 - x_2^2 + x_1(x_1^2 - 1)v_1 + x_2v_2$, $b(x) = x_1(x_1^2 - 1)$.

Select $\chi(s) = s^2$, then

$$a(x,v) - \chi(|v|) = \begin{pmatrix} x_1(x_1^2 - 1) \\ x_2 \\ v_1 \\ v_2 \end{pmatrix}^\top Q \begin{pmatrix} x_1(x_1^2 - 1) \\ x_2 \\ v_1 \\ v_2 \end{pmatrix} - \frac{1}{4}x_2^2 + 2.3x_1^2(x_1^2 - 1)^2,$$

where

$$Q = \begin{pmatrix} -2.3 & 1 & 0.5 & 0 \\ 1 & -0.75 & 0 & 0.5 \\ 0.5 & 0 & -1 & 0 \\ 0 & 0.5 & 0 & -1 \end{pmatrix}$$

is a negative definite matrix. Hence, we can take

$$\psi(x) = -\frac{1}{4}x_2^2 + 2.3x_1^2(x_1^2-1)^2 \geq a(x,v) - \chi(|v|).$$

Next, let

$$|x|_{\mathcal{W}} = \sqrt{x_2^2 + x_1^2(x_1^2-1)^2}$$

and $\alpha_3(s) = \frac{1}{4}s^2$, then we obtain

$$\Psi(x) = \psi(x) + \frac{1}{2}\alpha_3\left(|x|_{\mathcal{W}}\right),$$

and it is easy to check that

$$b(x) = 0 \Rightarrow \Psi(x) \leq -\frac{1}{2}\alpha_3\left(|x|_{\mathcal{W}}\right).$$

Consequently, V is a CLF and for any $\varepsilon > 0$ there is a $\delta > 0$ such that whenever $0 < |x|_{\mathcal{W}} < \delta$ there exists some control $|u| < \varepsilon$ such that

$$\Psi(x) + b(x)u < 0,$$

then SCP holds, and the control (3.49) is continuous in $\mathbb{R}^2$.

The behavior of the controlled system is shown in Fig.3.9(b). Note that with the applied control the two unstable foci become almost attractive in the closed-loop system. The effect for the noise for both the open-loop and closed-loop is also shown in Fig.3.9(c). Observe that by starting the system from the same initial conditions the control action forces the trajectories to different attractors. To generate the plots the noise signals were chosen $v_1(t) = v_2(t) = 0.2\sin(10t)$.

3.4.5 Brockett oscillator

The Brockett oscillator system [Brockett, 2013] has the following model:

$$\begin{aligned} \dot{x}_1(t) &= x_2(t) + v_1(t), \\ \dot{x}_2(t) &= -x_1(t) - \beta x_2(t)\left(|x(t)|^2 - 1\right) + \alpha u(t) + v_2(t), \end{aligned} \tag{3.58}$$

where again $x(t) = (x_1(t)\ x_2(t))^\top \in \mathcal{M} = \mathbb{R}^2$, $u(t) \in \mathbb{R}$ and $v(t) = (v_1(t)\ v_2(t))^\top \in \mathbb{R}^2$; $\alpha > 0$ and $\beta > 0$ are constant parameters. For $u = 0$ and $v = 0$ the system has the equilibrium at the origin and an attracting from almost all initial conditions limit cycle on the unit sphere $\mathbb{S} = \{x \in \mathbb{R}^2 : |x| = 1\}$, thus, $\mathcal{W} = \{(0,0),\mathbb{S}\}$ as shown in Fig.3.10(a) [Ahmed et al., 2018].

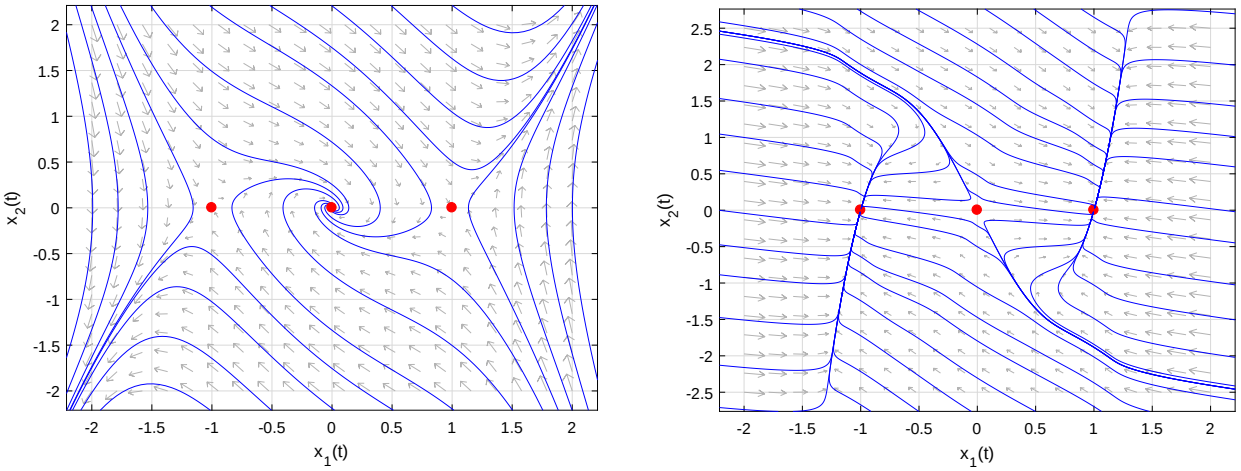

(a) (b)

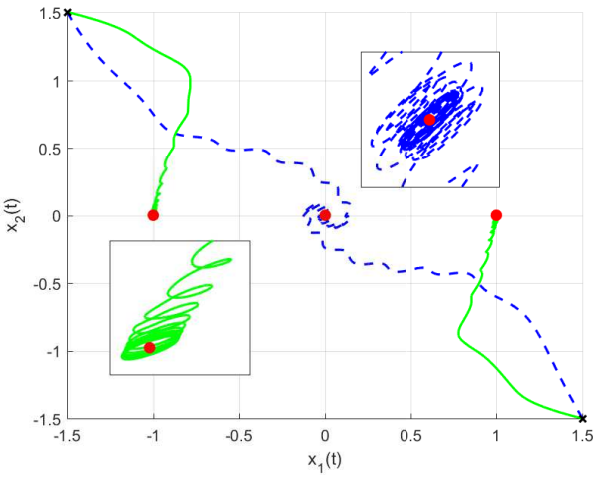

(c)

Figure 3.9: Phase portraits: (a) System without control (b) Controlled system with disturbance (c) Detail of a trajectory convergence for the system with disturbance: without control (dashed line), with control (solid line)

Assume that $\mathcal{A} = \{(0,0)\}$, which in our example will be locally attracting, and choose in this case as a CLF:

$$V(x) = \frac{1}{2}(x_1 + x_2)^2 + \frac{1}{2}x_1^2,$$

whose derivative for the Brockett oscillator admits $a(x,v) = -x_1^2 + (x_1 + x_2)x_2\,(1 + \beta - \beta|x|^2) + (2x_1 + x_2)v_1 + (x_1 + x_2)v_2$, $b(x) = \alpha(x_1 + x_2)$.

Select $\chi(s) = s^2$, and similarly we get

$$a(x,v) - \chi(|v|) = \begin{pmatrix} x_1 \\ x_1 + x_2 \\ v_1 \\ v_2 \end{pmatrix}^\top Q \begin{pmatrix} x_1 \\ x_1 + x_2 \\ v_1 \\ v_2 \end{pmatrix} - \frac{1}{2}x_1^2 + (x_1 + x_2)^2 + (x_1 + x_2)x_2[1 + \beta - \beta|x|^2],$$

where

$$Q = \begin{pmatrix} -0.5 & 0 & 0.5 & 0 \\ 0 & -1 & 0.5 & 0.5 \\ 0.5 & 0.5 & -1 & 0 \\ 0 & 0.5 & 0 & -1 \end{pmatrix}$$

is a negative definite matrix. Therefore, we can accept

$$\psi(x) = -\frac{1}{2}x_1^2 + (x_1 + x_2)^2 + (x_1 + x_2)x_2\left(1 + \beta - \beta|x|^2\right),$$

and, finally take

$$|x|_{\mathcal{W}} = \frac{|x|}{\sqrt{1 + |x|^2}}\sqrt{|1 - |x|^2|}$$

with $\alpha_3(s) = \frac{1}{4}s^2$. Then, as before

$$\Psi(x) = \psi(x) + \frac{1}{2}\alpha_3\left(|x|_{\mathcal{W}}\right),$$

and the main restriction for V to be a CLF,

$$b(x) = 0 \Rightarrow \Psi(x) \leq -\frac{1}{2}\alpha_3\left(|x|_{\mathcal{W}}\right)$$

is satisfied. However, it is impossible to demonstrate the SCP property in this case due to the term $(x_1 + x_2)x_2\,(1 + \beta - \beta|x|^2)$ in $\Psi(x)$ which is not approaching to zero while x becomes close to $\mathbb{S}$. Therefore, in this example the control (3.49) will be discontinuous on $\mathbb{S}$ and the solutions have to be understood in the sense of [Yakubovich et al., 2004].

The effect of the noise for both the open-loop and closed-loop systems with $\alpha = \beta = 1$ is shown in Fig.3.10(b). Again, observe that by initiating the system from the same initial conditions, the control action forces the trajectories to different attractors. In simulation the noise signals also were chosen as $v_1(t) = v_2(t) = 0.2\sin(10t)$.

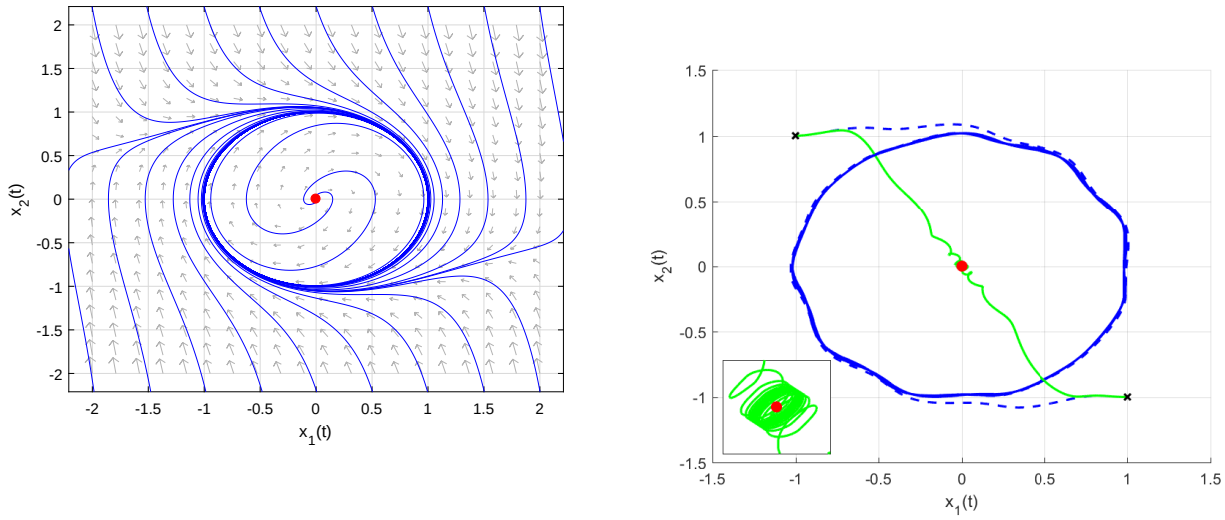

(a) (b)

Figure 3.10: Phase portraits: (a) System without control (b) Detail of a trajectory convergence for the system with disturbance: without control (dashed line), with control (solid line)

3.4.6 Noise-induced transition in a semiconductor-gas-discharge gap system

To illustrate the iISS CLF application in the multistable sense, we revisit the semiconductor-gas-discharge gap affected by parametric noise resonance [Kim et al., 2001, Astrov et al., 2008]:

$$\begin{aligned}\dot{x}_1 &= -\frac{x_1}{\tau} + \frac{x_1 x_2}{\tau(E_c + v)},\\ \dot{x}_2 &= -a_1 x_2 - b_1 x_1 x_2 + a_1 E_m,\end{aligned} \tag{3.59}$$

where, recalling the notation given in the previous section, x_1 is the density of free charge carries in the gap, x_2 is the electric field strength in the discharge gap, $\tau_E = 1/a_1$ is the characteristic time of the charging process, b_1 is a coefficient, $E_m = U_m/d$ is the maximal value of x_2 in the gap that can be provided by a source of constant voltage, U_m is the voltage of the fielding source, d is the length of the gap in the direction of the electric current, and τ defines the rate of a temporal variation of the charge carriers density when the electric field in the gap is not equal to some critical electric field strength E_c.

We are interested in robust stabilization of this system, using E_m as the input control, with respect to the disturbance input v which can drive the system from the conductive to the dielectric state. As before, we transform the original system (3.59) by means of an input signal in order to obtain a positive equilibrium point. For instance, let us consider

$$E_m = u_0 x_2 + \delta u, \tag{3.60}$$

thus the system (3.59) becomes

$$\begin{aligned}\dot{x}_1 &= -\frac{x_1}{\tau} + \frac{x_1 x_2}{\tau(E_c + v)},\\ \dot{x}_2 &= a_1(u_0 - 1)x_2 - b_1 x_1 x_2 + a_1 \delta u.\end{aligned} \tag{3.61}$$

which means that, by choosing $u_0 > 1$, the system will have a positive equilibrium point $n = \left(\frac{a_1(u_0-1)}{b_1}, E_c\right)$ and we can use

$$W(x) = b_1 x_1 - a_1(u_0 - 1)\ln(x_1) + \frac{x_2}{\tau E_c} - \frac{\ln(x_2)}{\tau} \tag{3.62}$$

as an energy function. In fact (3.62) is a conserved quantity for the unforced version of (3.61), *i.e.*, with $v \equiv 0$ and $\delta u \equiv 0$, which reveals the multistability character of the system by means of the existence of closed orbits around the equilibrium point n with different constant energy levels W. Therefore, a possible strategy to ensure robustness of the system consists, first, to select the level of energy W for $v \equiv 0$ guaranteeing the needed performance and, second, to design δu using the results of Section 3.1 in the presence of the perturbation v.

Universal formula

Introducing an auxiliary function

$$Q(x) = \frac{1}{2}(W - W^*)^2, \tag{3.63}$$

where W^* is a desired level of W, which is reached provided that $Q(x(t)) \to 0$ as $t \to +\infty$, and calculating its derivative along the trajectories of the system (3.61) we obtain

$$\begin{aligned}\dot{Q}(x,u) = (W(x) - W^*)a_1\left(\frac{x_2 - E_c}{\tau E_c x_2}\right)\delta u \\ + (W(x) - W^*)(a_1(u_0 - 1)x_2 - b_1 x_1 x_2)\frac{v}{\tau E_c(E_c + v)}.\end{aligned} \tag{3.64}$$

In this case, the set of all invariant solutions of the system for $v \equiv 0$ is chosen as $\mathcal{W} = n \cup \Gamma$, where $\Gamma = \{x \in \mathcal{M} : W(x) = W^*\}$. To design δu providing iISS property of the closed loop system with respect to $\mathcal{W}$ and the input v let us introduce a weak iISS CLF candidate function $U(x) = \ln(1 + Q(x))$ and calculate its derivative:

$$\dot{U}(x,u) = a(x,v) + b(x)\delta u$$

where $a(x,v) = r(x)\sigma(v)$, with

$$r(x) = \frac{(W(x) - W^*)(a_1(u_0 - 1)x_2 - b_1 x_1 x_2)}{1 + Q(x)}, \quad \sigma(v) = \frac{v}{\tau E_c(E_c + v)},$$
$$b(x) = \frac{(W(x) - W^*)a_1\left(\frac{x_2 - E_c}{\tau E_c x_2}\right)}{1 + Q(x)}.$$

Performing simple calculations we can observe that r is bounded by a constant $R \geq 0$. However, the boundedness of σ depends on the sign of v that cannot be equal to $-E_c$. Then, assuming $v \geq 0$ for $t \geq 0$ we can apply the Theorem 3.6 to design δu. Note that for the chosen output $y = h(x) = b(x)$ the weak zero-detectability property is already satisfied for $\delta u \equiv 0$ and $v \equiv 0$.

Selecting $\tilde{\chi}(s) = s + R\sigma(s)$ we define ψ_o as

$$\psi_o(x) = \sup_{v\geq 0} \{r(x)\sigma(v) - R\sigma(v) - v\} \leq 0,$$

therefore, $\Psi_o(x) = \psi_o(x) + \frac{1}{2}\alpha_4(|h(x)|)$ and $b(x) = 0$ imply $\Psi(x) \leq -\frac{1}{2}\alpha_4(|h(x)|)$ for any positive definite function α_4. Finally, by applying the control law (3.56) and choosing $\alpha_4(s) = s^2$ (a choice to guarantee SCP of $\mathcal{W}$), we obtain

$$\begin{aligned}\dot{U}(x,u) &= r(x)\sigma(v) - \sup_{v\geq 0} \{r(x)\sigma(v) - R\sigma(v) - v\} - \frac{1}{2}|h(x)|^2 - \sqrt{\Psi_o^2(x) + |h(x)|^4} \\ &\leq v + R\sigma(v) - \frac{1}{2}|h(x)|^2 - \frac{\sqrt{5}}{2}|h(x)|^2 \leq -\frac{1}{2}\,|h(x)|^2 + R\sigma(v) + v\end{aligned}$$

which shows that condition (1) of Definition 3.18 is satisfied for the closed-loop system. To show that the weak iISS CLF W satisfies the SCP property we analyze the amplitude of the control law (3.56):

$$|\delta u| = \frac{|\Psi_o(x) + \sqrt{\Psi_o^2(x) + |b(x)|^4}|}{|b(x)|} \leq 2|h(x)|. \tag{3.65}$$

As $h(x) = b(x)$ is a continuous output map $|h(x)| \leq \varepsilon$ whenever $0 < |x|_{\mathcal{Z}} < \delta$ for $\varepsilon > 0$ and $\delta > 0$ (in fact in this case we can choose $\varepsilon = \delta$) and $\delta u = K(x) < \varepsilon$.

To illustrate the behavior of the closed-loop system, we choose the parameters $a_1 = 20s^{-1}$, $b = 0.4cm^3/s$, $\tau = 5 \times 10^{-3}$, and $E_c = 5V/cm$. To simulate the perturbation, it is used a uniformly distributed stochastic noise with an amplitude equal to 0.025 witch represents 0.5% of the critical electric field strength E_c. These values are re-scaled from the real physical parameters of a real device, which can be found in [Astrov et al., 2008, Kim et al., 2001], to facilitate the result's simulation and analysis.

Recovering the control goal, we are interested in the robust stabilization of the system near to an appropriate operation region, which means near to the minimum energy level of W achieved when $x = n = (50,5)$. To exemplify we choose $W^* = 0.001$ and the control input applied to the original system is given by $Em = K(x) + u_0 x_2$ where $u_0 = 2$. Fig.3.11(a) shows the phase portrait for the system with and without disturbance. As we can see, for the former case, the state trajectories evolve inside a small region around the desired trajectory given by the latter case. The behavior of the function Q is shown in Fig.3.11(b) and we observe that $Q(x) \to 0$ as $t \to \infty$ for the system without disturbance and for the system with disturbance, the proposed control works to keep Q tending to zero as the time goes to infinity. By means of Fig.3.11(c) and 3.11(d) we can see the behavior of the open-loop system and the closed-loop system for the same disturbance signal and conclude that for the controlled version, the state oscillations are much smaller, which means that the system remains inside the desired operation region. The behavior of the control signal δu is shown in Fig.3.11(d) and illustrate the SCP for the weak iISS CLF.

3.5 Conclusion

In this chapter, iISS and ISS's conditions for passive and strictly passive systems have been studied in the context of multistable dynamics and correspondingly defined storage and

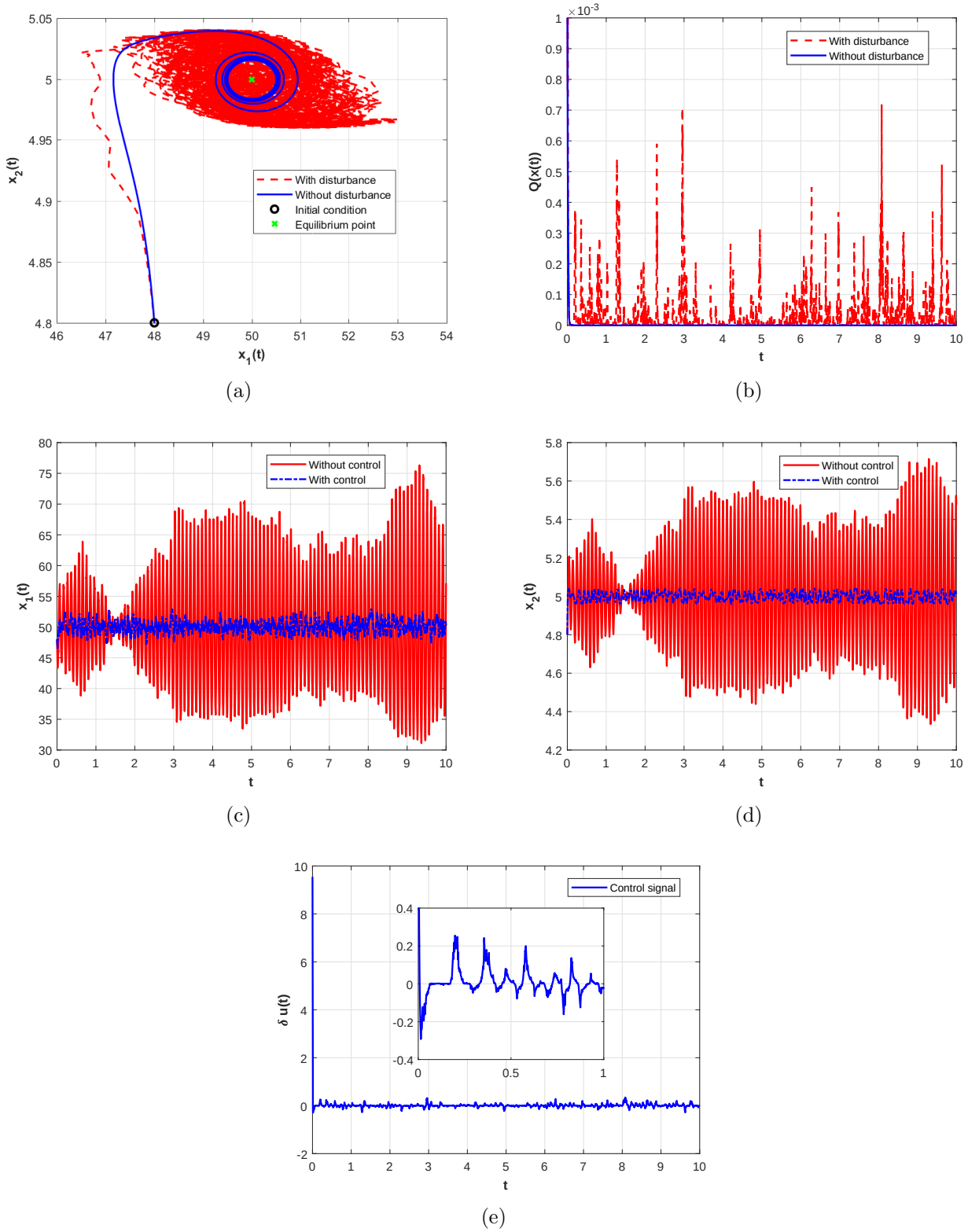

Figure 3.11: (a) Phase portrait for the controlled system (3.61) without (solid) and with (dashed) disturbance input (b) Behavior of the function Q (c) Time response of state $x_1(t)$ with (in blue) and without (in red) control (d) Time response of state $x_2(t)$ with (in blue) and without (in red) control (e) Control signal

supply functions. The problem was stated under the argumentation that passive and strict passive systems could be quite sensible to perturbations despite its stable nature. Therefore, the proposed conditions distinguished when additional output feedback was required or not to ensure robustness against exogenous perturbations in the input channel. The multispecies population dynamics model illustrated the obtained results, and in particular, it was shown that if all species are controlled, then the ISS property can be recovered. Still, if only a part of them can be regulated, then the iISS property is guaranteed. Another example dealt with a noise-induced transition problem in a semiconductor-gas-discharge gap system where a control transformation was necessary to change the invariant set shape to guarantee the system's robust stability using a speed-gradient control.

The development of a general design method for iISS or ISS stabilization of multistable systems also was considered. We studied a subclass of nonlinear multistable dynamical systems affine in the input with exogenous disturbances. In this case, our main problem was to establish conditions for the existence of a feedback control rendering the iISS (ISS) stability property with respect to input disturbances. We have appropriately extended the notions of iISS (ISS) CLF and SCP within the multistability framework in this direction. It has also been shown that such properties can also be extended to the iISS case using the existence of a continuous output map that makes the system smooth dissipative and weak zero detectable, giving rise to a weak iISS CLF notion and corresponding SCP. It was verified that a iISS (ISS) CLF or a weak iISS CLF satisfying the SCP imply the existence of a feedback control law that can be explicitly designed by the universal formula strategy. To illustrate the iISS (ISS) CLF application, such a feedback control was designed to stabilize two different nonlinear multistable systems robustly. The noise-induced transition problem in a semiconductor-gas-discharge gap system was revisited to exemplify the weak iISS CLF application.

The existing results on CLF deal with the concept of stability with respect to an equilibrium point or a single attractive set. The multistability framework deal with all compact invariant solutions (satisfying Assumption 3.1), including locally stable and unstable ones, which compose a finite and disjoint family of compact invariant sets. For this new scenario, the changes from the classic results seem to be subtle since basically the reference for stability conditions changes from an attractor to a finite and disjoint family of compact invariant sets. However, the facts that they are disjoint and (some of them) unstable are the main sources of complicacy, which influence, for example, the control continuity. To apply the universal formula we have to require $\frac{\partial V(x)}{\partial x} = 0$ for any $x \in \mathcal{W}$ for an ISS or iISS CLF V, or that $b(x) = 0$ for all $x \in \mathcal{Z}$ for a weak iISS CLF. The notion of weak iISS CLF has less sense in the conventional case, while in the multistable scenario it allows the design constraints to be relaxed greatly. All these small changes are not so straightforward complementing the existent CLF theory to the studied general stabilization problem.

CHAPTER

FOUR

GENERAL CONCLUSIONS AND FUTURE WORK

4.1 Living behavior

Chapter 1 provided a brief background on climate change problematics, from the most general aspect of climate comportment, through the effects on ecological systems, to the specific problems we dealt with in this thesis, *i.e.*, on detecting a climate change in Arctic using a mollusk-based biosensor. The objective was to give a general idea about how climate and ecology are coupled and how disturbances on these complex systems could influence the bivalves' behavior. Such a feature is the basic principle and motivation for valvometry, which, in turn, faces a major challenge to understand, isolate, and connect the information contained in the data with environmental or climate change entrances.

We also have recalled in Chapter 1 that the Arctic zone is the most sensitive area to climate variability. The importance of this ecosystem is global and has mobilized many initiatives for protection and conservation. One of these initiatives is the WaQMoS project in which this thesis work is inserted. We reviewed the basics of the MolluSCAN Eye biosensor, focusing on the applied mathematical point of view. That interprets the MolluSCAN Eye as a system with multiple inputs and one output, from which many estimates can be derived. We emphasized the challenges over this perspective and the importance of proposing mathematical and data processing methods to provide suitable variables with aggregated biological meaning. Then, we limited our first research object, *i.e.*, to provide a set of time-scaled populational behavioral variables to be related to bioclimatic ones such as the temperature, the main input-driver. Next, also motivated by the complex nature of climate and ecological systems, we defined our complementary route to study multistable system's robust stability.

In Chapter 2, we obtained a set of time-scaled populational behavioral variables calculated from the distance signal measured along seven years (2012-2018) of data acquisition in Ny Alesund, Svalbard, Norway from scallops *Chlamys Islandica*. The population monthly base variables were the average distance, the percentage of valve opening/closing, the average velocity, and the movement index. For this objective, a sequence of data processing tools was proposed. The first action was to complete the missing measurement, due to Internet connection losses or electronic cards failure. Secondly, we normalized the data to compensate for individual features

such as the size and growth rate. Such procedures were important to calculate the behavioral variables for the population.

Next, following a practical demand, we developed an intelligent adaptive filter. Such a filter was proposed to filter a harmonic electronic noise present in the data set measured in 2017 and in 2018. The intelligent filter development's motivation was to suppress a specific frequency with minor interference on the original signal since the noise component occupied an important frequency band. Such a result was not possible with conventional approaches, especially with low order passive filters due to its rigid structure. Therefore, using the DREM method combined with the fixed/finite-time parameter estimation approach, a more flexible filter structure with relative freedom in the parameter dependencies was obtained. Besides its simple structure, composed only by the first term of Fourier series and a noise term, the obtained result showed excellent performance in suppressing so specific frequency constraint keeping good characteristics on low, medium, and high-frequency regions, minimizing the losses of essential pieces of information. The filter application in all distance data, since 2012, also contributed to another essential aspect of data processing: harmonizing these data, generating comparability between the signals collected in different technical conditions of the data acquisition system. Such a feature is critical for the intended application.

Once we treated the distance signals properly, the next step was to estimate the velocity from it. For this purpose, the homogeneous finite-time differentiator was used. With the advantage of having the signal filtered as input, the differentiator parameters were tuned to obtain a more accurate estimation avoiding a second filter effect. Finally, we reach the end of chapter 2 by obtaining the five behavior variables mentioned above. The first three variables were derived from the distance signal and the last two from the velocity signal. The variables were calculated for each individual. Then an average was done to obtain the equivalent for the population. As living beings, individual behaviors are more challenging to map. Besides, we chose a monthly time base for analysis since smaller time-scale variations are less obvious, requiring more sophisticated analysis methods. This is not the scope of this work. However, it is a perspective.

We also compared, qualitatively, the behavior variables obtained from the filtered and unfiltered signal. In this sense, the distance signal-related behavioral variables did not show differences in these two cases. However, a small change occurred in the trend lines of the variables related to speed since the data collected in 2017 and 2018 presented harmonic noises that possibly influenced this trend. Once again, we make clear that analyzing the signals from the point of view of biology and determining correlations and trends meaning are not the focus of this work; however, observing the signals of air and water temperature and the speed-related behavioral signals, it was possible to note a visual correlation, which should be explored *a posteriori*. Therefore, we can only affirm that the obtained behavioral variables, especially the speed-related ones, show promise as potential tools, for example, to measure the bivalves' level of stress, which can be converted into a welfare and adaptation measurement for these animals regarding environmental temperature variation.

Most of the present work was dedicated to valvometry data processing. From this point of view, it is noted that there exists a gap in the standardization of the treatment of these

data until they are finally ready for analysis. This is a general problem, mainly in trait-based approaches, which is a promising direction in the study of rapidly changing ecosystems [Degen et al., 2018]. Therefore, a practical consequence of this work should be in this direction. Once there exists a consensus about basic parameters, such as sampling time, missing data, noise characteristics, filtering, harmonization, and regularization, most of the effort can be devoted to causes and effects. In this way, correlating the distance and velocity outputs with bioclimatic inputs would be crucial as the first action to infer dynamical models for climate change detection. Another consequence of the present work was the model-based adaptive filter obtained. The filter proved to be effective in filtering a specific frequency. It could also be useful to isolate other characteristic frequencies, In this way, correlating more precision in spawning detection [Ahmed et al., 2016c] and identifying biological rhythms. Guessing a hypothetic period, one could isolate the specific frequency and study the residual between the original signal and the filtered signal to verify if the hypothesis would be correct [Cornelissen, 2014].

4.2 Multistability

In Chapter 3, based on the framework of ISS and iISS, we provided robustness conditions for stability and stabilization of two subclasses of affine nonlinear multistable systems. The study was done using the framework defined in Angeli and Efimov [2015]. Therefore, we started the chapter by presenting this theory. It was shown that the multistability framework deal with all compact invariant solutions, satisfying the constraint on the decomposition of the compact invariant set $\mathcal{W}$ (Assumption 3.1), including locally stable and unstable ones. For this new scenario, the classic results' changes seem to be subtle since the reference for stability conditions changes from a single attractor to a finite and disjoint family of compact invariant sets. However, the facts that they are disjoint and (some of them) unstable are the main sources of complicacy, which influence, for example, the control continuity. Next, it was presented the robust stability notions with respect to $\mathcal{W}$ already available in the literature, including iISS notions [Forni and Angeli, 2017].

Chapter 3 first development was about iISS and ISS's conditions for passive and strictly passive systems. We studied this class of systems in the context of multistable dynamics and correspondingly defined storage and supply functions. The problem was stated under the argumentation that passive and strict passive systems could be quite sensible to perturbations despite its stable nature. Therefore, the proposed stability conditions distinguished when additional output feedback was required or not to ensure robustness against exogenous perturbations in the input channel. Using the multispecies population dynamics model, we illustrated the obtained results. In particular, it was shown that if all species were controlled, then the ISS property could be recovered. Still, if only a part of them could be regulated, which is a more practical case, then the iISS property was guaranteed. An interpretation of these results is that under the suggested control, populations' diversity and coexistence can be preserved under various environmental perturbations. Another example dealt with a noise-induced transition problem in a semiconductor-gas-discharge gap system. In this case, a control transformation was necessary to change the invariant set shape to guarantee the system's robust stability using

a speed-gradient control.

The development of a general design method for iISS or ISS stabilization of multistable systems also was considered in this chapter. We studied a subclass of nonlinear multistable dynamical systems affine in the input with exogenous disturbances. In this case, we established conditions for a feedback control rendering the iISS (ISS) stability property with respect to input disturbances. We appropriately extended the notions of iISS (ISS) CLF and SCP within the multistability framework and shown that such properties can also be extended to the iISS case using the existence of a continuous output map that makes the system smooth dissipative and weak zero detectable, giving rise to a weak iISS CLF notion and corresponding SCP. It was verified that an iISS (ISS) CLF or a weak iISS CLF satisfying the SCP imply the existence of a feedback control law that can be explicitly designed by the universal formula strategy. To illustrate the iISS (ISS) CLF application, such a feedback control was designed to robustly stabilize two academic nonlinear multistable systems. Also, the more practical and realistic problem on noise-induced transition in a semiconductor-gas-discharge gap system was revisited to exemplify the weak iISS CLF application. The notion of weak iISS CLF has less sense in the conventional single attractor case. Simultaneously, it allows the design constraints to be relaxed greatly in the multistable scenario, which is not so straightforward, complementing the existent CLF theory to the studied general stabilization problem.

The practical application of multistability is increasing and due to the complexity of multistable dynamical systems controlling is a challenge. In some cases, the multistability needs to be avoided, or the desired state has to be stabilized against a noisy environment. On the other hand, the coexistence of different stable states could offer great flexibility in system performance [Pisarchik and Feudel, 2014]. These control goals were illustrated in this thesis. Different energy levels could be selected for ecological equilibrium in a predator-prey example, while other equilibria must be avoided to guarantee a semiconductor working on the right operational region. The technique using ISS and iISS framework version for multistable systems showed potential; however, it is just a begin in this field and must be expanded to other systems and control classes such as network, time-delay, switched, and hybrid systems. Moreover, convergence aspects and relaxation on decomposition constraints must be investigated.

BIBLIOGRAPHY

H. Ahmed, R. Ushirobira, D. Efimov, D. Tran, and J-C. Massabuau. Velocity estimation of valve movement in oysters for water quality surveillance. *IFAC-PapersOnLine*, 48(11):333–338, 2015.

H. Ahmed, R. Ushirobira, D. Efimov, and W. Perruquetti. Robust synchronization for multistable systems. *IEEE Transactions on Automatic Control*, 61(6):1625–1630, 2016a.

H. Ahmed, R. Ushirobira, D. Efimov, D. Tran, M. Sow, P. Ciret, and J-C. Massabuau. Monitoring biological rhythms through the dynamic model identification of an oyster population. *IEEE Transactions on Systems, Man, and Cybernetics: Systems*, 47(6):939–949, 2016b.

H. Ahmed, R. Ushirobira, D. Efimov, D. Tran, M. Sow, L. Payton, and J. Massabuau. A fault detection method for automatic detection of spawning in oysters. *IEEE Transactions on Control Systems Technology*, 24(3):1140–1147, 2016c.

H. Ahmed, R. Ushirobira, and D. Efimov. Robust global synchronization of brockett oscillators. *IEEE Transactions on Control of Network Systems*, 2018. doi: 10.1109/tcns.2018.2813927.

A. K. Al-Habahbeh, S. Kortsch, B. A. Bluhm, F. Beuchel, B. Gulliksen, C. Ballantine, D. Cristini, and R. Primicerio. Arctic coastal benthos long-term responses to perturbations under climate warming. *Philosophical Transactions of the Royal Society A*, 378(2181): 20190355, 2020.

H. Andrade, J-C. Massabuau, S. Cochrane, P. Ciret, D. Tran, M. Sow, and L. Camus. High frequency non-invasive (HFNI) bio-sensors as a potential tool for marine monitoring and assessments. *Frontiers in Marine Science*, 3, 2016. doi: https://doi.org/10.3389/fmars.2016.00187.

D. Angeli. An almost global notion of input-to-state stability. *IEEE Trans. Automatic Control*, 49:866–874, 2004.

D. Angeli and D. Efimov. Characterization of input-to-state stability for systems with multiple invariant sets. *IEEE Transactions on Automatic Control*, 60:3242–3256, 2015.

D. Angeli, E. D. Sontag, and Y. Wang. A characterization of integral input-to-state stability. *IEEE Transactions on Automatic Control*, 45:1082–1097, 2000.

D. Angeli, J. E. Ferrell, and E. D. Sontag. Detection of multistability, bifurcations and hysteresis in a large class of biological positive-feedback systems. *Proc. Natl. Acad. Sci. USA*, 101:1822–1827, 2004.

S. Aranovskiy, A. Bobtsov, R. Ortega, and A. Pyrkin. Performance enchancement of parameter estimators via dynamic regressor extension and mixing. *IEEE Transactions on Automatic Control*, 62:3546–3550, 2017.

M. Arcak and P. Kokotović. Nonlinear observers: a circle criterion design and robustness analysis. *Automatica*, 37(12):1923–1930, 2001.

Z. Artstein. Stabilization with relaxed controls. *Nonlinear Analysis, Theory, Methods and Applications*, 7:1163–1173, 1983.

Yu. A. Astrov, A. L. Fradkov, and P. Yu Guzenko. Control of a noise-induced transition in a nonlinear dynamical system. *Physical Review*, 77:026201:1–7, 2008.

M. E. Biresselioglu, M. H. Demir, B. Solak, A. Kayacan, and S. Altinci. Investigating the trends in arctic research: The increasing role of social sciences and humanities. *Science of The Total Environment*, page 139027, 2020.

S. Bosheim, M. L. Carroll, S. Denisenko, A. Voronkov, W. Jr. Ambrose, G. Henkes, et al. Arctic bivalves as indicators of environmental variation-baseline data. In *SPE International Conference on Health, Safety, and Environment in Oil and Gas Exploration and Production*. Society of Petroleum Engineers, 2008.

J. Bremner, S. I. Rogers, and C. L. J. Frid. Methods for describing ecological functioning of marine benthic assemblages using biological traits analysis (bta). *Ecological Indicators*, 6(3): 609–622, 2006.

R. Brockett. Synchronization without periodicity. *Mathematical systems theory, a volume in honor of U. Helmke*, pages 65–74, 2013.

M. Chaves, T. Eissing, and F. Allgöwer. Bistable biological systems: A characterization through local compact input-to-state stability. *IEEE Transactions on Automatic Control*, 45:87–100, 2008.

M. Cisek, P. Makuch, and T. Petelski. Comparison of meteorological conditions in svalbard fjords: Hornsund and kongsfjorden. *Oceanologia*, 59(4):413–421, 2017.

G. Cornelissen. Cosinor-based rhythmometry. *Theoretical Biology and Medical Modelling*, 11 (1):16, 2014.

P. J. Cranford, J. E. Ward, S. E. Shumway, et al. Bivalve filter feeding: variability and limits of the aquaculture biofilter. *Shellfish aquaculture and the environment*, pages 81–124, 2011.

R. Degen, M. Aune, B. A. Bluhm, C. Cassidy, M. Kędra, C. Kraan, L. Vandepitte, M. Włodarska-Kowalczuk, I. Zhulay, P. G. Albano, et al. Trait-based approaches in rapidly changing ecosystems: A roadmap to the future polar oceans. *Ecological Indicators*, 91:722–736, 2018.

M. Dolbeth, D. Crespo, S. Leston, and M. Solan. Realistic scenarios of environmental disturbance lead to functionally important changes in benthic species-environment interactions. *Marine environmental research*, 150:104770, 2019.

W. W. Dowd and G. N. Somero. Behavior and survival of mytilus congeners following episodes of elevated body temperature in air and seawater. *Journal of Experimental Biology*, 216(3): 502–514, 2013.

D. Dudkowski, S. Jafari, T. Kapitaniak, N. V. Kuznetsov, G. A. Leonov, and A. Prasad. Hidden attractors in dynamical systems. *Physics Reports*, 637:1–50, 2016. doi: http://dx.doi.org/10.1016/j.physrep.2016.05.002.

J. M. Durant, J-C. Molinero, G. Ottersen, G. Reygondeau, L. C. Stige, and O. Langangen. Contrasting effects of rising temperatures on trophic interactions in marine ecosystems. *Scientific reports*, 9(1):1–9, 2019.

C. Ebenbauer, T. Raff, and F. Allgöwer. Dissipation inequalities in systems theory: An introduction and recent results. In *Invited lectures of the international congress on industrial and applied mathematics*, volume 2007, pages 23–42, 2009.

M. Edwards and A. J. Richardson. Impact of climate change on marine pelagic phenology and trophic mismatch. *Nature*, 430(7002):881–884, 2004.

D. Efimov. Passivity and input-to-state stability of nonlinear systems. *IFAC Proceedings Volumes*, 39:285–290, 2006.

D. Efimov. Global lyapunov analysis of multistable nonlinear systems. *SIAM Journal on Control and Optimization*, 50(5):3132–3154, 2012.

D. Efimov and A. L. Fradkov. Adaptive input-to-output stabilization of nonlinear systems. *International Journal of Adaptive Control and Signal Processing*, 22:949–967, 2008.

D. Efimov, J. Schiffer, N. Barabanov, and R. Ortega. A relaxed characterization of iss for periodic systems with multiple invariant sets. *European Journal of Control*, 37:1–7, 2017.

D. V. Efimov. Universal formula for output asymptotic stabilization. *IFAC Proceedings Volumes*, 35:239–244, 2002a.

D. V. Efimov. A condition of CLF existence for affine systems. *Proceedings of the 41st IEEE Conference on Decision and Control*, pages 1882–1887, 2002b.

I. Eisenman and J. S. Wettlaufer. Nonlinear threshold behavior during the loss of arctic sea ice. *Proceedings of the National Academy of Sciences*, 106(1):28–32, 2009.

G. Enciso and E. D. Sontag. Monotone systems under positive feedback: multistability and a reduction theorem. *Systems & Control Lett.*, 54:159–168, 2005.

U. Feudel, A. N. Pisarchik, and K. Showalter. Multistability and tipping: From mathematics and physics to climate and brain - minireview and preface to the focus issue. 2018.

C. B. Field, M. J. Behrenfeld, J. T. Randerson, and P. Falkowski. Primary production of the biosphere: integrating terrestrial and oceanic components. *science*, 281(5374):237–240, 1998.

F. Forni and R. Sepulchre. Differential analysis of nonlinear systems: Revisiting the pendulum example. In *Proc. 53rd IEEE Conference on Decision and Control*, pages 3848–3859, Los Angeles, US, 2014.

P. Forni and D. Angeli. Output-to-state stability for systems on manifolds with multiple invariant sets. *IEEE Conference on Decision and Control*, 55:453–458, 2016a.

P. Forni and D. Angeli. Input-to-state-stability for cascade systems with multiple invariant sets. *Systems & Control Letters*, 98:97–110, 2016b.

P. Forni and D. Angeli. Characterization of integral input-to-state stability for systems with multiple invariant sets. *IEEE Transactions on Automatic Control*, 62:3729–3743, 2017.

A. L. Fradkov. *Cybernetical Physics: From Control of Chaos to Quantum Control*. Understanding Complex Systems. Springer-Verlag, London, 2007.

M. Ghil and V. Lucarini. The physics of climate variability and climate change. *arXiv preprint arXiv:1910.00583*, 2019.

J. Guckenheimer and P. J. Holmes. *Nonlinear Oscillations, Dynamical Systems, and Bifurcations of Vector Fields*, volume 42 of *Applied Mathematical Sciences*. Springer-Verlag, New York, 1983.

I. Hanssen-Bauer, E. J. Førland, H. Hisdal, S. Mayer, A. B. Sandø, and A. Sorteberg. Climate in svalbard 2100. *A knowledge base for climate adaptation*, 2019.

C. Hayachi. *Nonlinear oscillations in physical systems*. McGraw-Hill Book Company, New York, 1964.

D. Hill and P. Moylan. Dissipative dynamical systems: Basic input-output and state properties. *Journal of the Franklin Institute*, 309:327–357, 1980.

J. H. R. Kim, H. Maurer, Yu. A. Astrov, M. Bode, and H. G. Purwinst. High-speed switch-on of a semiconductor gas discharge image converter using optimal control methods. *Journal of Computational Physics*, 170:395–414, 2001.

K. J. M. Kramer, H. A. Jenner, and D. de Zwart. The valve movement response of mussels: a tool in biological monitoring. *Hydrobiologia*, 188(1):433–443, 1989.

S. Kröger and R. J. Law. Sensing the sea. *Trends in biotechnology*, 23(5):250–256, 2005.

B. P. Lathi. *Signal Processing and Linear Systems*. Oxford University Press, Oxford, 2009.

M. Laurent and N. Kellershohn. Multistability: a major means of differentiation and evolution in biological systems. *Trends Biochem. Sci.*, 24:418–422, 1999.

E. League, P. Kabat, P. Egerton, O. Baddour, L. Paterson, C. Nullis, S. Castonguay, M. Walsh, et al. United in science: high-level synthesis report of latest climate science information convened by the science advisory group of the un climate action summit 2019. 2019.

D. Liberzon, E. D. Sontag, and Y. Wang. On integral-input-to-state stabilization. *Proceedings of the American Control Conference*, 3:1598–1602, 1999.

D. Liberzon, E. D. Sontag, and Y. Wang. Universal contruction of feedback laws achieving ISS and integral-ISS disturbance attenuation. *System & Control Letters*, 46:111–127, 2002.

Y. Lin and E. D. Sontag. Control-lyapunov universal formulas for restricted inputs. *Control-Theory and Advanced Technology*, 10:1–22, 1995.

R. Lindsey. Climate and earths energy budget. *NASA Earth Observatory, Greenbelt, MD, accessed Oct*, 9:2017, 2009.

V. Lucarini and T. Bódai. Edge states in the climate system: exploring global instabilities and critical transitions. *Nonlinearity*, 30(7):R32, 2017.

R. M. May. Thresholds and breakpoints in ecosystems with a multiplicity of stable states. *Nature*, 269(5628):471–477, 1977.

B. M. Millman. Mechanisms of contraction in molluscan muscle. *American Zoologist*, 7(3): 583–591, 1967.

G. Neukermans, L. Oziel, and M. Babin. Increased intrusion of warming atlantic water leads to rapid expansion of temperate phytoplankton in the arctic. *Global change biology*, 24(6): 2545–2553, 2018.

H. Nijmeijer and A. J. van der Schaft. *Nonlinear Dynamical Control Systems*. Springer-Verlag, 1990.

Z. Nitecki and M. Shub. Filtration, decompositions, explosions. *American Journal of Mathematics*, 97:1029–1047, 1975.

M. I. O'Connor, M. F. Piehler, D. M. Leech, A. Anton, and J. F. Bruno. Warming and resource availability shift food web structure and metabolism. *PLoS Biol*, 7(8):e1000178, 2009.

R. Ortega, A. Loría, P. J. Nicklasson, and H. J. Sira-Ramirez. *Passivity-based Control of Euler-Lagrange Systems: Mechanical, Electrical and Elctromechanical Aoolications*. Springer-Verlag, London, 1998.

J. Overland, E. Dunlea, J. E. Box, R. Corell, M. Forsius, V. Kattsov, M. S. Olsen, J. Pawlak, L-O Reiersen, and M. Wang. The urgency of arctic change. *Polar Science*, 21:6–13, 2019.

R. K. Pachauri, L. Gomez-Echeverri, and K. Riahi. Synthesis report: summary for policy makers. 2014.

D. Padfield, C. Lowe, A. Buckling, R. Ffrench-Constant, Student Research Team, S. Jennings, F. Shelley, J. S. Ólafsson, and G. Yvon-Durocher. Metabolic compensation constrains the temperature dependence of gross primary production. *Ecology Letters*, 20(10):1250–1260, 2017.

I. Pchelkina and A. L. Fradkov. Control of oscillatory behavior of multispecies populations. *Ecological Modelling*, 227:1–6, 2012.

F. Pernet, N. Malet, A. Pastoureaud, A. Vaquer, and C. Quéréand L. Laurent. Marine diatoms sustain growth of bivalves in a mediterranean lagoon. *Journal of sea research*, 68:20–32, 2012.

W. Perruquetti, T. Floquet, and E. Moulay. Finite-time observers: application to secure communication. *IEEE Transactions on Automatic Control*, 53(1):356–360, 2008.

A. K. Pettersen, C. R. White, and D. J. Marshall. Metabolic rate covaries with fitness and the pace of the life history in the field. *Proceedings of the Royal Society B: Biological Sciences*, 283(1831):20160323, 2016.

A. N. Pisarchik and U. Feudel. Control of multistability. *Physics Reports*, 540:167–218, 2014.

A. Polyakov. *Generalized Homogeneity in Systems and Control*. Springer, 2020.

H. Ríos, D. Efimov, J. A. Moreno, W. Perruquetti, and J. G. Rueda-Escobedo. Time-varying parameter identification algorithms: Finite and fixed-time convergence. *IEEE Transactions on Automatic Control*, 62:3670–3678, 2017.

H. Ríos, D. Efimov, and W. Perruquetti. An adaptive sliding-mode observer for a class of uncertain nonlinear systems. *International Journal of Adaptive Control and Signal Processing*, 32:3670–3678, 2018.

N. Rouche, P. Habets, and M. Laloy. *Stability Theory by Liapunov's Direct Method*. Applied Mathematical Sciences. Springer-Verlag, New York, 1977.

V. V. Rumyantsev and A. S. Oziraner. *Stability and stabilization of motion with respect to part of variables*. Nauka, Moscow, 1987. [in Russian].

S. E. Harris S. L. Burch. *Understanding climate change: science, policy, and practice*. University of Toronto Press, 2014.

M. Solan, P. Archambault, P. E. Renaud, and C. März. The changing arctic ocean: consequences for biological communities, biogeochemical processes and ecosystem functioning, 2020.

E. D. Sontag. A "universal" construction of Artstein's theorem on nonlinear stabilization. *Systems & Control Letters*, 13:117–123, 1989.

E. D. Sontag. Further facts about input-to-state stabilization. *IEEE Transactions on Automatic Control*, 35:473–476, 1990.

E. D. Sontag. Coments on integral variants of ISS. *Systems & Control Letters*, 34:93–100, 1998.

E. D. Sontag and Y. Wang. On characterizations of the input-to-state stability property. *Systems & Control Letters*, 24:351–359, 1995.

E. D. Sontag and Y. Wang. New characterizations of the input-to-state stability. *IEEE Transactions on Automatic Control*, 41:1283–1294, 1996.

G. B. Stan and R. Sepulchre. Analysis of interconnected oscillators by dissipativity theory. *IEEE Trans. Automatic Control*, 52:256–270, 2007.

T. C. Telfer, H. Atkin, and R. A. Corner. Review of environmental impact assessment and monitoring in aquaculture in europe and north america, 2009.

Y. Thomas, C. Cassou, P. Gernez, and S. Pouvreau. Oysters as sentinels of climate variability and climate change in coastal ecosystems. *Environmental Research Letters*, 13(10):104009, 2018.

D. Tran, M. Sow, L. Camus, P. Ciret, J. Berge, and J-C. Massabuau. In the darkness of the polar night, scallops keep on a steady rhythm. *Scientific reports*, 6(1):1–9, 2016.

V. I. Vorotnikov. *Partial Stability and Control*. Birkhauser, Boston, 1998.

J. Wang, D. Efimov, S. Aranovskiy, and A. Bobtsov. Fixed-time estimation of parameters for non-persistent excitation. *European Journal of Control*, 2019.

J. C. Willems. Dissipative dynamical systems part i: General theory. *Archive for rational mechanics and analysis*, 45(5):321–351, 1972.

V. A. Yakubovich, G. A. Leonov, and A. Kh. Gelig. *Stability of Stationary Sets in Control Systems with Discontinuous Nonlinearities*. World Scientific, Singapore, 2004. in Russian.